NASA TN D-57

7N-02
195455
80P.

TECHNICAL NOTE
D-57

LOW-SPEED WIND-TUNNEL INVESTIGATION OF A WINGLESS JET VTOL TRANSPORT MODEL

By M. O. McKinney, Jr.

Langley Research Center
Langley Field, Va.

NATIONAL AERONAUTICS AND SPACE ADMINISTRATION

WASHINGTON

October 1959

NATIONAL AERONAUTICS AND SPACE ADMINISTRATION

TECHNICAL NOTE D-57

LOW-SPEED WIND-TUNNEL INVESTIGATION OF A WINGLESS JET VTOL TRANSPORT MODEL

By M. O. McKinney, Jr.

L
5
7
5

SUMMARY

A wind-tunnel investigation has been made of the static stability and lift and drag characteristics of a small-scale model which represented a wingless turbojet-powered vertical-take-off-and-landing (VTOL) transport airplane, which might have some performance advantage over a winged airplane for cruise at high subsonic speeds at very low altitudes. The model consisted of a fuselage with conventional tail surfaces at the rear and with 12 simulated jet engines near the center which could be tilted from a horizontal attitude for normal forward flight to a vertical attitude for hovering flight. The investigation consisted of power-off and power-on longitudinal stability and lift and drag tests and power-off lateral stability tests. The results of the investigation showed that satisfactory static longitudinal stability characteristics could be obtained and that a maximum trimmed lift-drag ratio of about 5 could be obtained at a lift coefficient of about 0.15 which is approximately the lift coefficient for a Mach number of 0.6 at sea level for a full-scale airplane of the type represented by the model.

INTRODUCTION

Preliminary design studies have shown that for an airplane designed for high-speed low-altitude flight (for example, a Mach number of 0.8 at sea level), the use of wings detracts from the performance of the airplane in this design condition. This fact is illustrated in figure 1 which shows the type of lift-drag polars that would be obtained with winged and wingless airplane configurations having the same body and tails. The winged airplane has a much higher maximum lift-drag ratio than the wingless configuration; however, at a low lift coefficient corresponding to that required for high subsonic speeds at sea level, the wingless configuration has the higher lift-drag ratio. A further advantage of a wingless configuration for high-speed low-altitude operation is that it would ride more smoothly because of its low lift-curve slope. By the use of vertical-take-off-and-landing principles, it is possible to eliminate the need for a wing for take-off and landing; thus, a wingless airplane becomes technically feasible from a

MODEL COMPONENT DESIGNATIONS

B_1 body with symmetrical afterbody (see fig. 3(a))

B_2 body with upswept afterbody (see fig. 3(b))

N nacelles

$H_1,H_2,\ldots H_5$ horizontal tails (see fig. 4)

$V_1,V_2,\ldots V_8$ vertical tails (see fig. 5)

L
5
7
5

APPARATUS AND TESTS

Three-view sketches of the model are shown in figure 3, sketches of the various tails used in the tests are shown in figures 4 and 5, and photographs of the model are presented in figure 6. The model was intended to represent a turbojet-powered VTOL transport airplane with 12 engines - 4 engines in the nacelles and 8 engines mounted in turntables recessed into the sides of the fuselage with retractable inlet doors and with the jets exhausting out the sides of the turntables at an angle of 15° with respect to the airplane center line. The turntables together with the nacelles could be rotated to a vertical attitude for vertical take-off and landing. These turntables show up much more clearly in the photographs of figure 6 than in the drawing of figure 3(a). The retractable inlet doors were not simulated on the model. For power-on tests, the flow from both the pod-mounted engines and the recessed engines was simulated by compressed air which was supplied to the model through thin-wall flexible hoses as illustrated in the sketch of figure 7. During the power-off tests the inlet pipes, which can be seen protruding from the sides of the nacelles in the photographs of figure 6, were removed and the plugs in the inlets of the nacelles were removed to permit air flow through the nacelles. Two of the horizontal tails, H_4 and H_5, were equipped with 25-percent-chord elevators for longitudinal control tests.

The tests were made in the Langley free-flight tunnel which has a 12-foot octagonal cross section. Most of the tests were made at an airspeed of about 45 miles per hour which gave an effective Reynolds number of about 4.5×10^6 based on the fuselage length. All the tests were made with transition strips of No. 60 carborundum grit 2 inches behind the nose of the fuselage and at the 5-percent-chord station of the tails.

The model was sting mounted with a strain-gage balance located with its moment center at the center of gravity. No corrections were applied to the data except a buoyancy correction to the drag which resulted from the static-pressure gradient along the tunnel, and a correction for the drag of the compressed-air hoses in the power-on tests.

The investigation consisted of power-off longitudinal stability and control and lateral stability tests of the model with bodies B_1 and B_2 and with various horizontal and vertical tails; and power-on longitudinal stability and control tests of the model with body B_1, with horizontal tails H_3 and H_5, and with various angles of incidence of the jets from 0° to 80°. No lateral stability tests were made with the power on because of the restraint of the hoses supplying compressed air to the model.

RESULTS AND DISCUSSION

Longitudinal Stability and Control

Power-off tests.- The effects of various model components including the various-size horizontal tails are shown in figure 8 for configurations with body B_1. The principal result of these tests is that the model was longitudinally unstable with tails H_1 and H_2 and was stable with tails H_3 and H_4. The lift-drag ratios from these tests for the complete configurations with the horizontal tails which provided stability and for the tail-off configuration are presented in figure 9. These data show that maximum values of L/D for the stable configurations $B_1NV_1H_3$ and $B_1NV_5H_4$ are about 5 at a lift coefficient of about 0.15. The results of the elevator-effectiveness tests for the model with the horizontal tail H_4 are presented in figure 10. These data show that the model can be trimmed over the entire angle-of-attack range covered in the tests (0° to 30°) and that it trims with 0° elevator deflection at lift coefficients of about 0.20 which are slightly higher than that required for high-speed low-altitude cruise.

The results of the longitudinal tests with the body B_2 are presented in figure 11. These data show that the model was unstable with tail H_1 but was stable with tail H_2. The variation of L/D with C_L for the stable configuration (B_2NH_2) is presented in figure 12. In order to show the effect of the two different bodies, the lift-drag ratios are also presented in figure 12 for corresponding configurations with body B_1.

These data show that the configurations with body B_1 have somewhat higher maximum values of L/D, either with the same horizontal tail H_2 or with a horizontal tail which gave about the same degree of longitudinal stability H_4. This difference results mainly from the difference in minimum drag coefficient which was about 0.020 for configurations with B_1 and about 0.025 for configurations with B_2.

Power-on tests.- The results of the power-on longitudinal stability and control tests are presented in figures 13 to 19. As pointed out previously, the retractable inlets proposed for the recessed engines were not represented on the model. The data show that power caused a reduction in longitudinal stability so that the model was neutrally stable or unstable for jet incidence angles of 20° or more with horizontal tail H_3, with which it had been stable in the power-off tests or in the power-on tests at a jet incidence of 0°. The data also show that, with the larger tail H_5, the model was longitudinally stable over the entire range of power and jet-incidence conditions covered in the tests except for some of the cases with 20° down-elevator deflection. These latter cases are not very significant, however, since in all of these cases the model had large nose-down pitching moments and was stable with an elevator setting more nearly that required for trim. The lift-drag ratios of the model with tail H_5, taken from the $T_c' = 0$ run of figure 13, are presented in figure 20. This curve shows a maximum value of L/D of nearly 6 with an elevator deflection of 0° and a maximum trimmed value of L/D of 5 at a lift coefficient of about 0.15. This value would be the lift coefficient at a Mach number of about 0.6 at sea level for the 30,000-pound hypothetical airplane that the model was designed to represent at a scale of 1/9.

L
5
7
5

The data of figures 13 to 17 also show that, for the angles of jet incidence for which control effectiveness tests were run $\left(i_j = 0^\circ \text{ to } i_j = 40^\circ\right)$, the model could be trimmed with elevator deflections less than 20° for all power conditions.

Lateral Stability

The results of the lateral stability tests, which were made only for the power-off condition, are presented in figures 21 to 32 for the case of body B_1. The lateral stability derivatives presented in alternate figures of this group were taken from the slopes at small angles of sideslip from the results of the immediately preceding sideslip tests.

The data of figure 23(a) show that with the original vertical tail V_1 the model was directionally unstable at an angle of attack of 0° for small angles of sideslip. With the larger tail V_2 in approximately the same location as V_1 (see fig. 25), the model was directionally stable at an angle of attack of 0°; however, it was much less stable at small angles of sideslip than at large angles. Analysis of the data indicated that the effectiveness of these tails was only about 60 percent as great as would be expected, perhaps because of unfavorable sidewash effects or vortex flow from the body such as that discussed in reference 1. Since the effectiveness of these tails was low for this rearward position, it seemed logical to try some more forward tail locations. Tails V_3 and V_4, which were about the same size as tails V_1 and V_2, respectively, were therefore tested. Comparison of the data for tails V_3 and V_4 from figures 27 to 30 with the data for tails V_1 and V_2 from figures 23 to 26 shows that the tails in the forward position gave more directional stability at an angle of attack of 0° than the corresponding tails in the rearward position. Their greater contribution to directional stability resulted from the fact that they produced more side force than the corresponding rearward tails, evidently because of the end-plate effect of the horizontal tail or because of a more favorable sidewash.

Tail V_5 was intended to represent a reasonably optimum vertical tail with regard to both size and position. The data for this tail are presented in figures 31 and 32. These data show that the model was directionally stable throughout the angle-of-attack range except that it was not stable at angles of sideslip above 10° at an angle of attack of 30°. It also had a positive dihedral effect of a magnitude which would be acceptable for a conventional airplane. In this configuration, therefore, the model seemed to have reasonably good lateral stability characteristics from static considerations.

The results of the lateral stability tests for configurations with body B_2 are presented in figures 33 to 40. These data show that with the original tail (tail V_6) the model was directionally unstable at angles of attack of 10° or more. With the same tail moved to a more forward position (tail V_7) the stability at high angles of attack was improved but the model was not stable at angles of attack of 20° and 30°. With the somewhat larger tail (tail V_8) in the forward position the model was generally directionally stable except at the higher angles of attack and sideslip. With vertical tails of about the same size, the directional stability of the model was generally somewhat lower with body B_2 than with body B_1. This condition was particularly true for the case of $B_1NH_2V_4$ in figure 30 and $B_2NH_2V_7$ in figure 38 and was less definite in the case of $B_1NH_2V_1$ in figure 24 and $B_2NH_2V_6$ in figure 36.

CONCLUSIONS

An experimental investigation was conducted to determine the lift and drag and static stability characteristics of a small-scale model which represented a wingless turbojet-powered vertical-take-off-and-landing (VTOL) airplane since analysis had indicated that such a configuration might have some performance advantages for cruise at high subsonic speeds at very low altitudes. The results of the investigation showed that satisfactory static longitudinal and lateral stability could be obtained with the wingless jet VTOL transport configuration represented by the model and that the model has a maximum trimmed lift-drag ratio of about 5 at a lift coefficient of 0.15, which is approximately the lift coefficient for high subsonic speeds at sea level for a full-scale airplane of this type.

Langley Research Center,
National Aeronautics and Space Administration,
Langley Field, Va., May 19, 1959.

REFERENCE

1. Stone, Ralph W., Jr., and Polhamus, Edward C.: Some Effects of Shed Vortices on the Flow Fields Around Stabilizing Tail Surfaces. Rep. 108, AGARD, North Atlantic Treaty Organization (Paris), Apr.-May 1957.

L-575

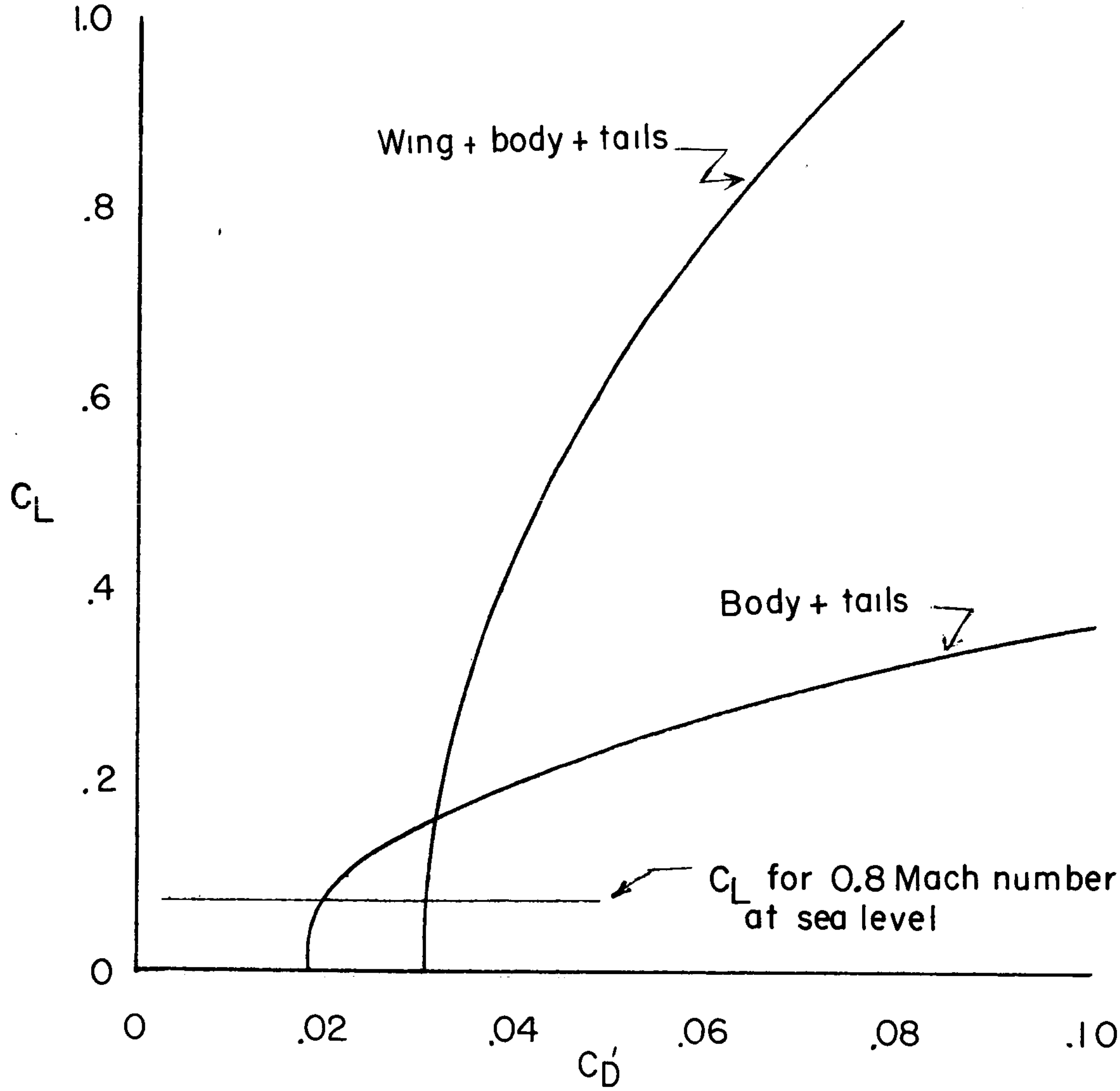

Figure 1.- Comparison of lift-drag polars for winged and wingless configurations. C_L and C_D' are lift and drag coefficients based on plan-form area of body which was the same in both cases.

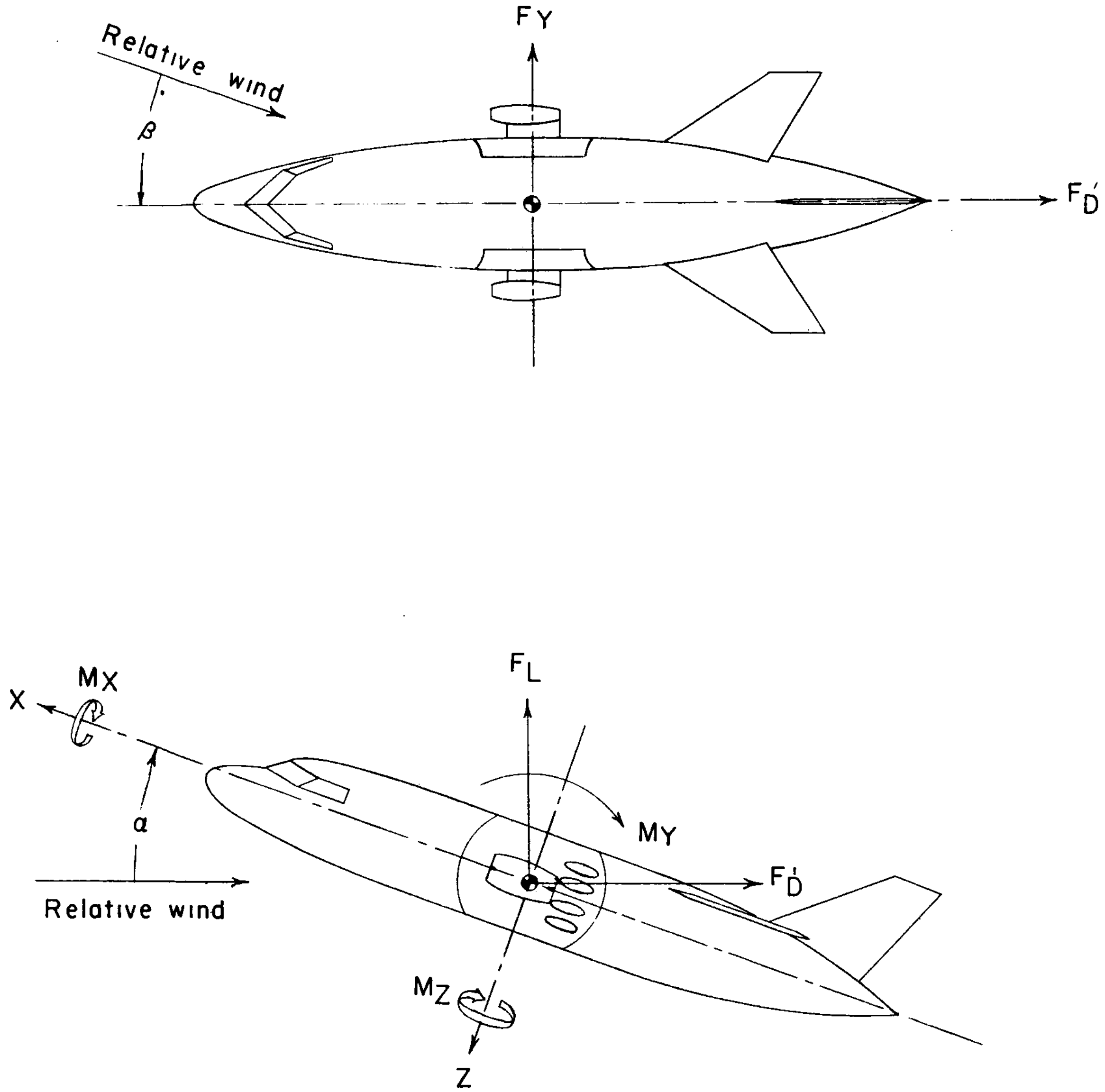

Figure 2.- Sketch of axes showing positive direction of forces, moments, and angles.

L-575

L-575

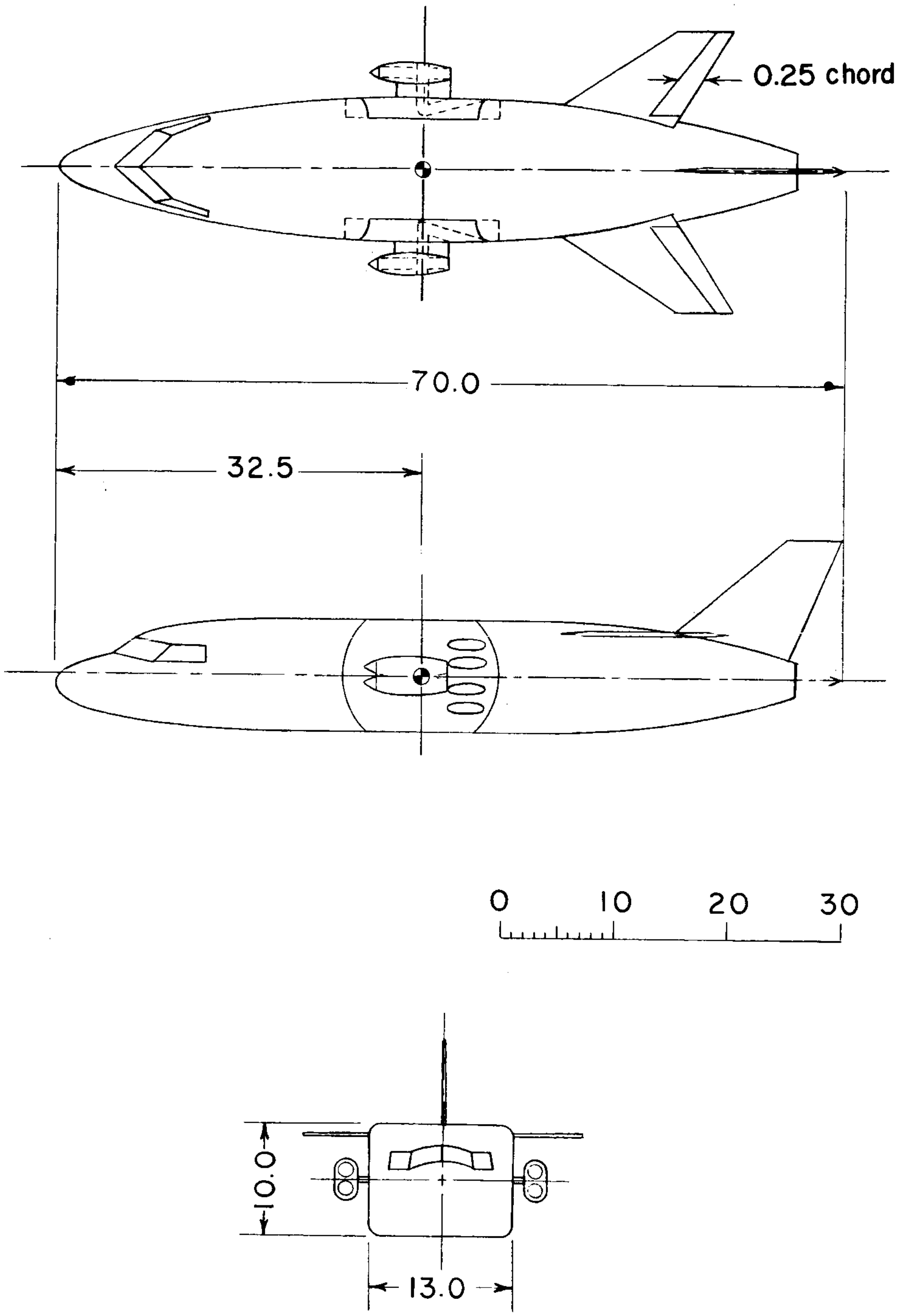

(a) Model with body B_1.

Figure 3.- Sketches of models. All dimensions are in inches.

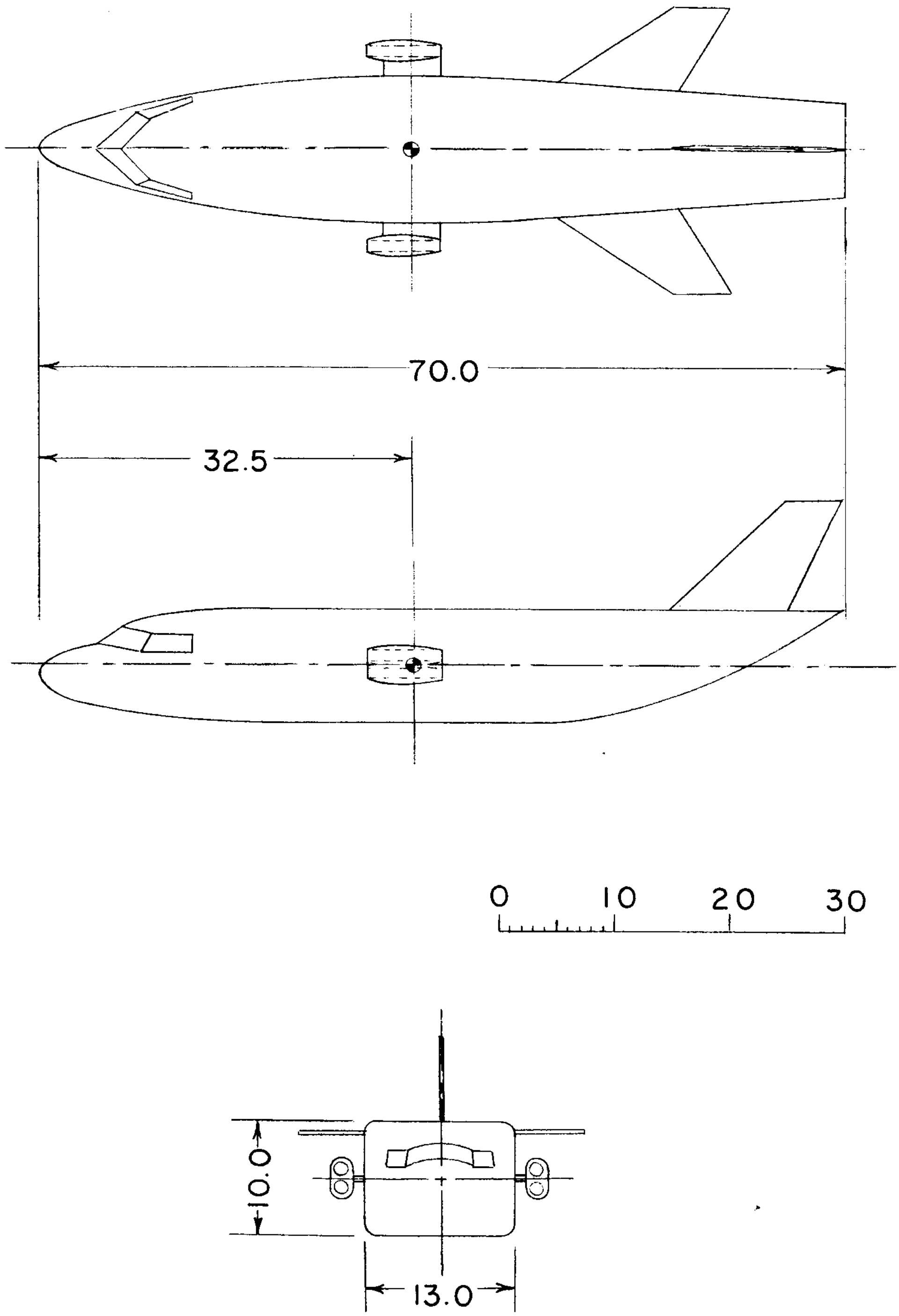

(b) Model with body B_2.

Figure 3.- Concluded.

L-575

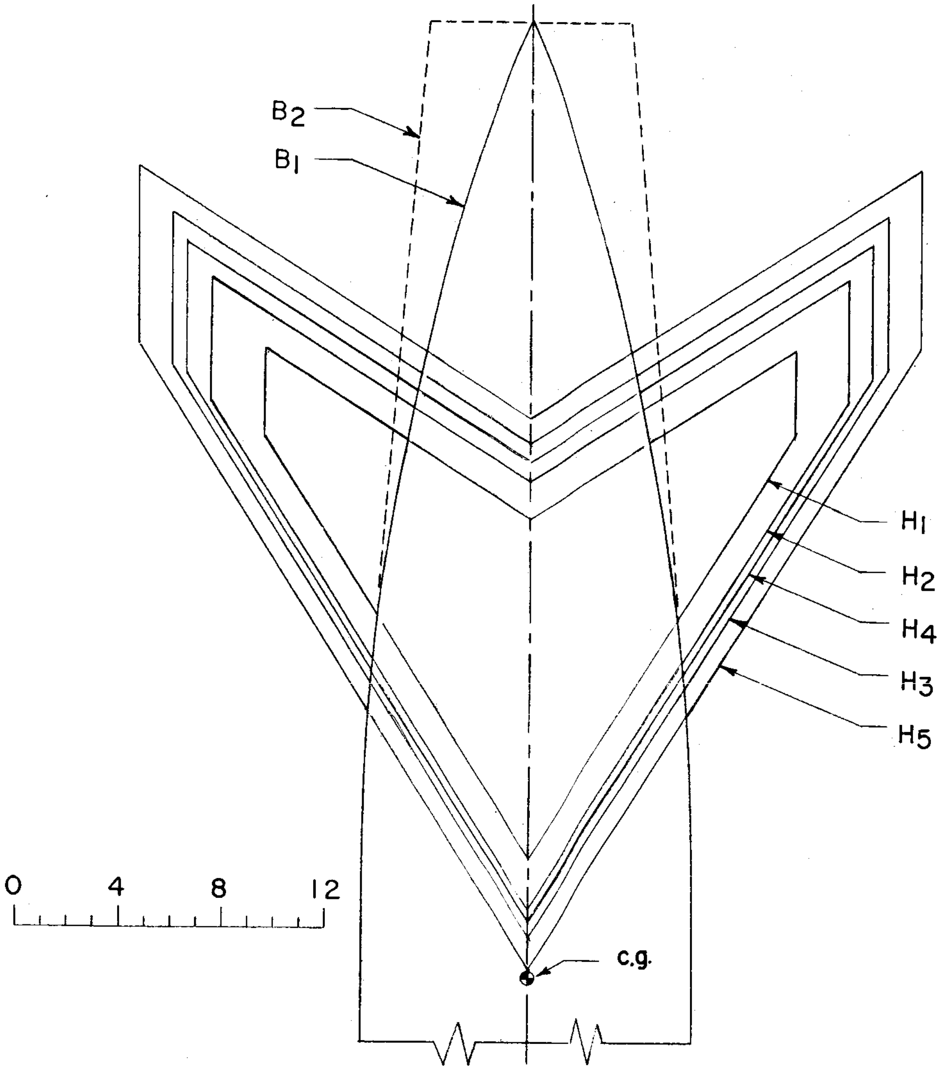

Tail	Root chord, in.	Tip chord, in.	Span, in.	L.E. root chord behind c.g., in.	Area, sq ft
H_1	13.3	3.5	20.8	4.7	1.22
H_2	16.7	4.8	25.0	2.8	1.86
H_3	19.3	6.0	28.0	1.7	2.46
H_4	17.9	5.2	26.8	2.3	2.15
H_5	21.5	7.0	30.6	.5	3.03

Figure 4.- Sketch of horizontal tails used on model.

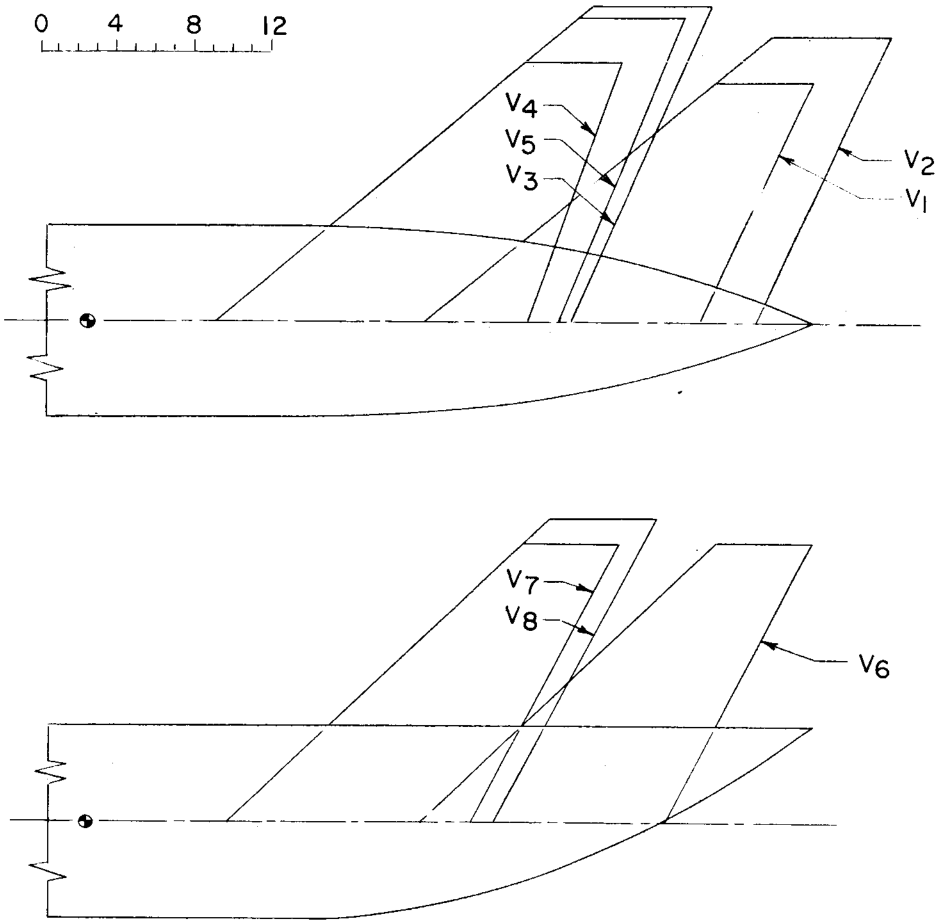

Tail	Root chord at center line, in.	Tip chord, in.	Height center line to tip, in.	L. E. root chord behind c.g., in.	Exposed area, sq ft
V_1	14.1	5.0	12.5	17.4	0.53
V_2	17.0	6.0	14.8	17.4	.86
V_3	18.3	6.0	16.4	6.6	.86
V_4	16.0	5.0	13.5	6.6	.53
V_5	17.6	5.4	15.8	6.6	.77
V_6	12.7	5.0	14.5	17.3	.50
V_7	12.7	5.0	14.5	7.3	.50
V_8	13.8	5.5	15.8	7.3	.63

Figure 5.- Sketch of vertical tails used on model.

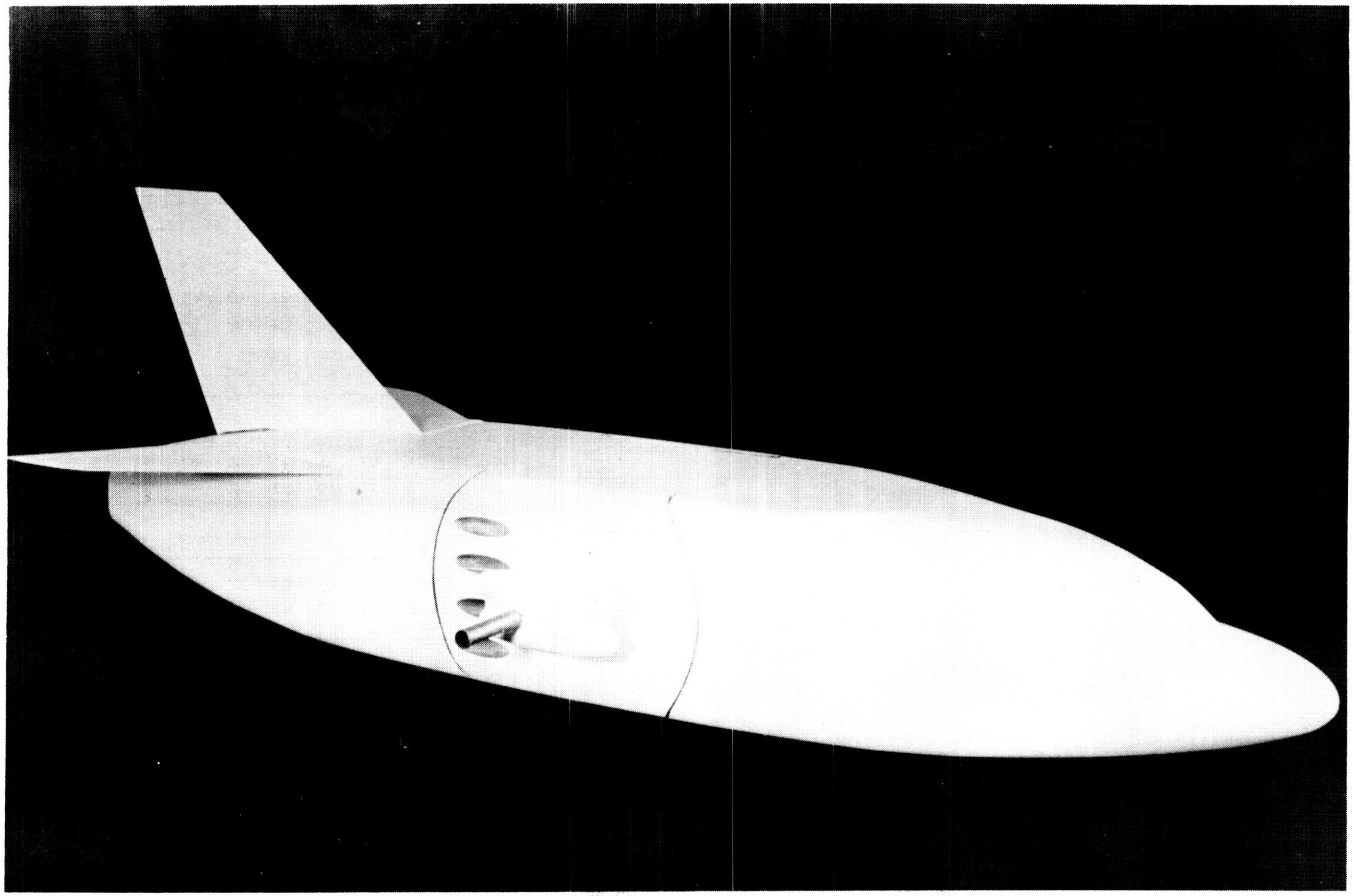

(a) Model with body B_1 and with jets at 0° incidence. L-59-656

Figure 6.- Photographs of models.

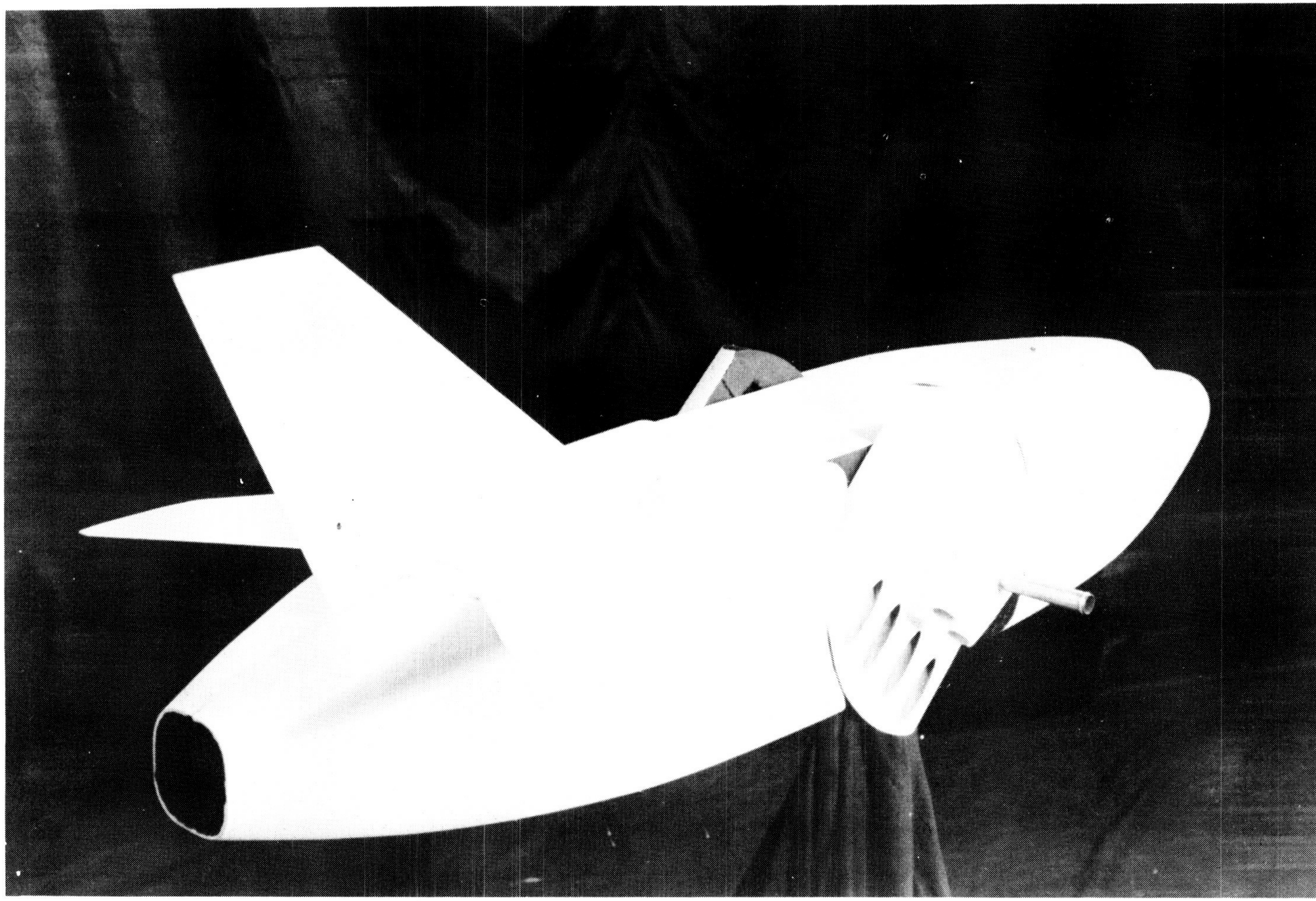

(b) Model with body B_1 and with jets at 30° incidence. L-59-657

Figure 6.- Concluded.

L-575

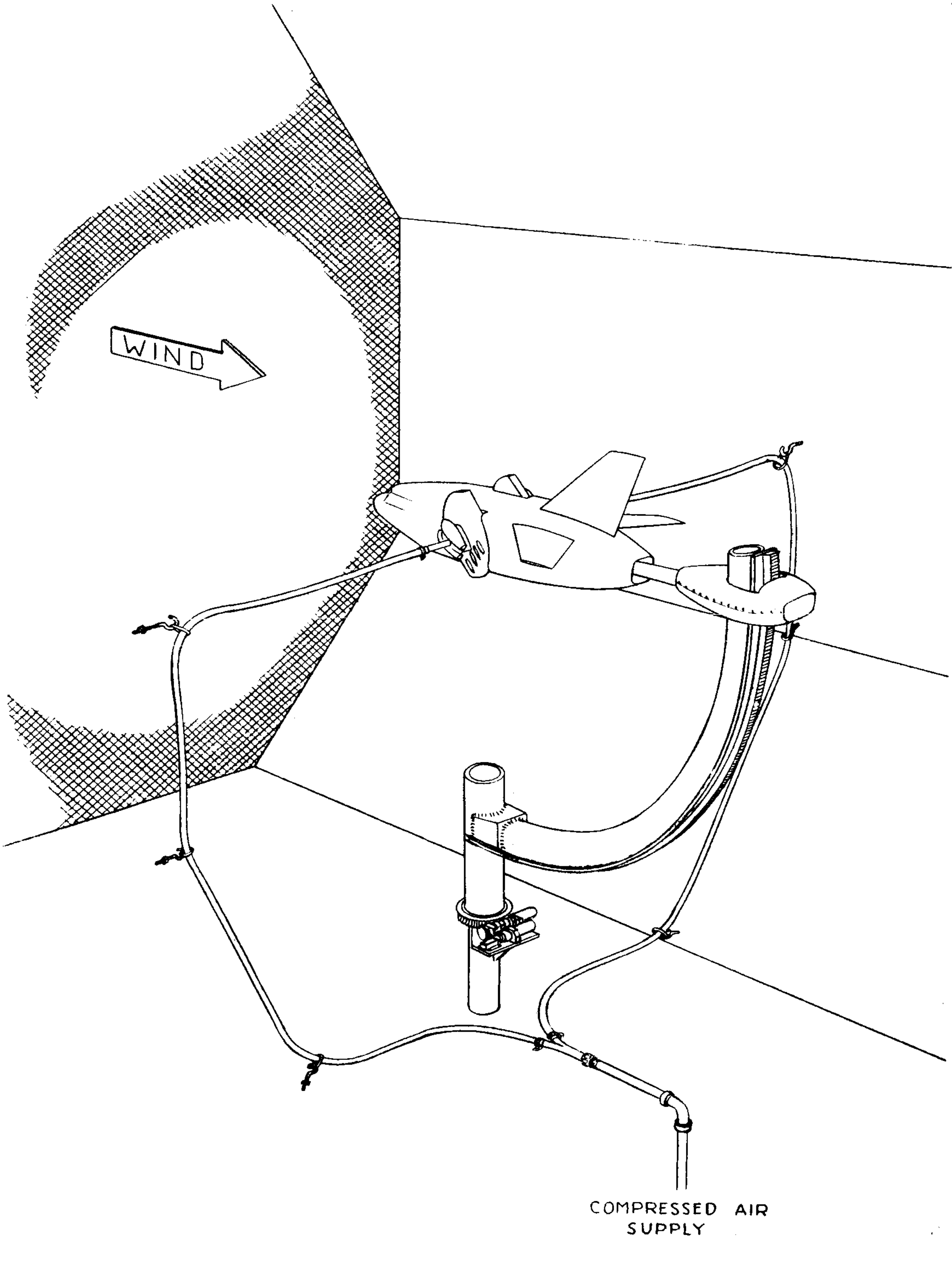

Figure 7.- Setup used in power-on tests.

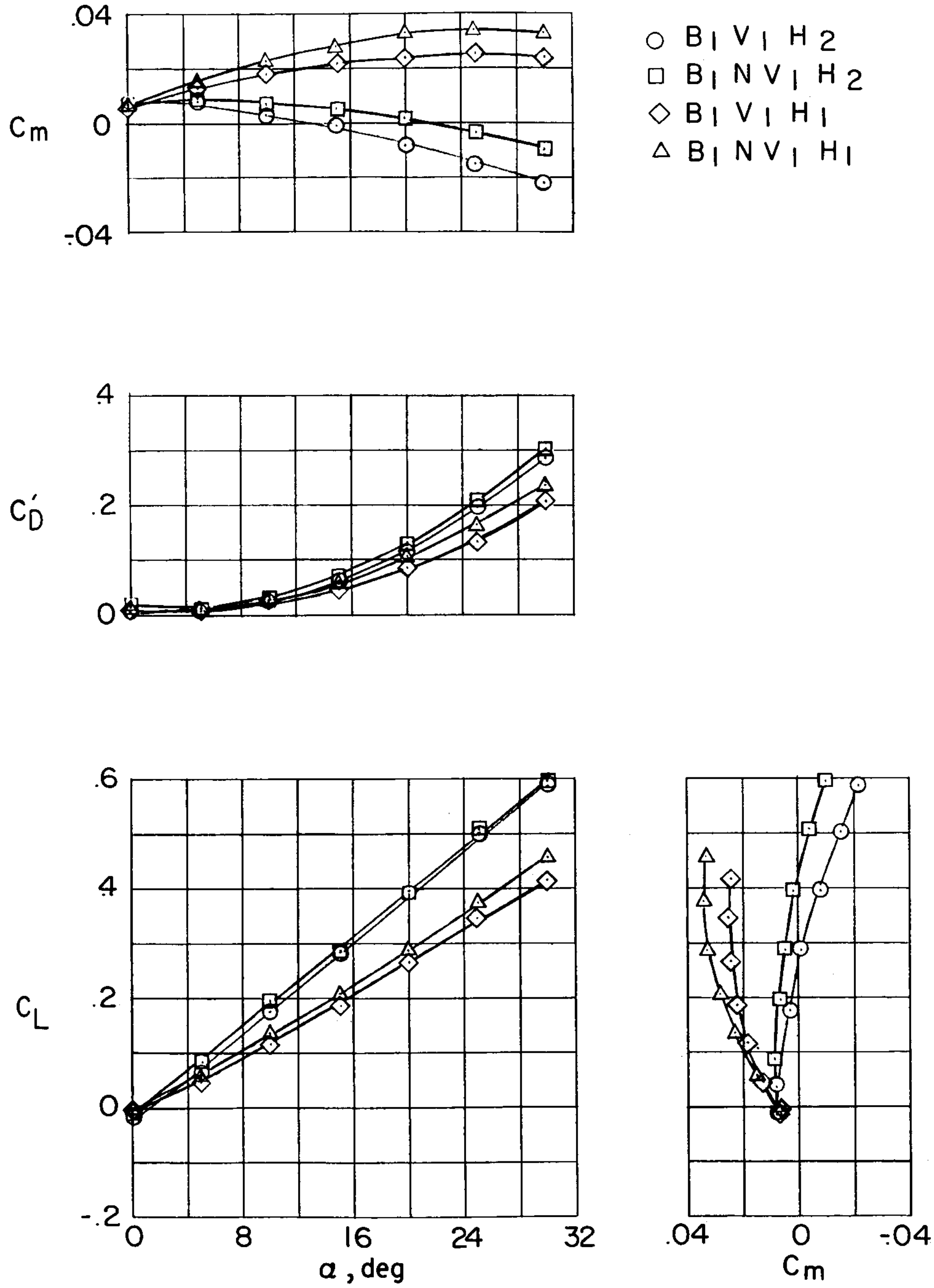

L-575

(a) Effect of components including H_1 and H_2.

Figure 8.- Power-off longitudinal characteristics of model with body B_1. $i_j = 0^{\circ}$.

L-575

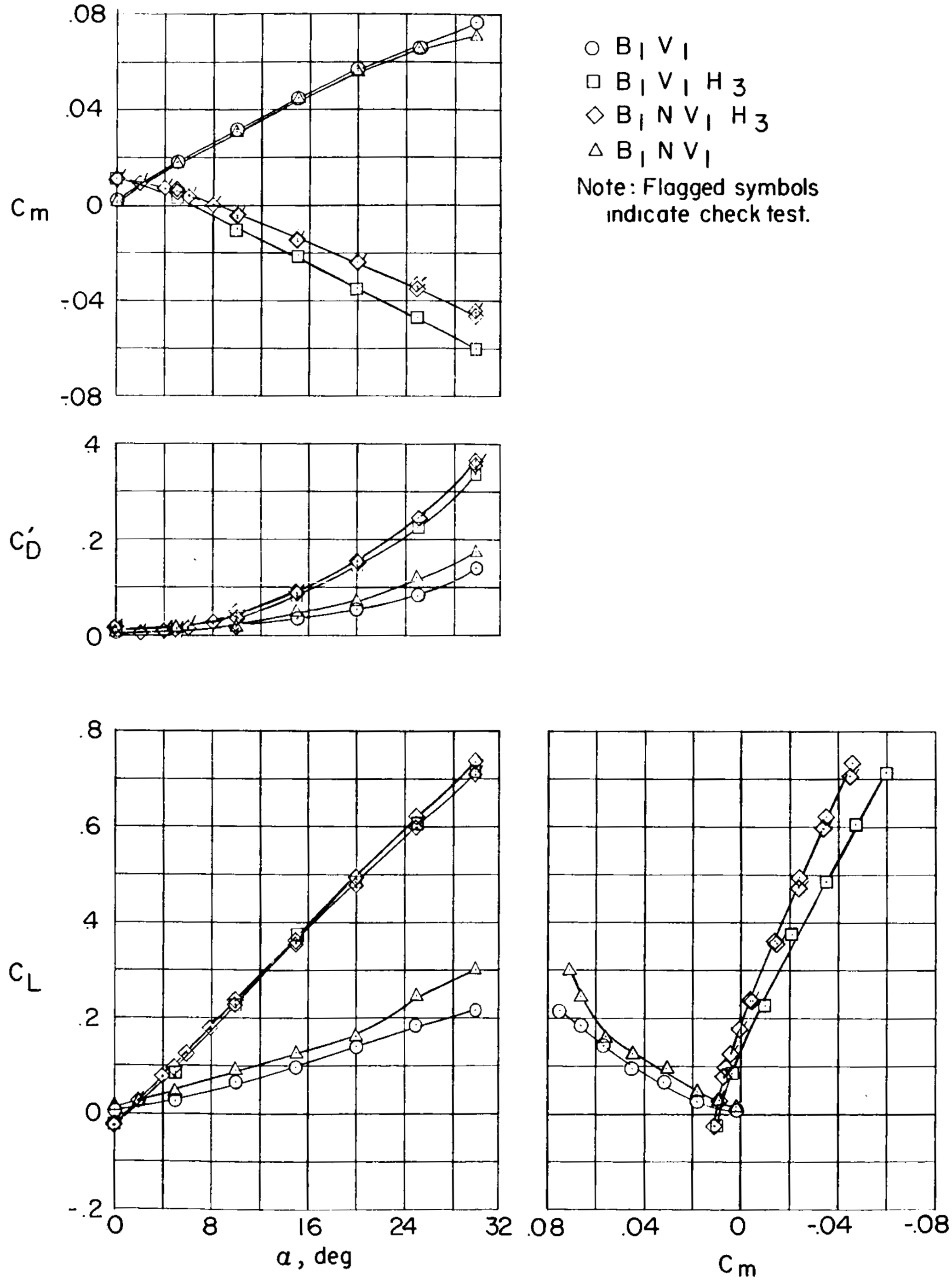

(b) Effect of components including H_3.

Figure 8.- Continued.

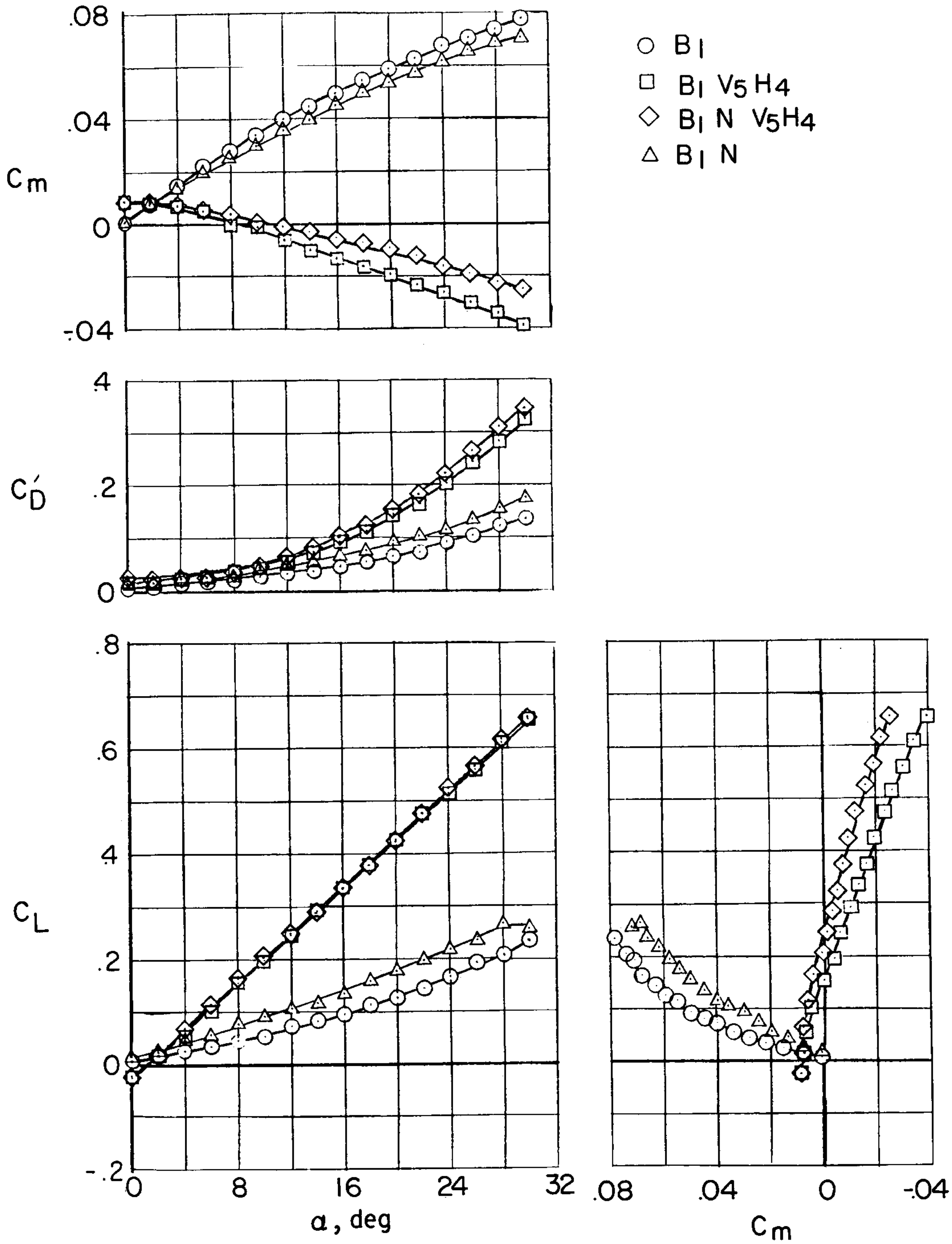

(c) Effect of components including H_4.

Figure 8.- Concluded.

L-575

L-575

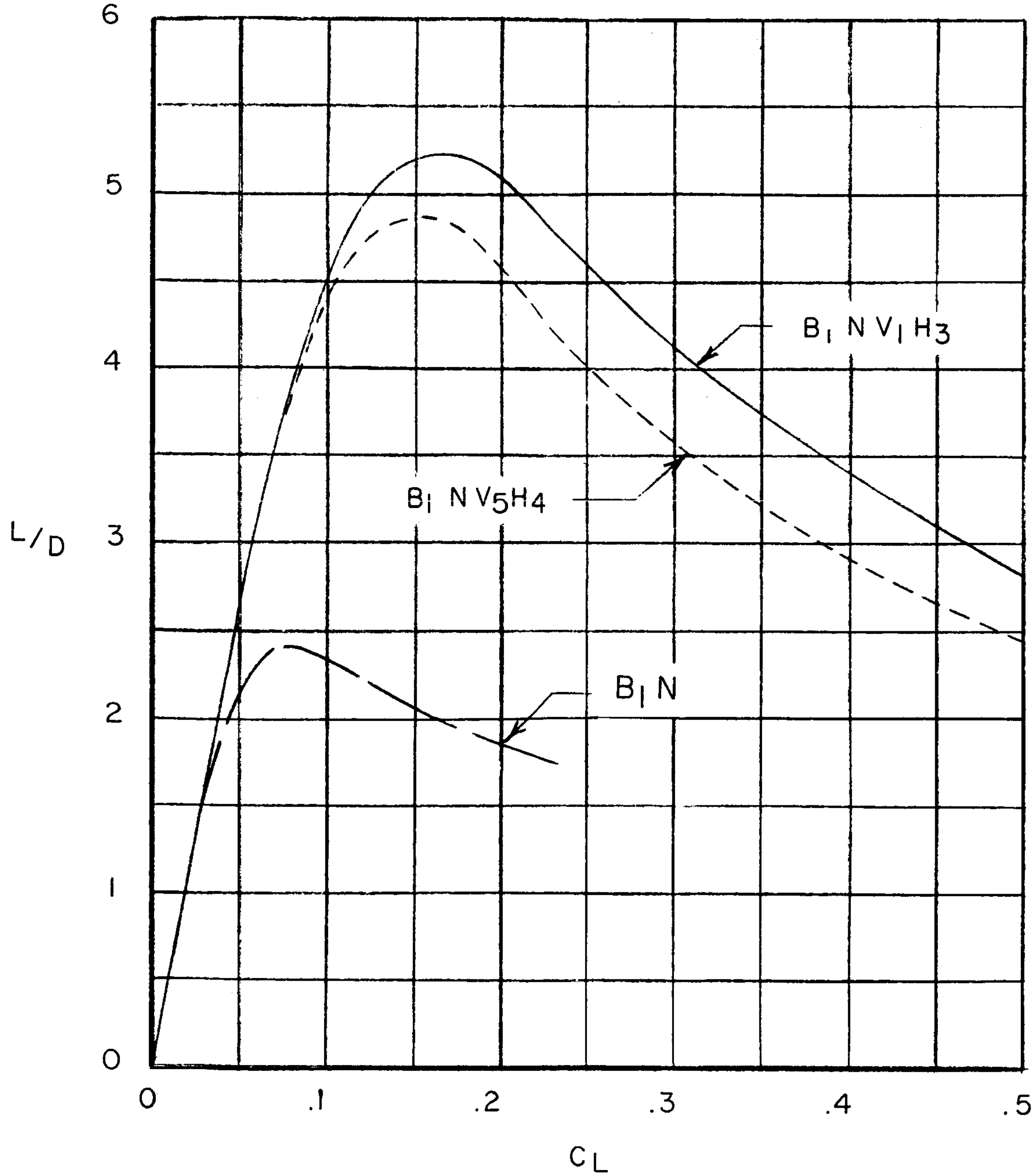

Figure 9.- Lift-drag ratio of model with body B_1 and tails which provided longitudinal stability. Power off; $i_j = 0^{\circ}$.

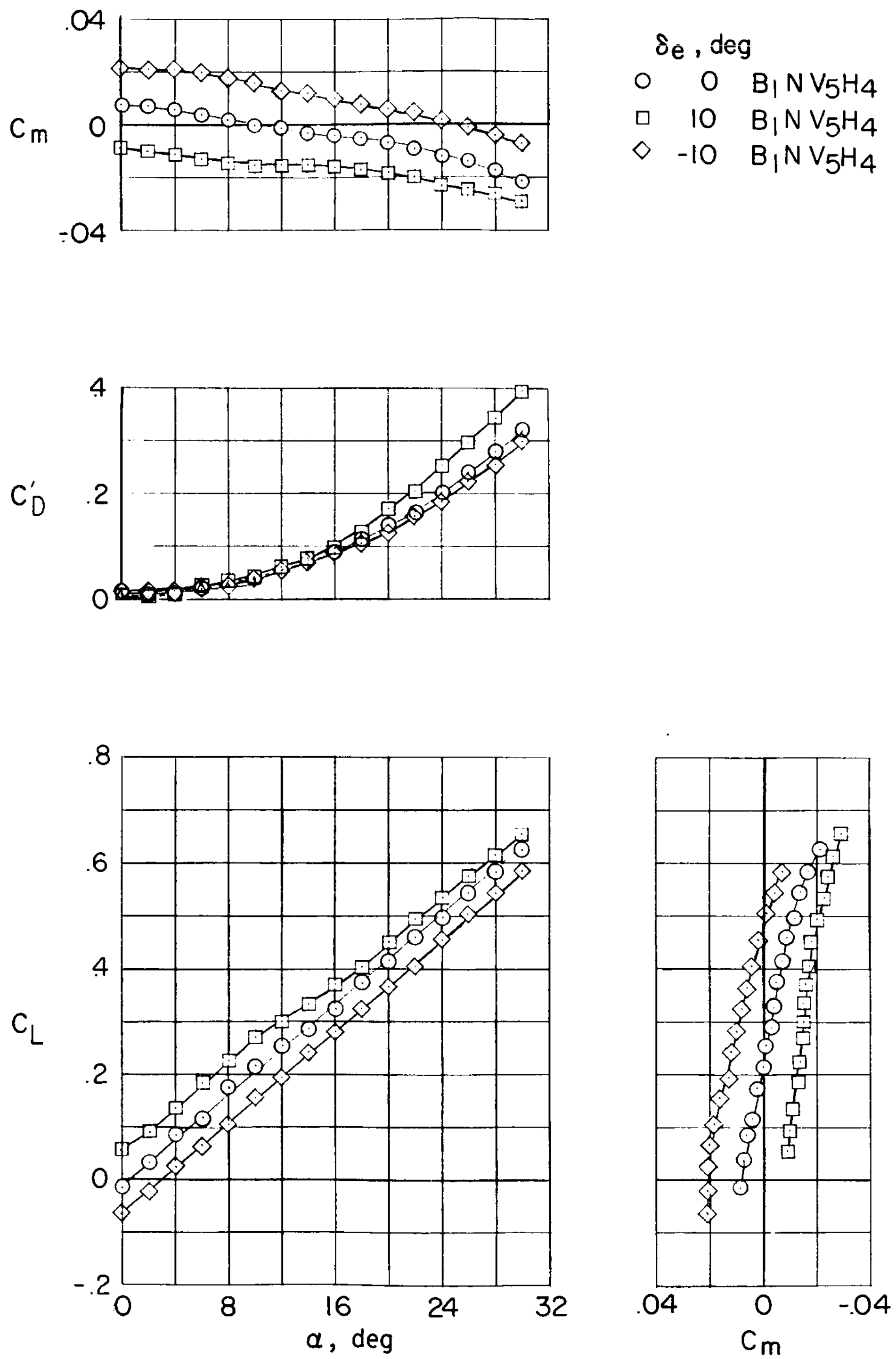

Figure 10.- Elevator effectiveness of model in configuration $B_1NV_5H_4$. Power off; $i_j = 0^o$.

L-575

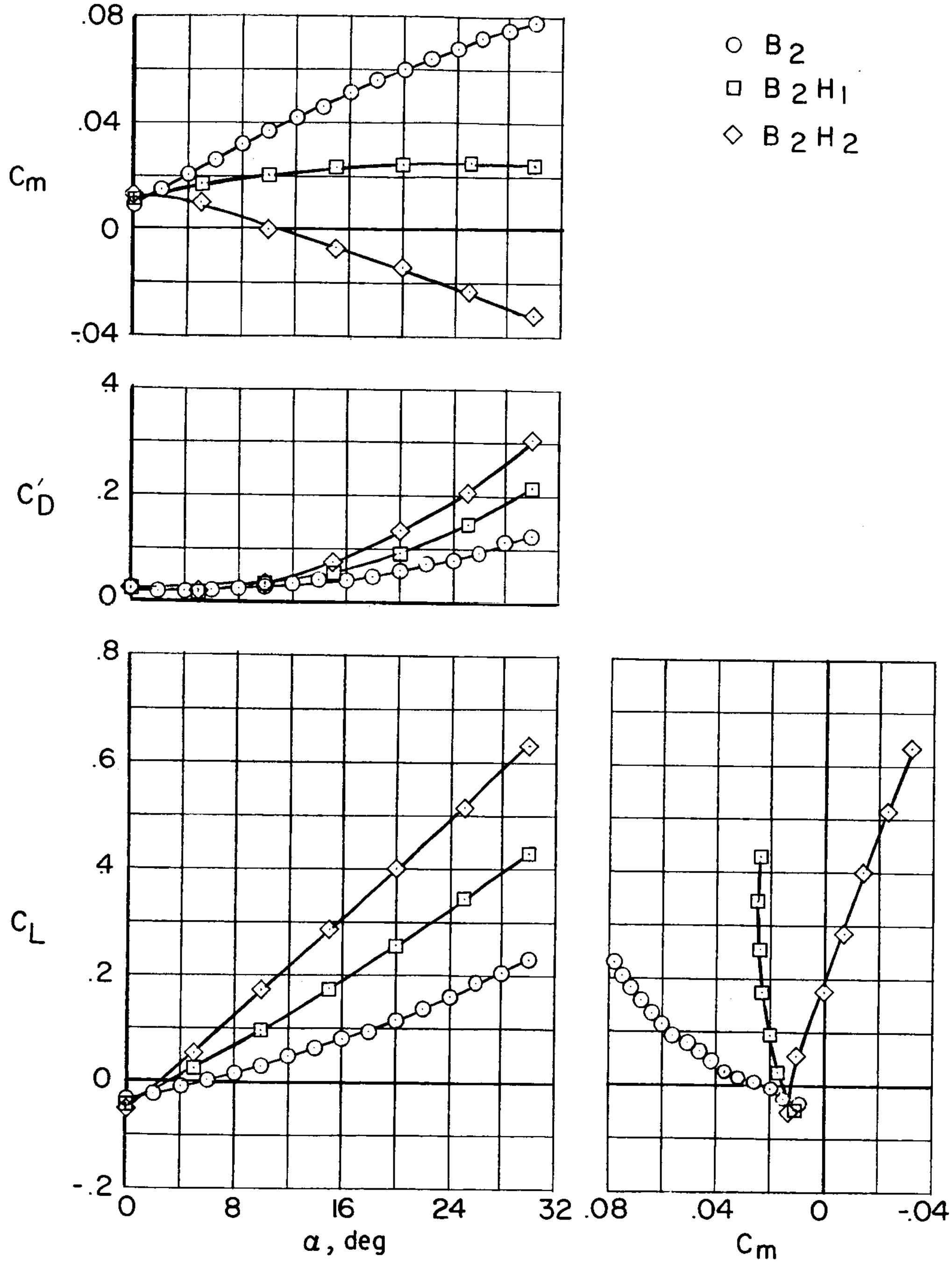

(a) Effect of components; nacelles off.

Figure 11.- Power-off longitudinal characteristics of model with body B_2. $i_j = 0^{\circ}$.

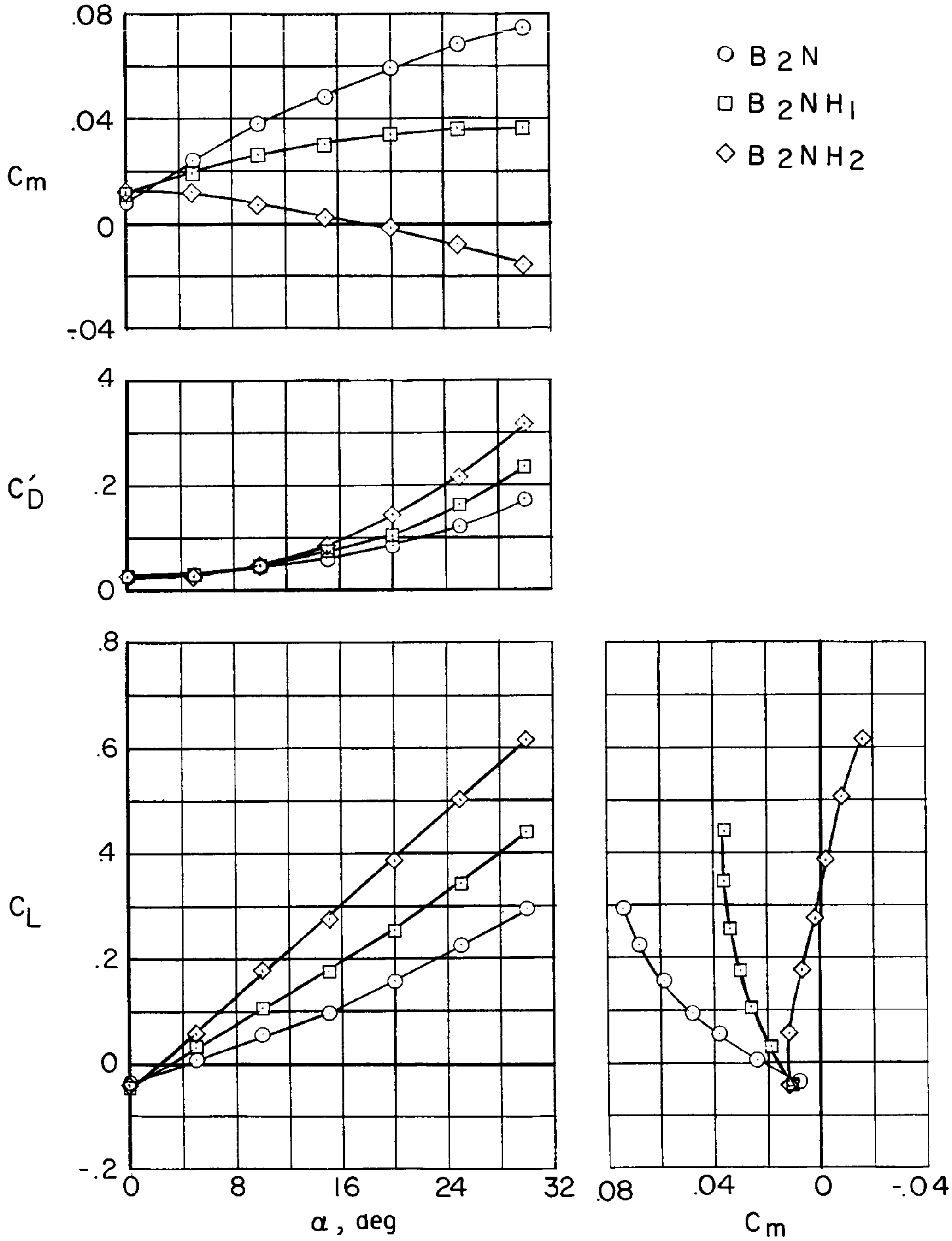

(b) Effect of components; nacelles on.

Figure 11.- Concluded.

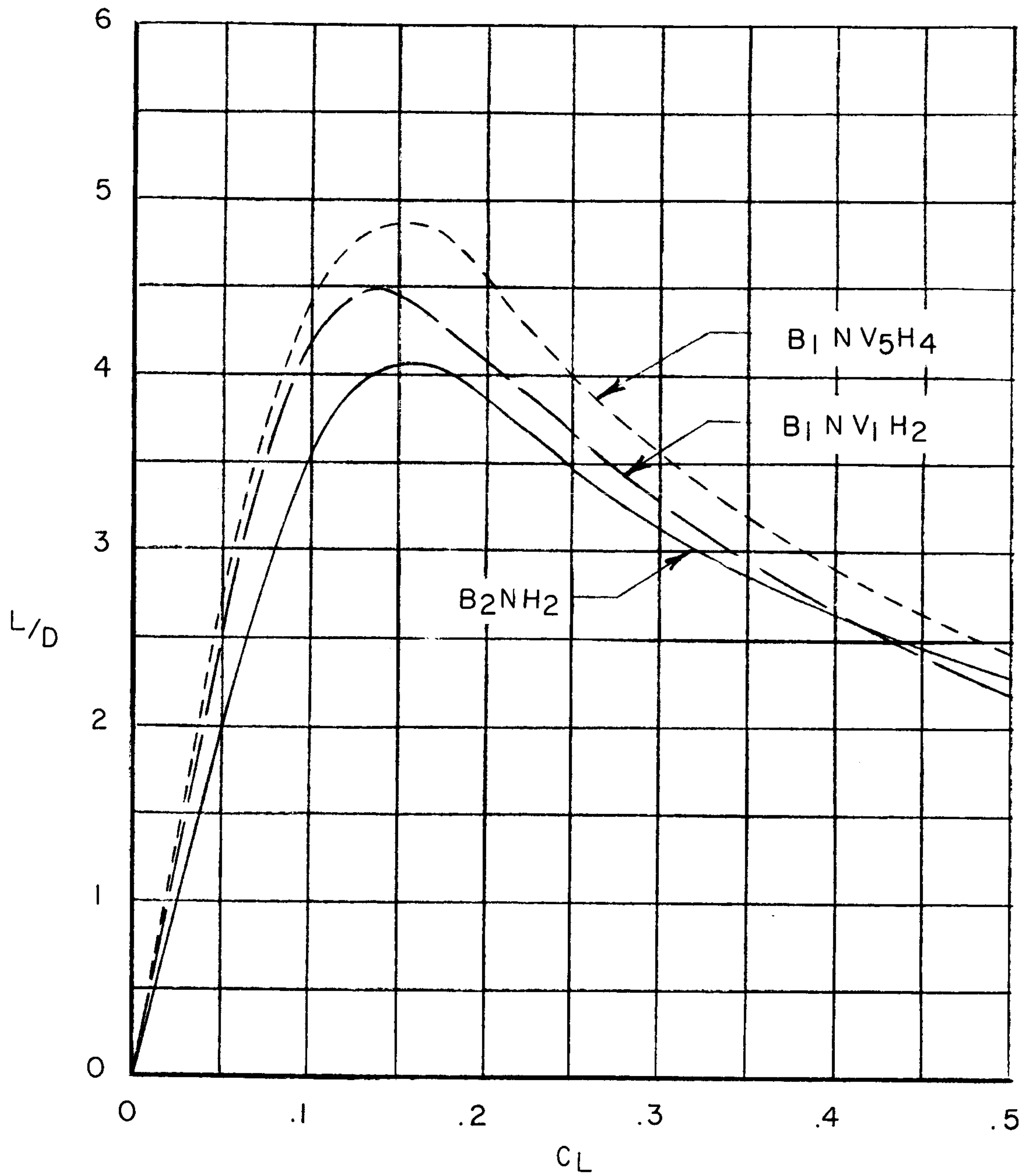

Figure 12.- Comparison of lift-drag ratios of models with bodies B_1 and B_2. Power off; $i_j = 0^o$.

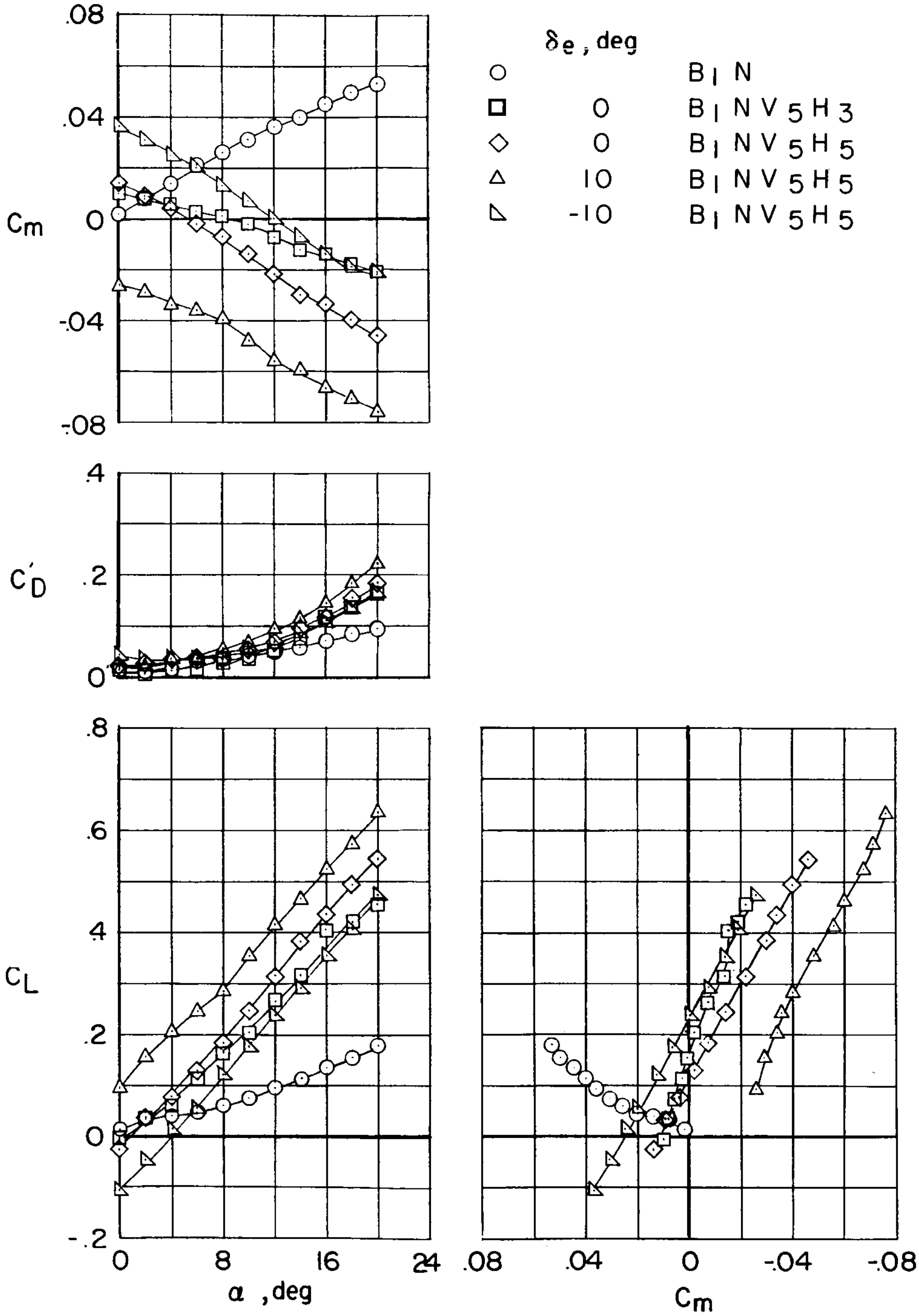

(a) $T_c' = 0$.

Figure 13.- Power-on longitudinal characteristics of model with $i_j = 0^{\circ}$.

L-575

L-575

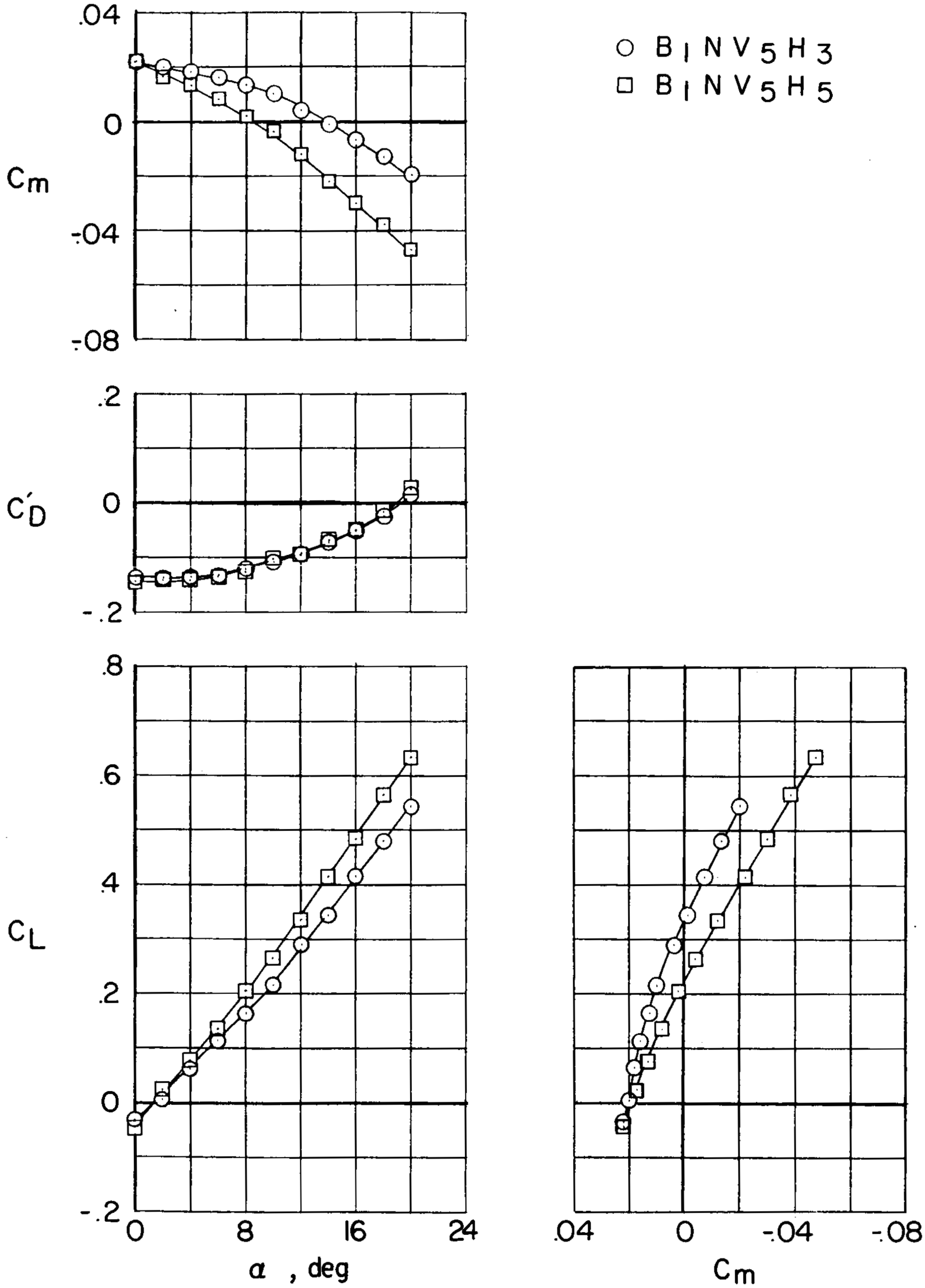

(b) $T_c' = 0.17$.

Figure 13.- Continued.

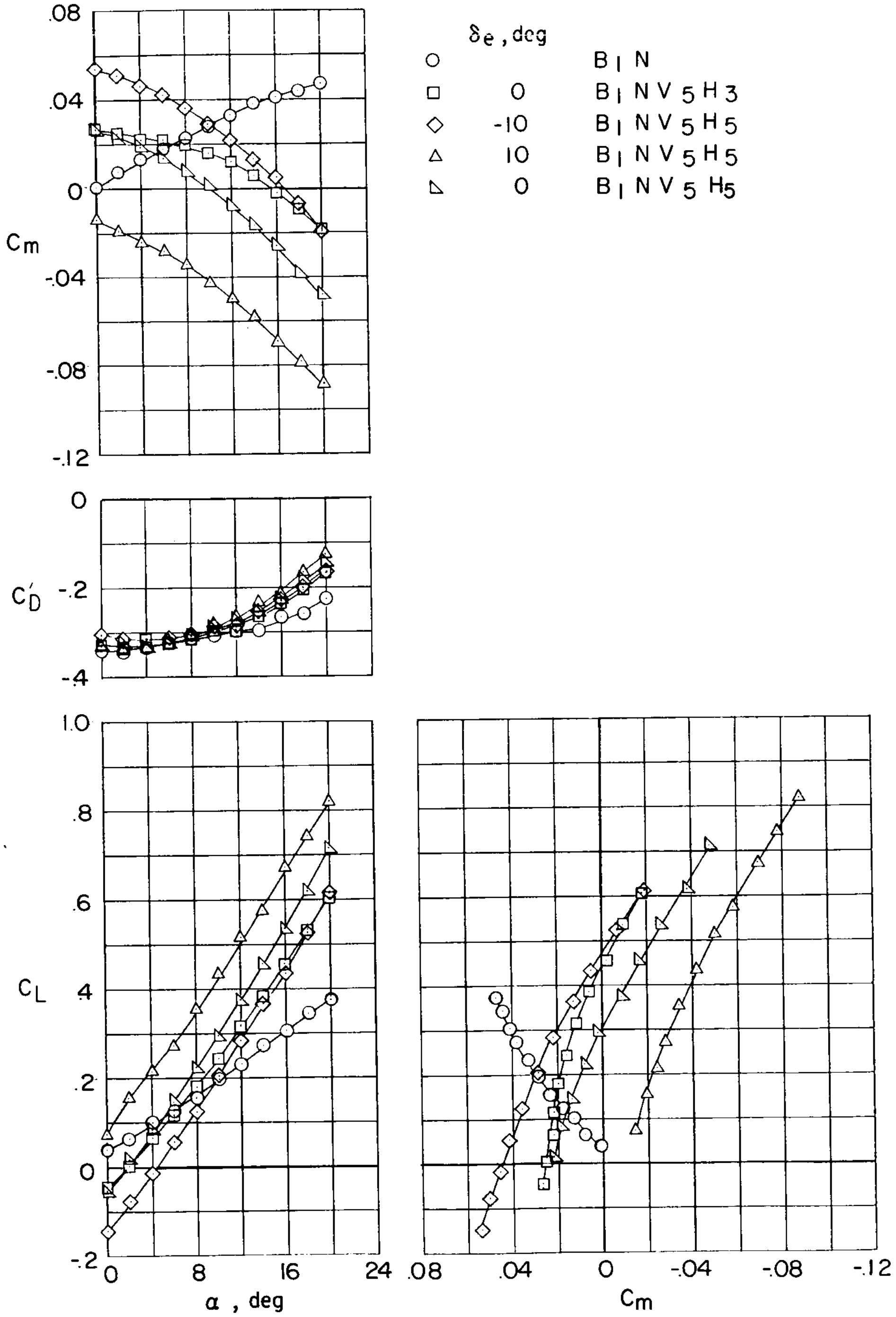

(c) $T_c' = 0.35$.

Figure 13.- Concluded.

L-575

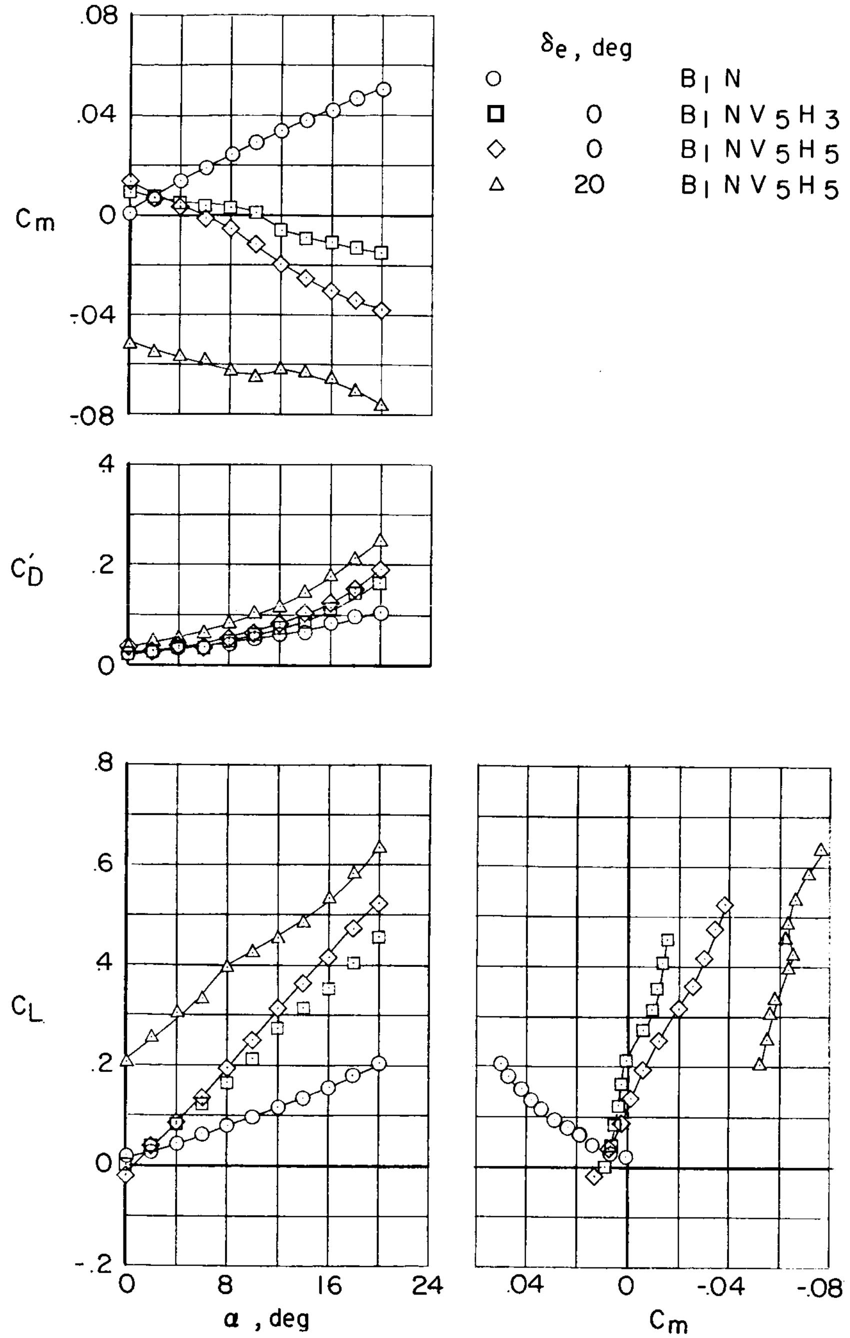

(a) $T_c' = 0$.

Figure 14.- Power-on longitudinal characteristics of model with $i_j = 10^{\circ}$.

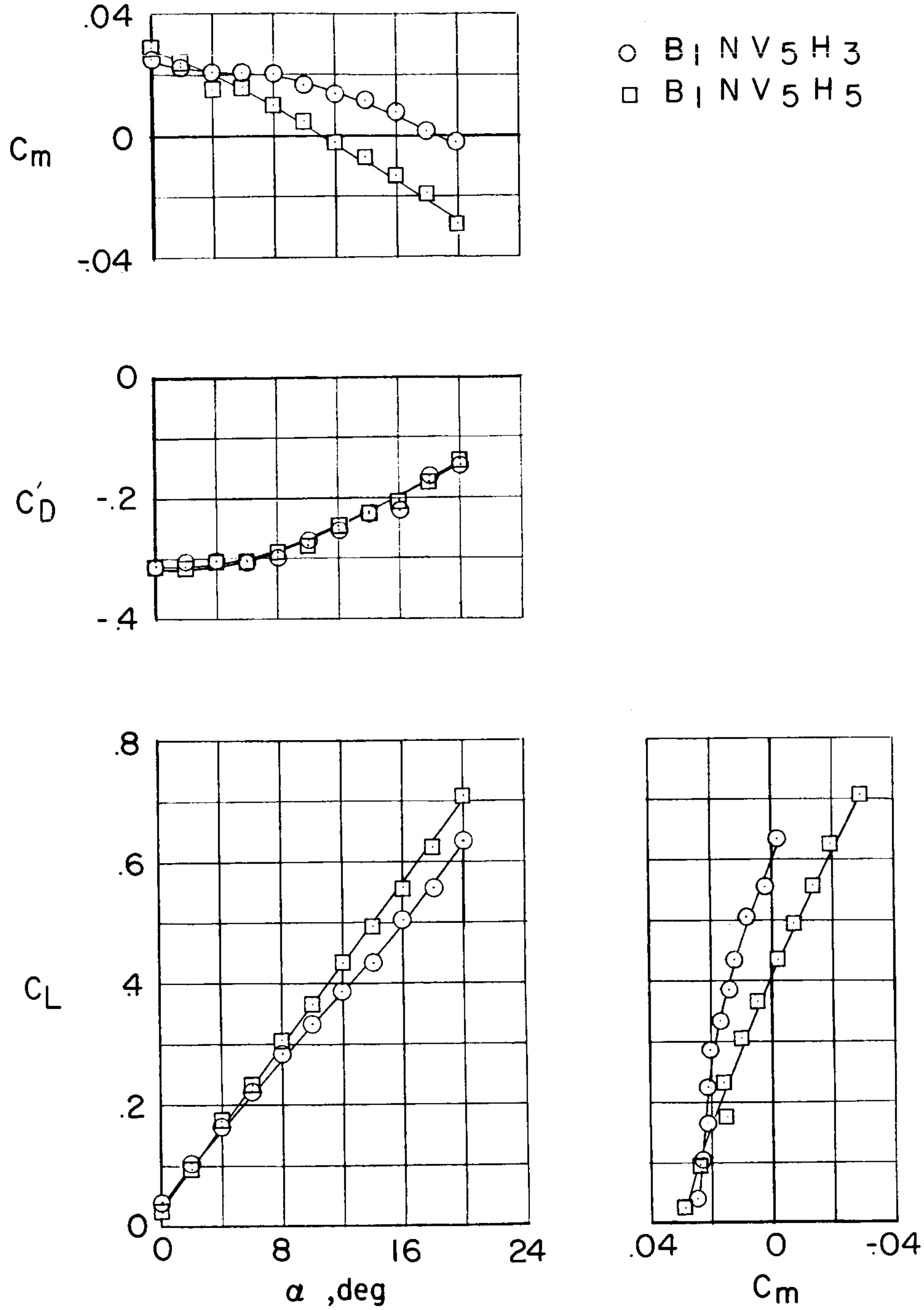

(b) $T_c' = 0.35$.

Figure 14.- Continued.

L-575

L-575

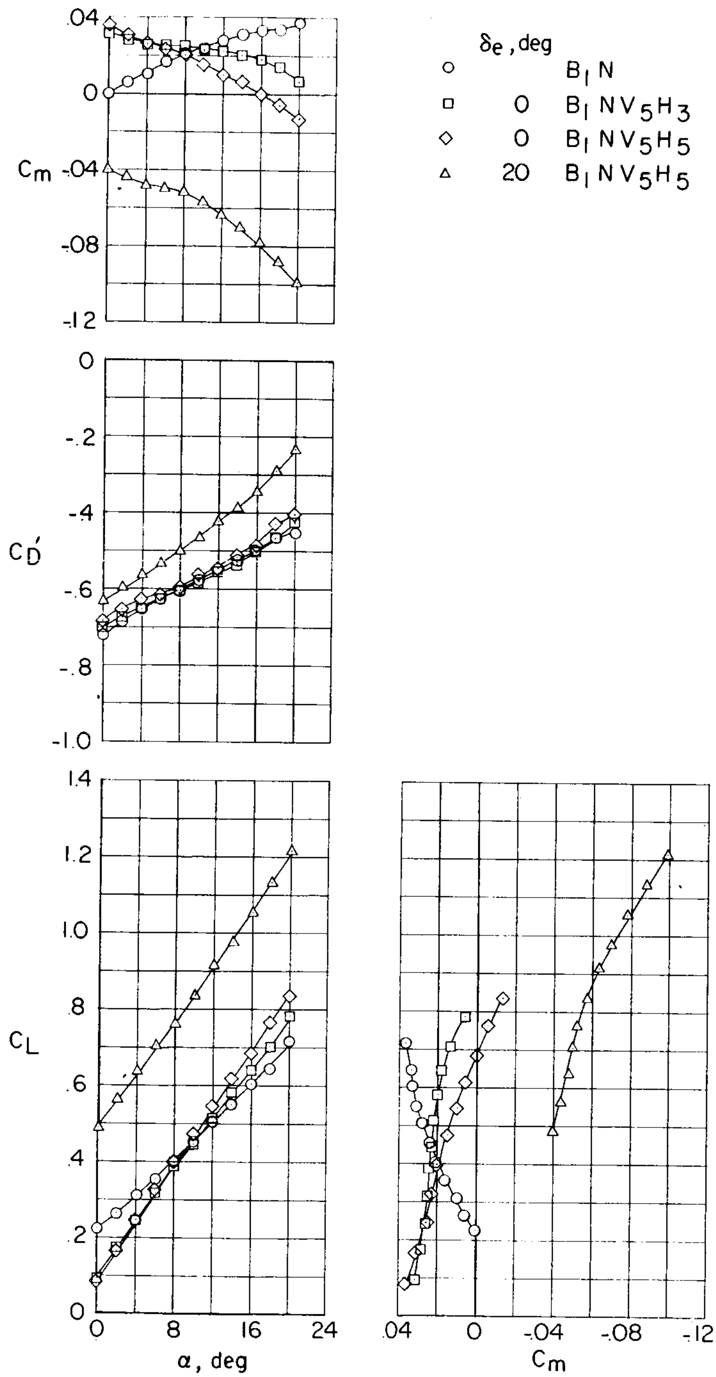

(c) $T_c' = 0.7$.

Figure 14.- Concluded.

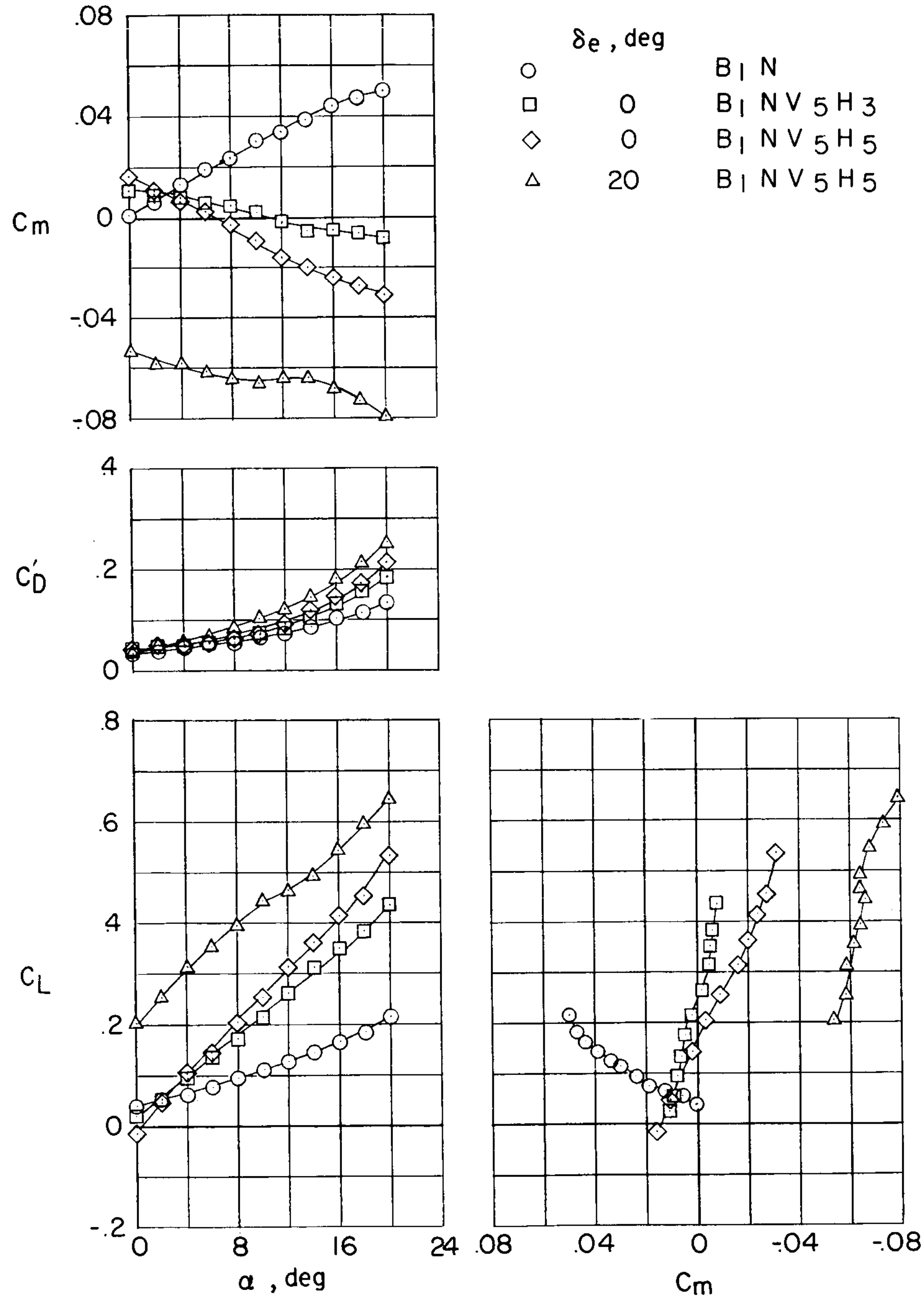

(a) $T_c' = 0$.

Figure 15.- Power-on longitudinal characteristics of model with $i_j = 20^{\circ}$.

L-575

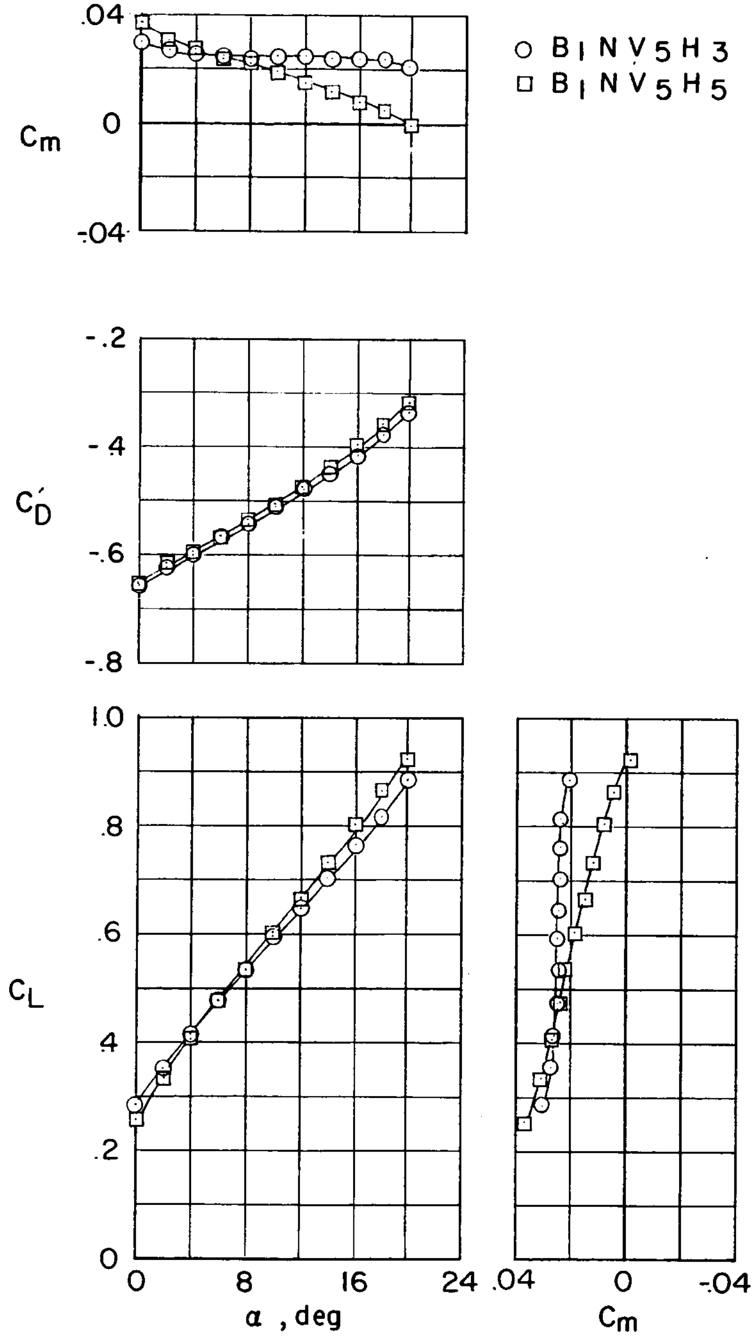

(b) $T_c' = 0.7$.

Figure 15.- Continued.

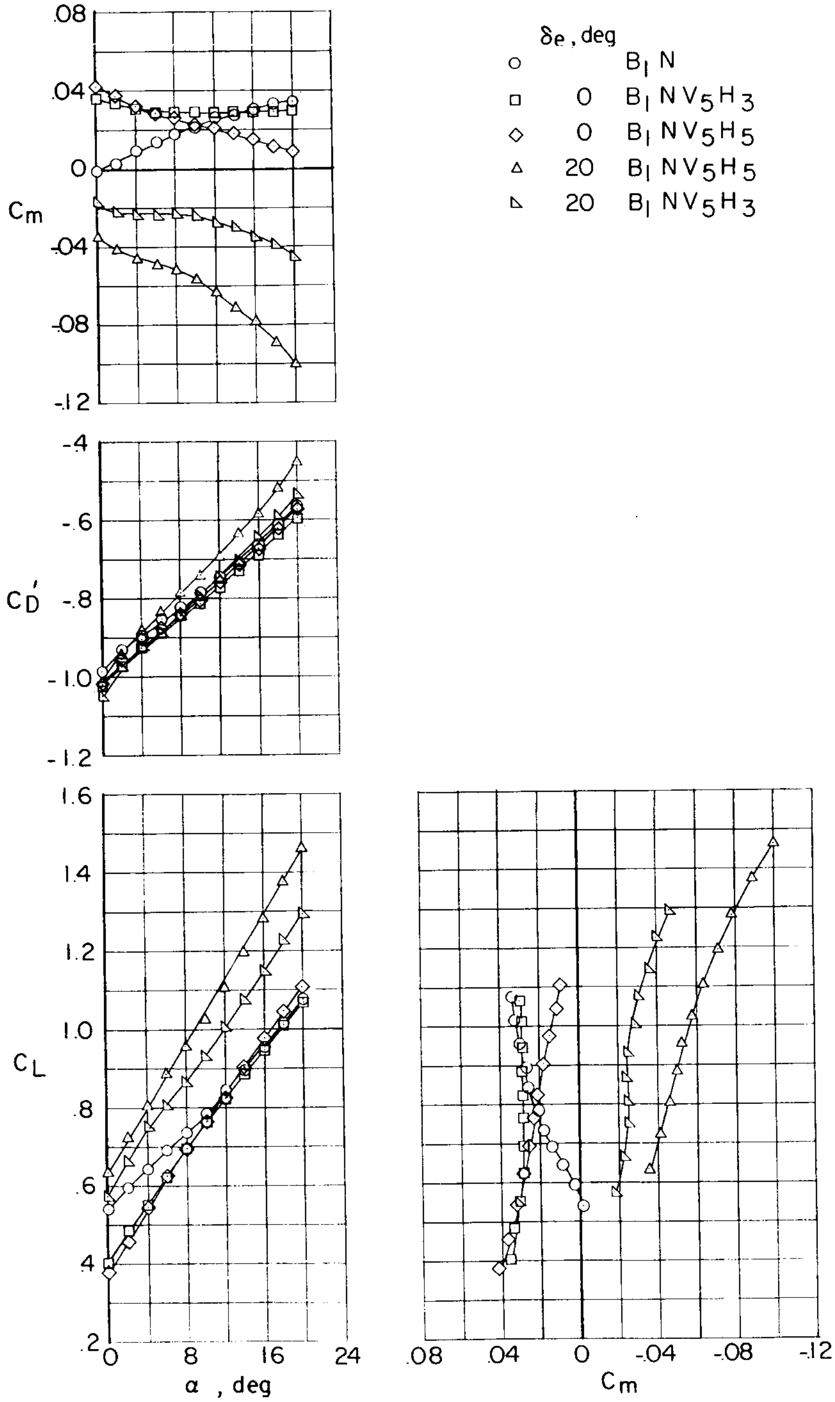

(c) $T_c' = 1.1$.

Figure 15.- Concluded.

L-575

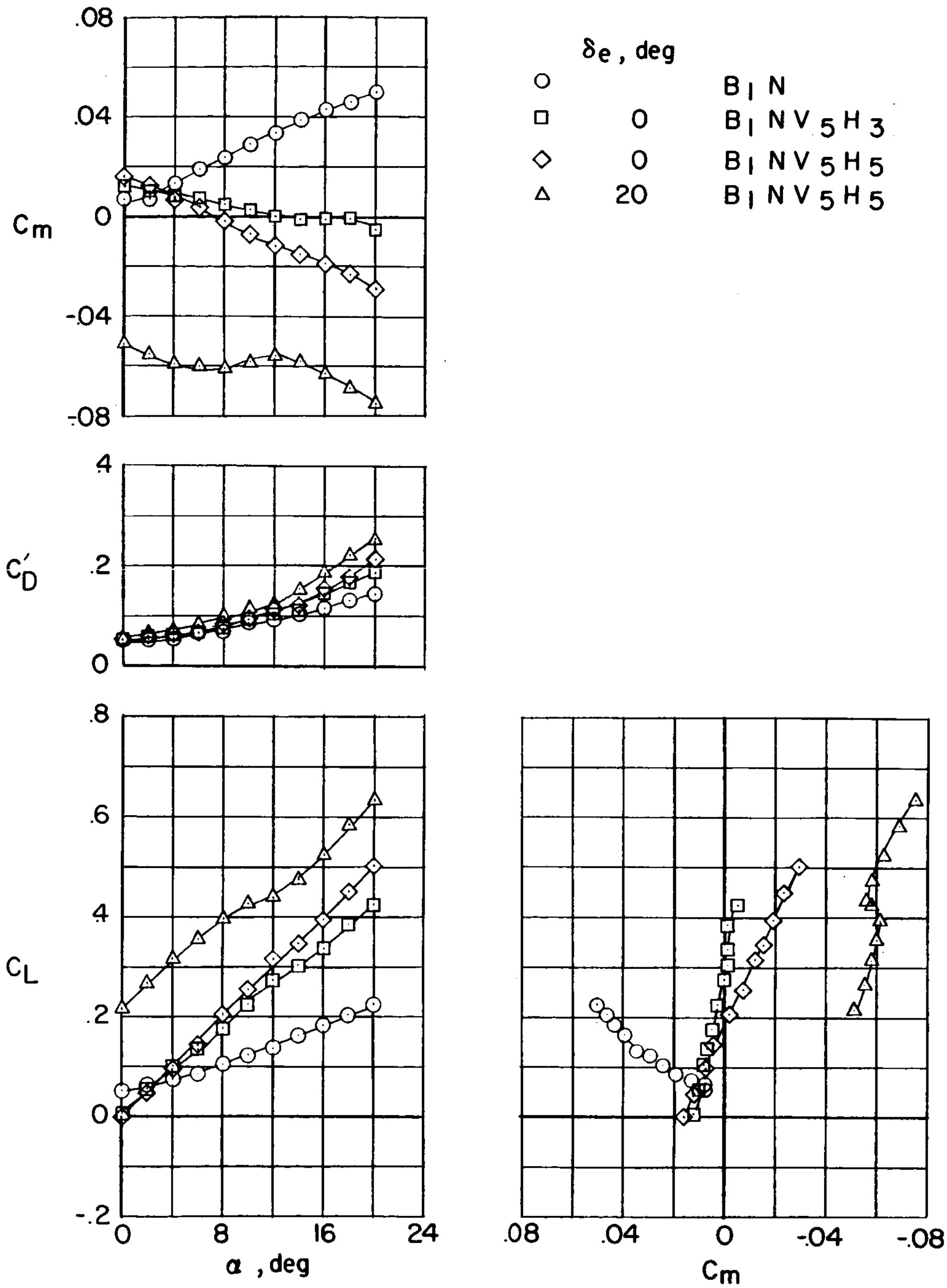

(a) $T_c' = 0$.

Figure 16.- Power-on longitudinal characteristics of model with $i_j = 30^\circ$.

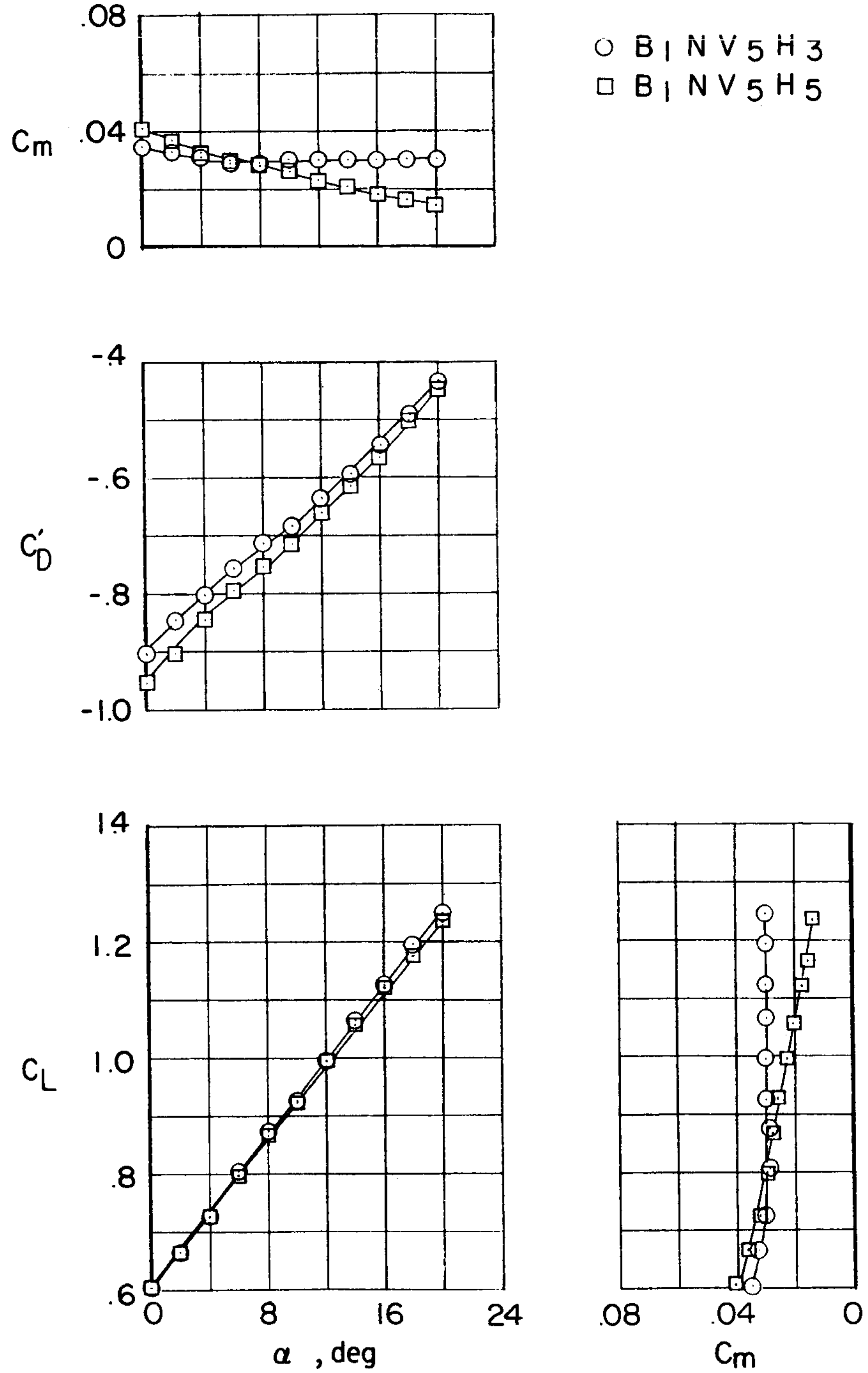

(b) $T_c' = 1.1$.

Figure 16.- Continued.

L-575

L-575

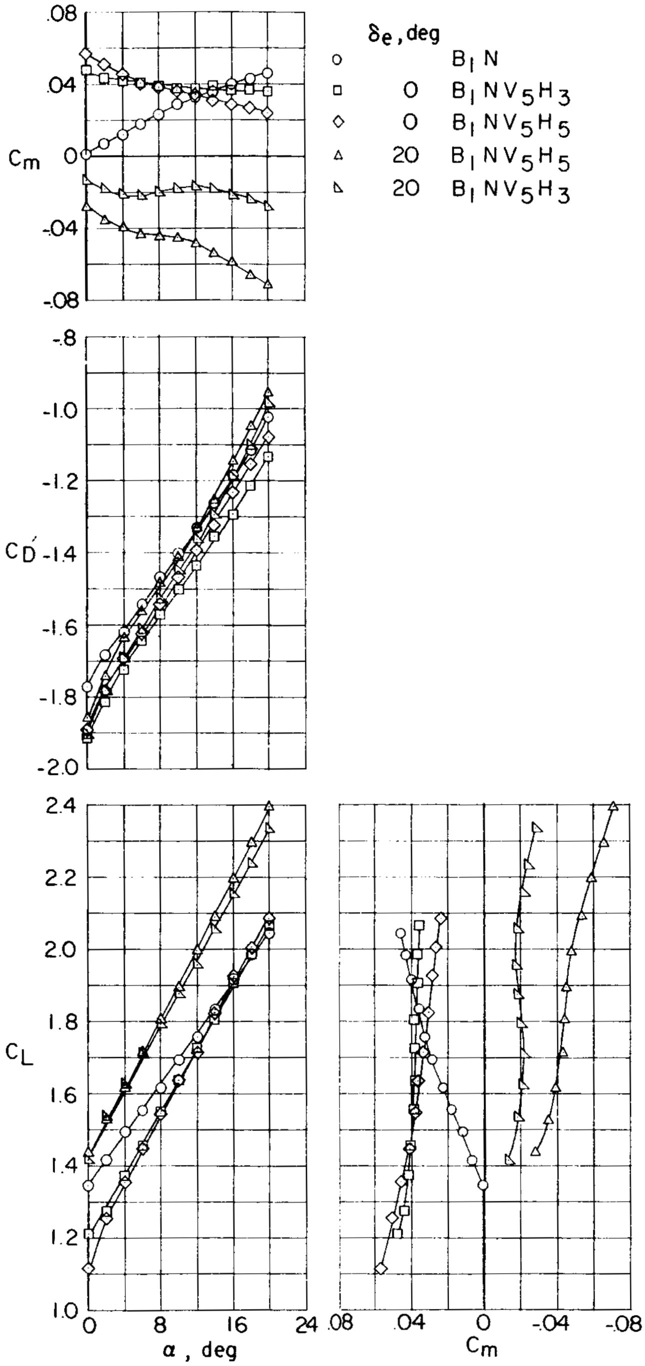

(c) $T_c' = 2.3$.

Figure 16.- Concluded.

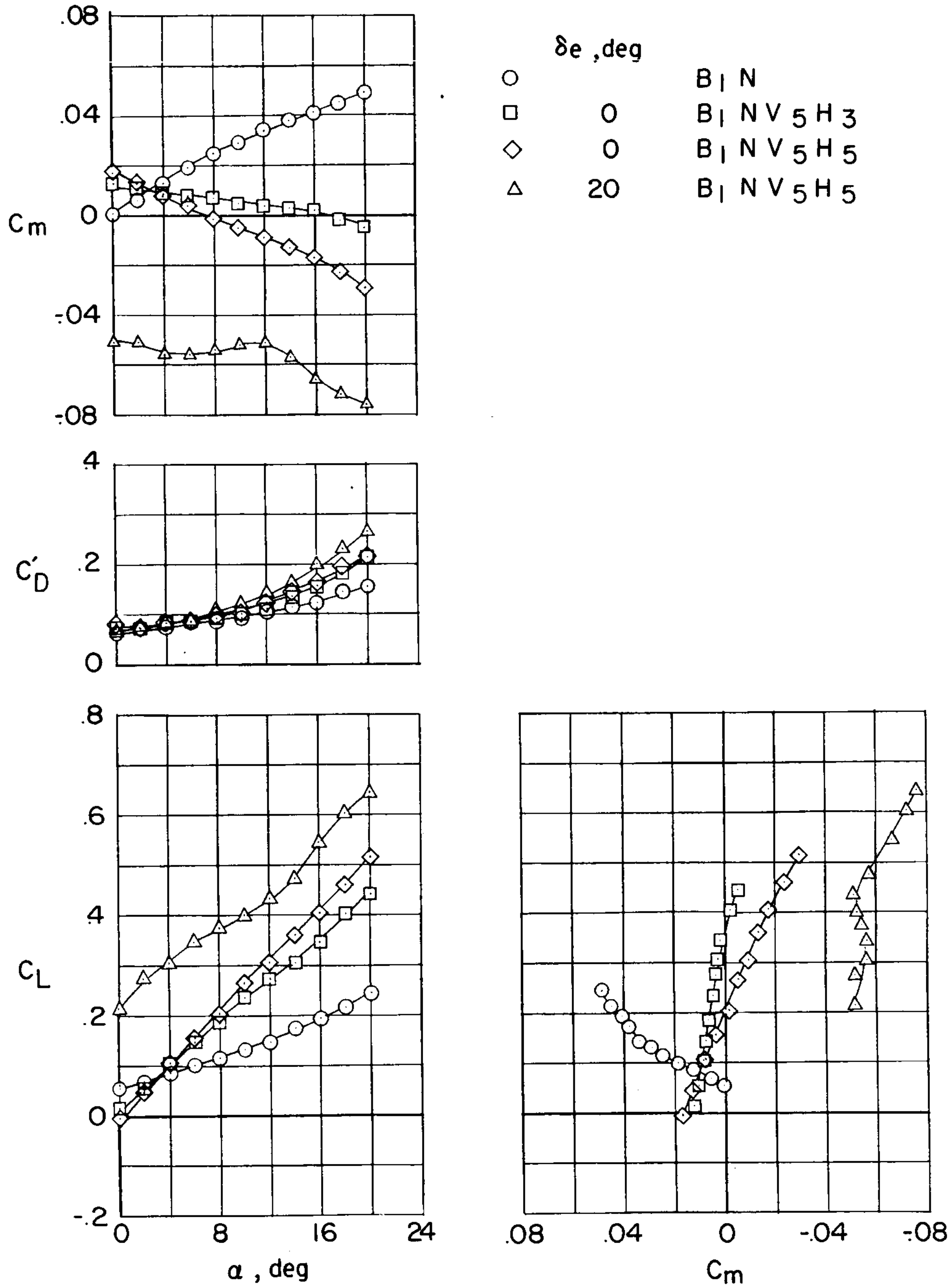

(a) $T_c' = 0$.

Figure 17.- Power-on longitudinal characteristics of model with $i_j = 40^\circ$.

L-575

L-575

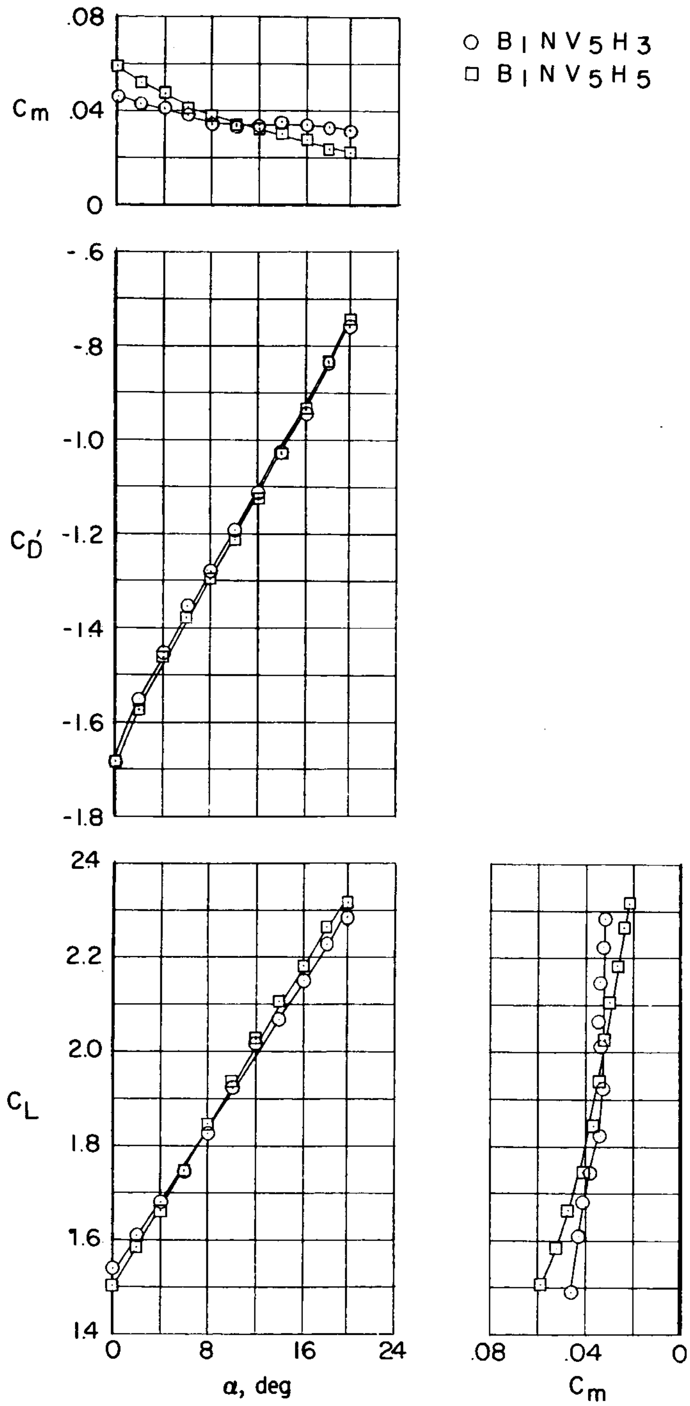

(b) $T_c' = 2.3$.

Figure 17.- Continued.

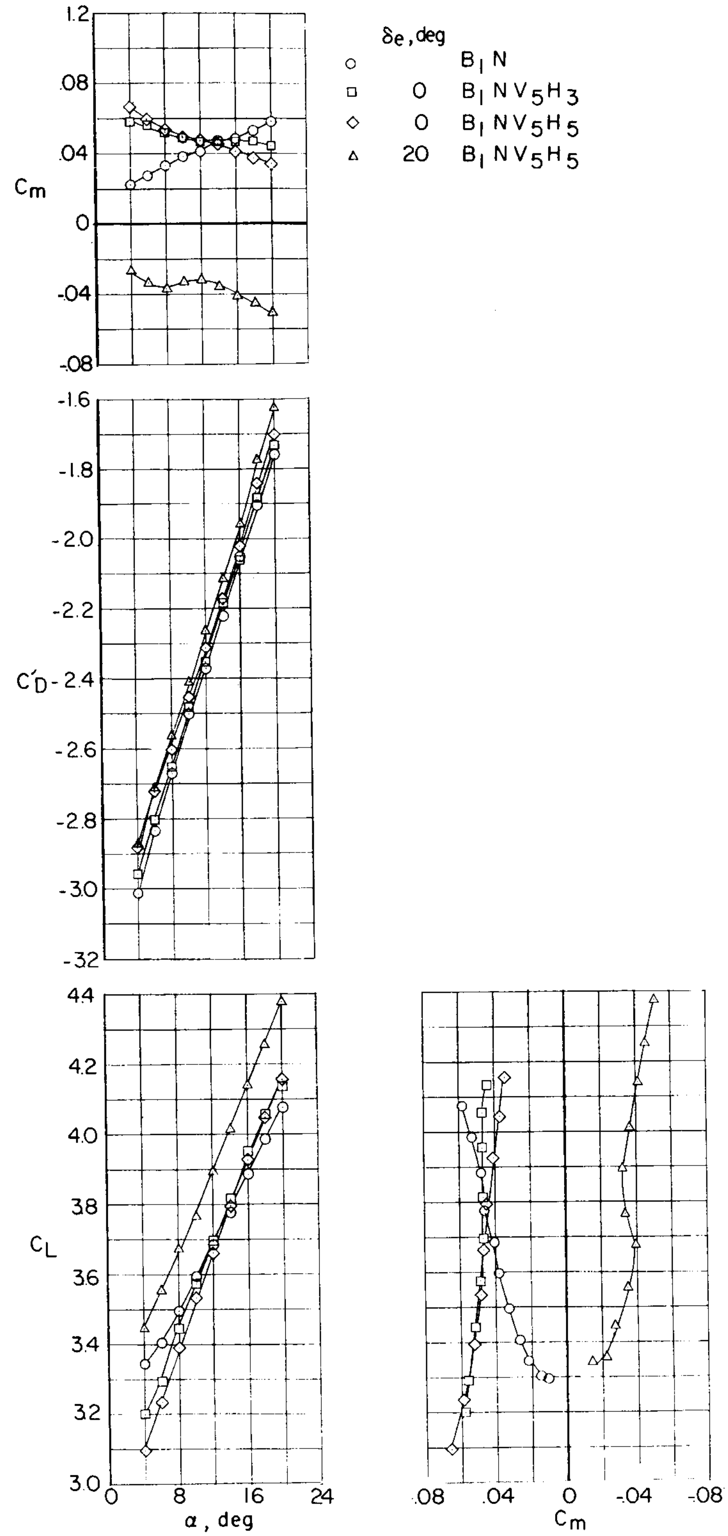

(c) $T'_c = 4.7$.

Figure 17.- Concluded.

L-575

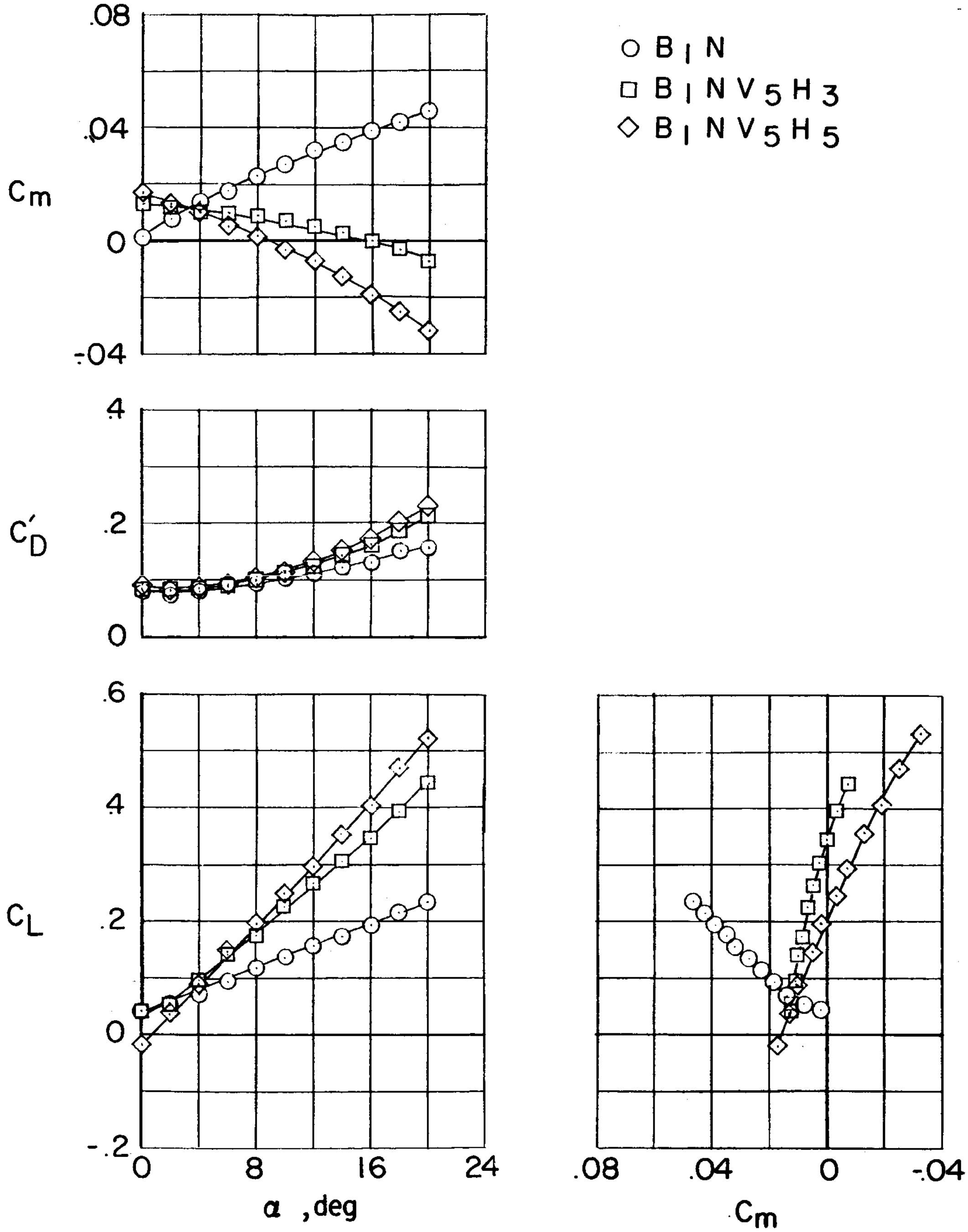

(a) $T_c' = 0$.

Figure 18.- Power-on longitudinal characteristics of model with $i_j = 60^{\circ}$.

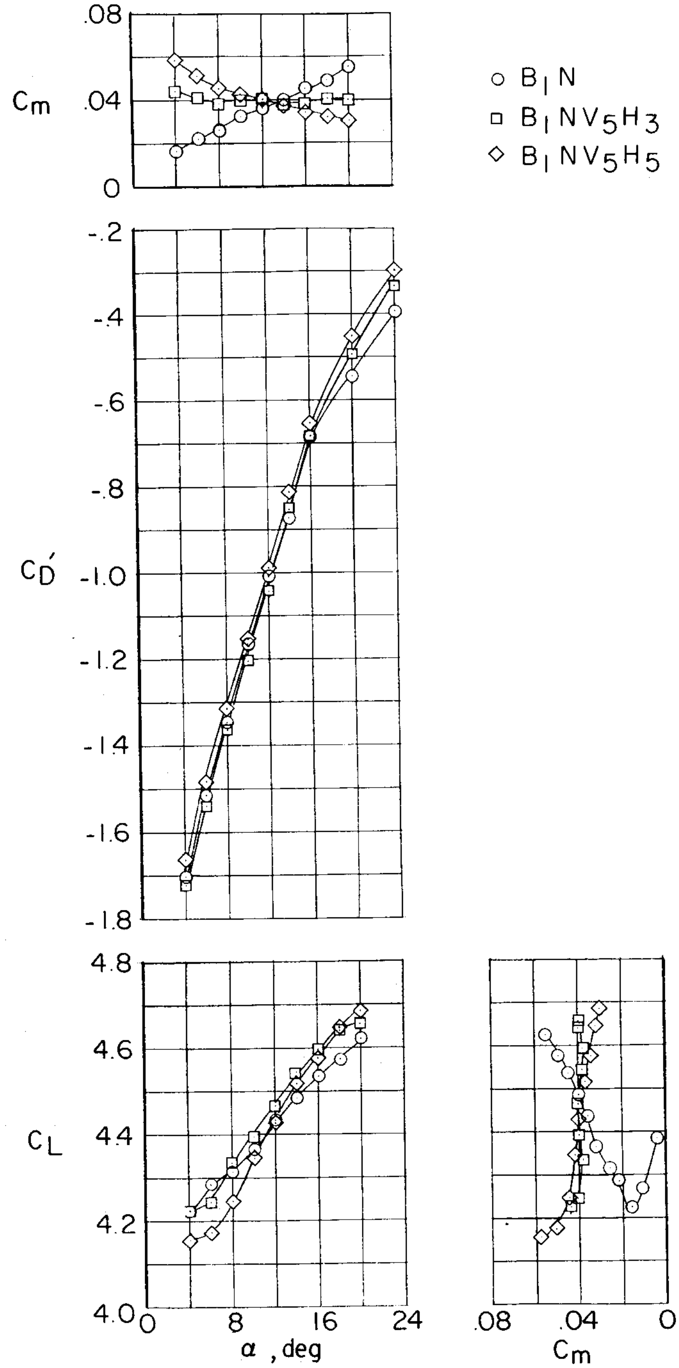

(b) $T_c' = 4.7$.

Figure 18.- Concluded.

L-575

L-575

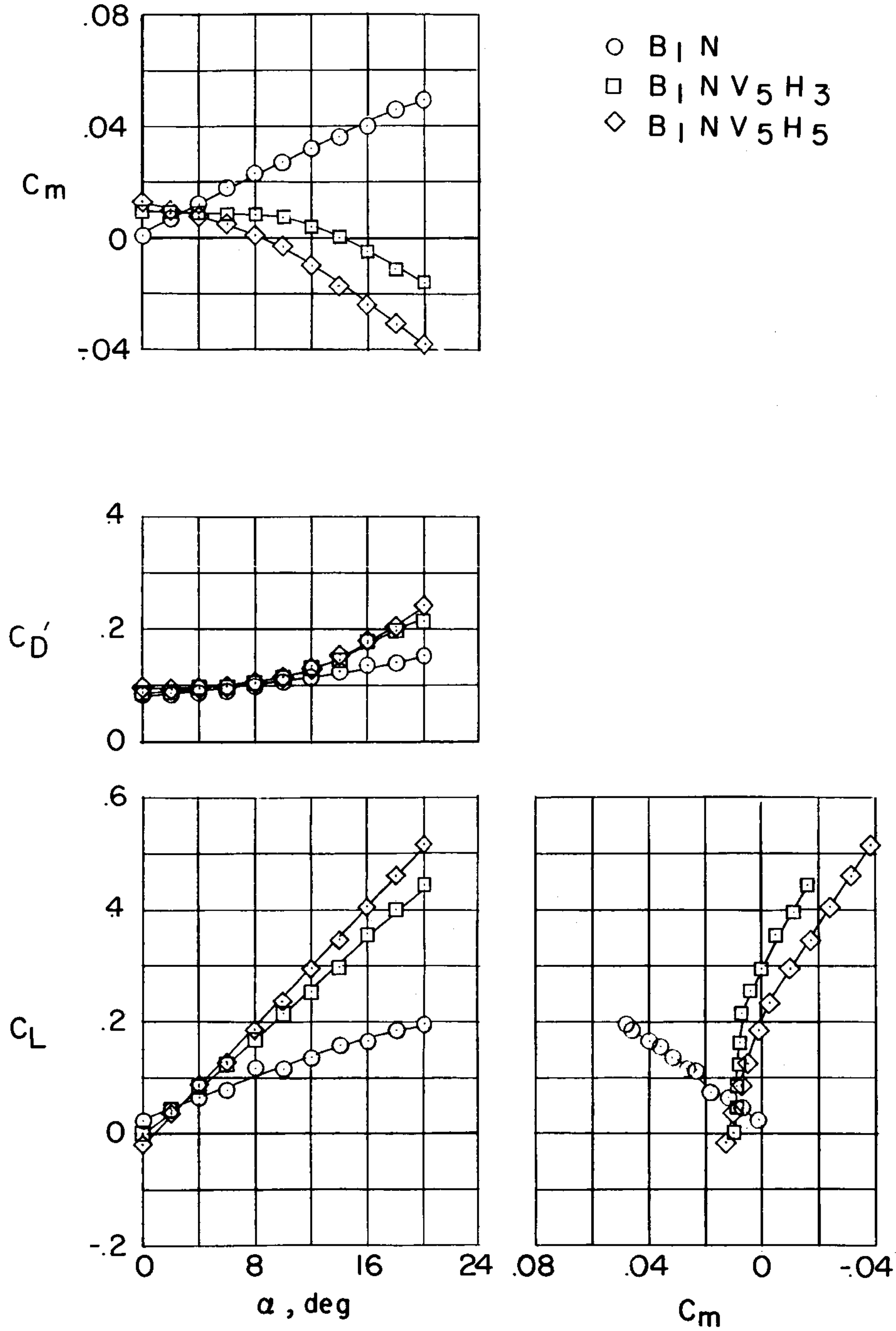

(a) $T_c' = 0$.

Figure 19.- Power-on longitudinal characteristics of model with $i_j = 80^\circ$.

L-575

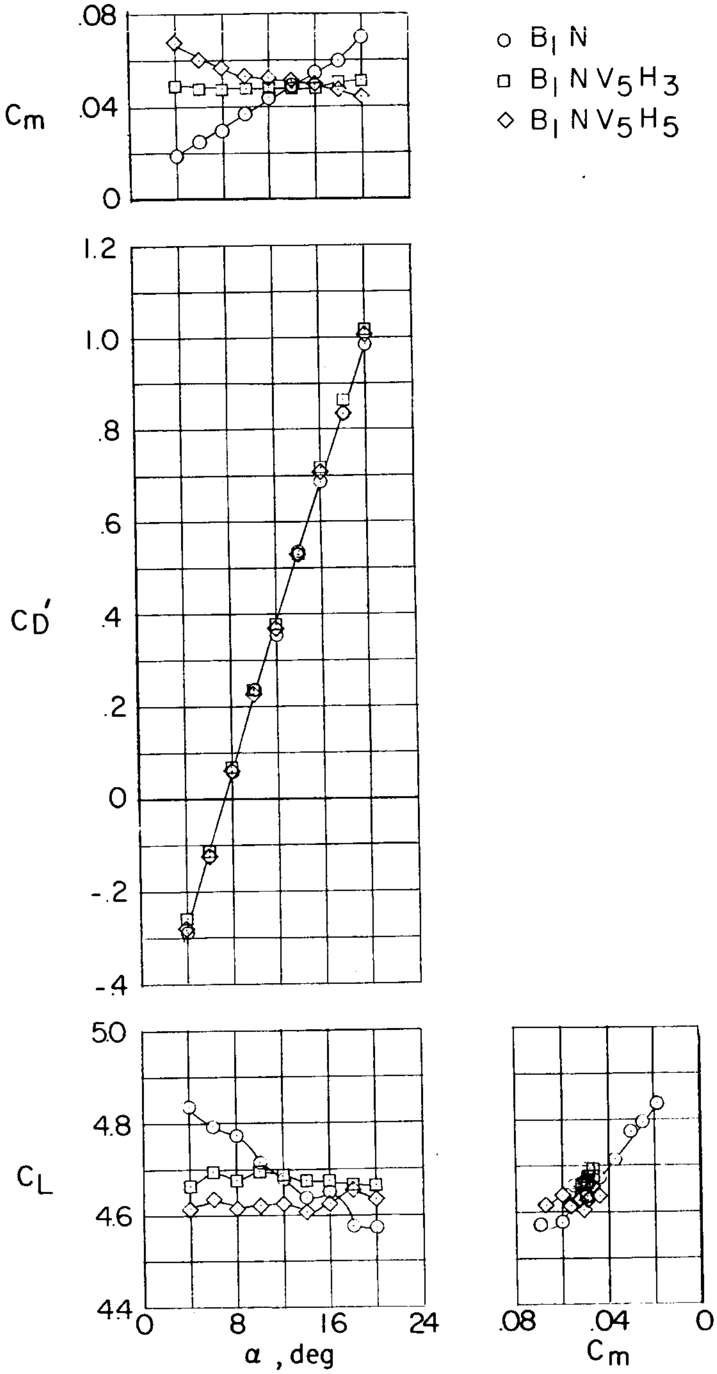

(b) $T_c' = 4.7$.

Figure 19.- Concluded.

L-575

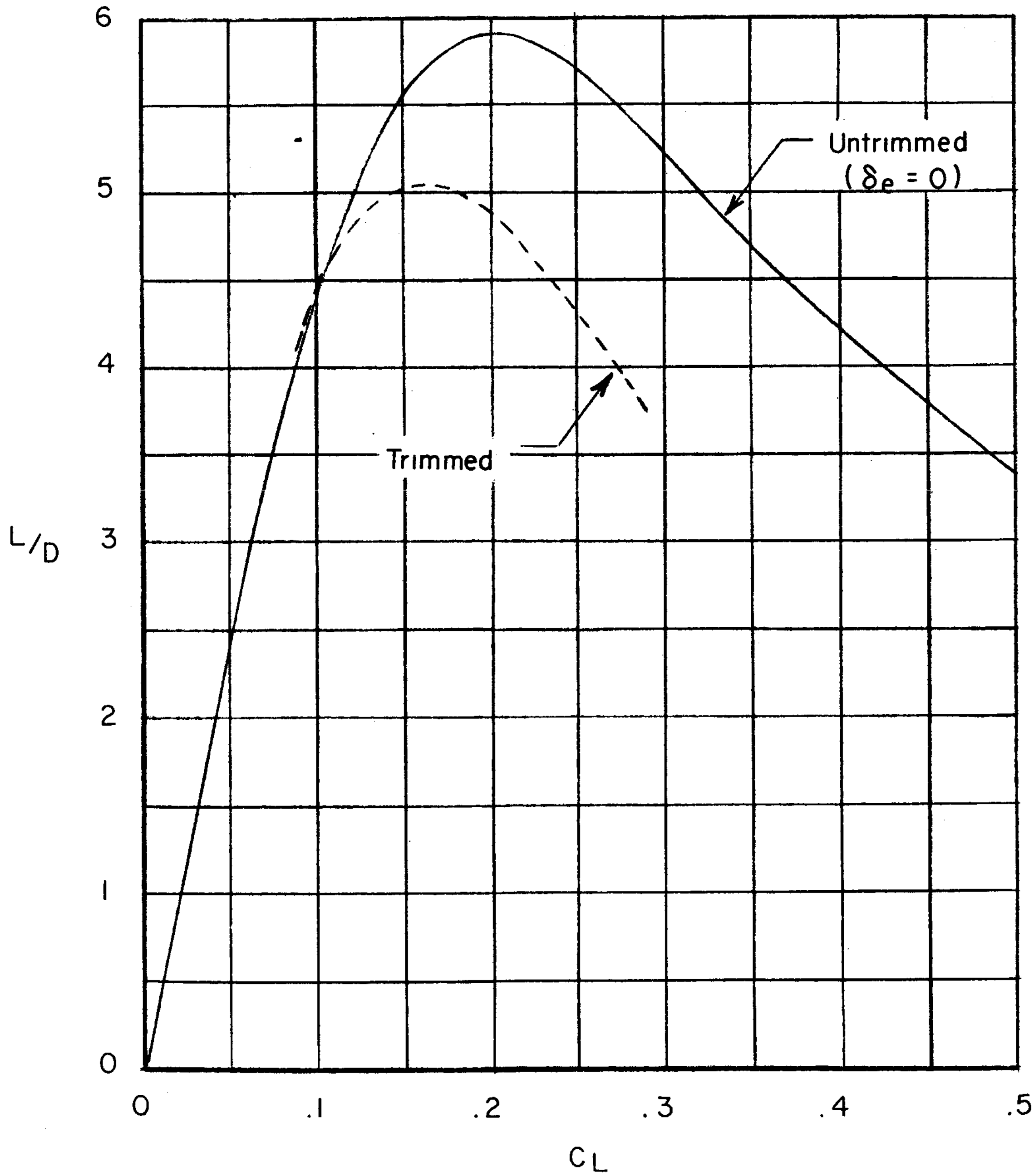

Figure 20.- Lift-drag ratios of model in configuration $B_1NV_5H_5$. $i_j = 0^o$; $T_c' = 0$.

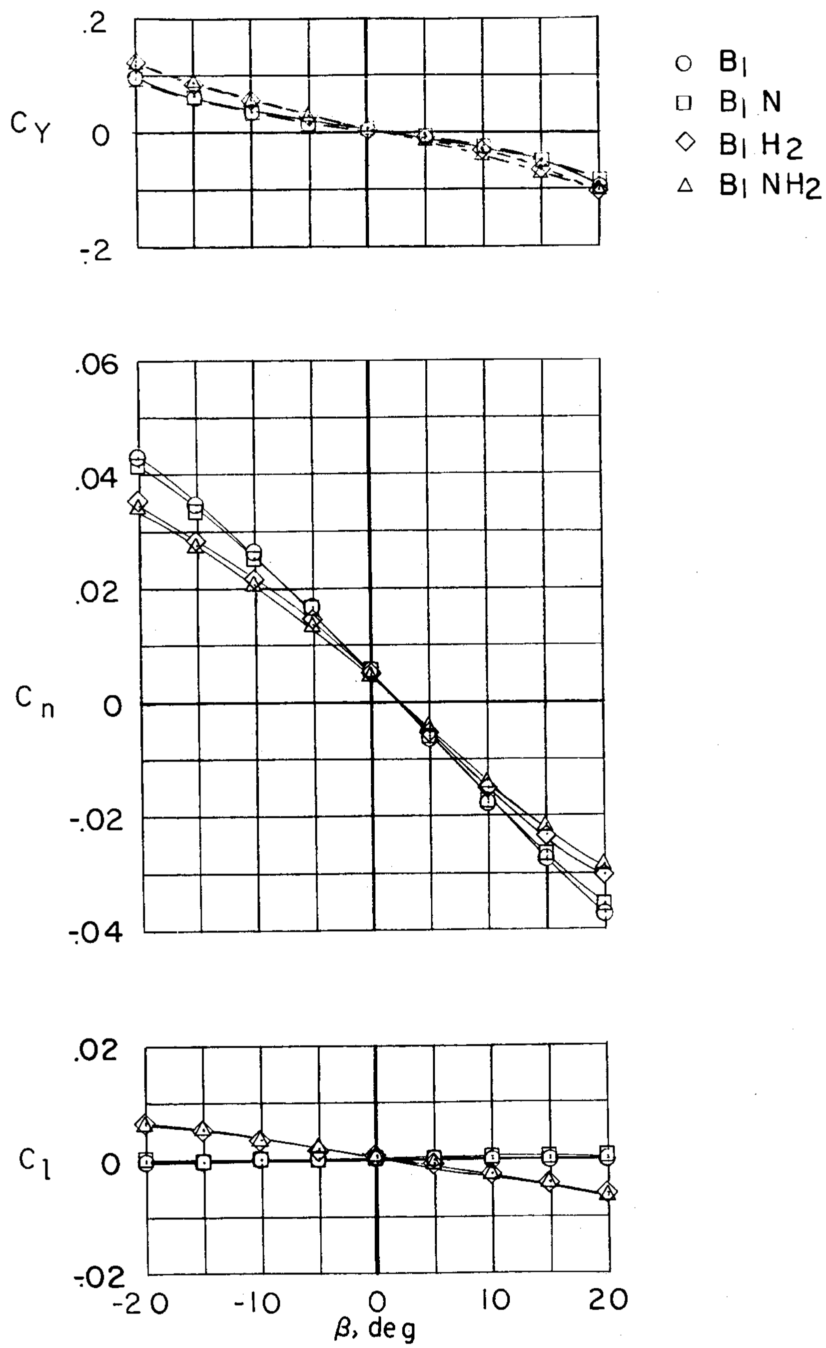

(a) $\alpha = 0^\circ$.

Figure 21.- Effect of components on lateral characteristics of model with body B_1 and vertical tail off. Power off; $i_j = 0^\circ$.

L-575

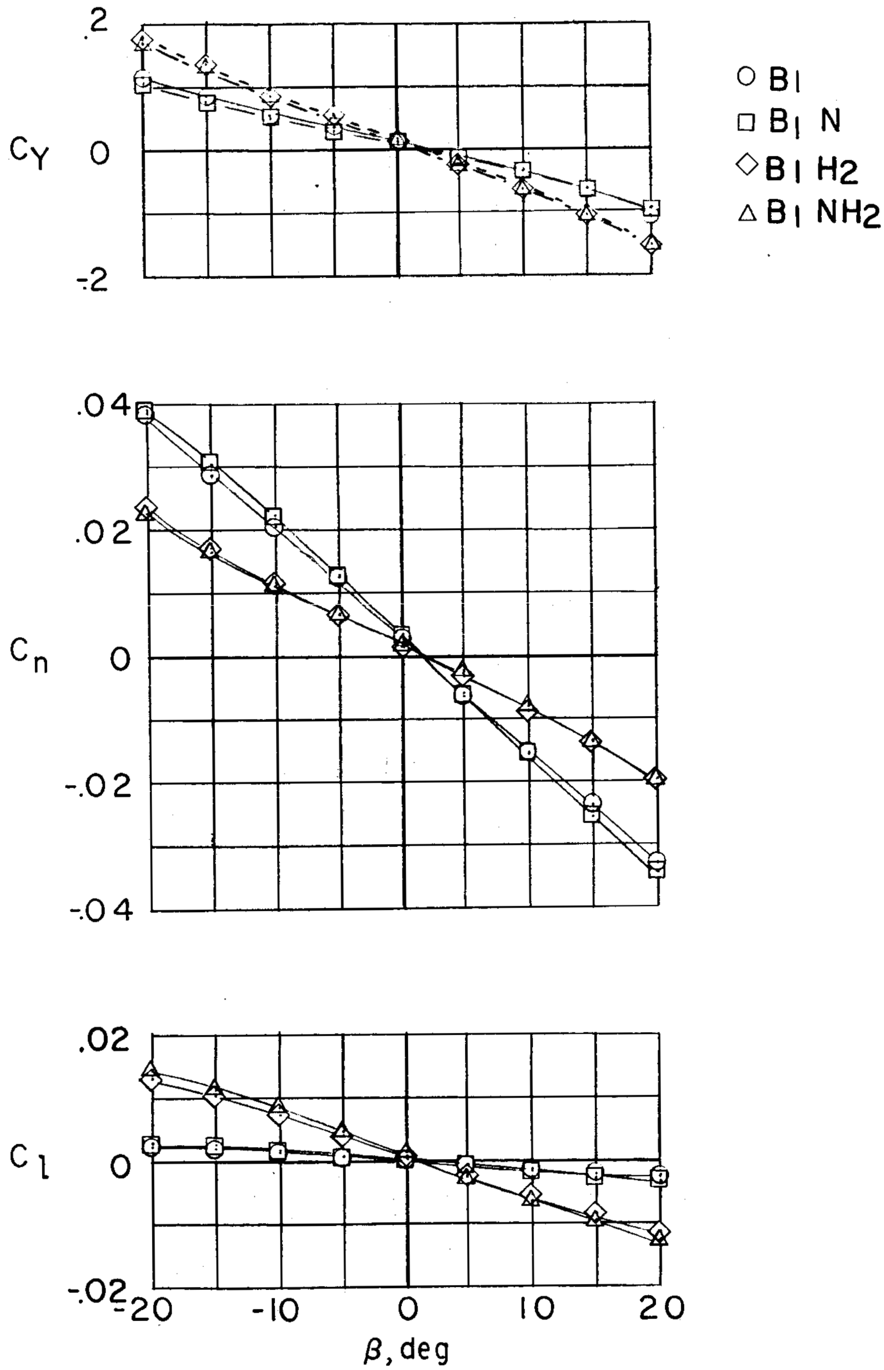

(b) $\alpha = 10^{\circ}$.

Figure 21.- Continued.

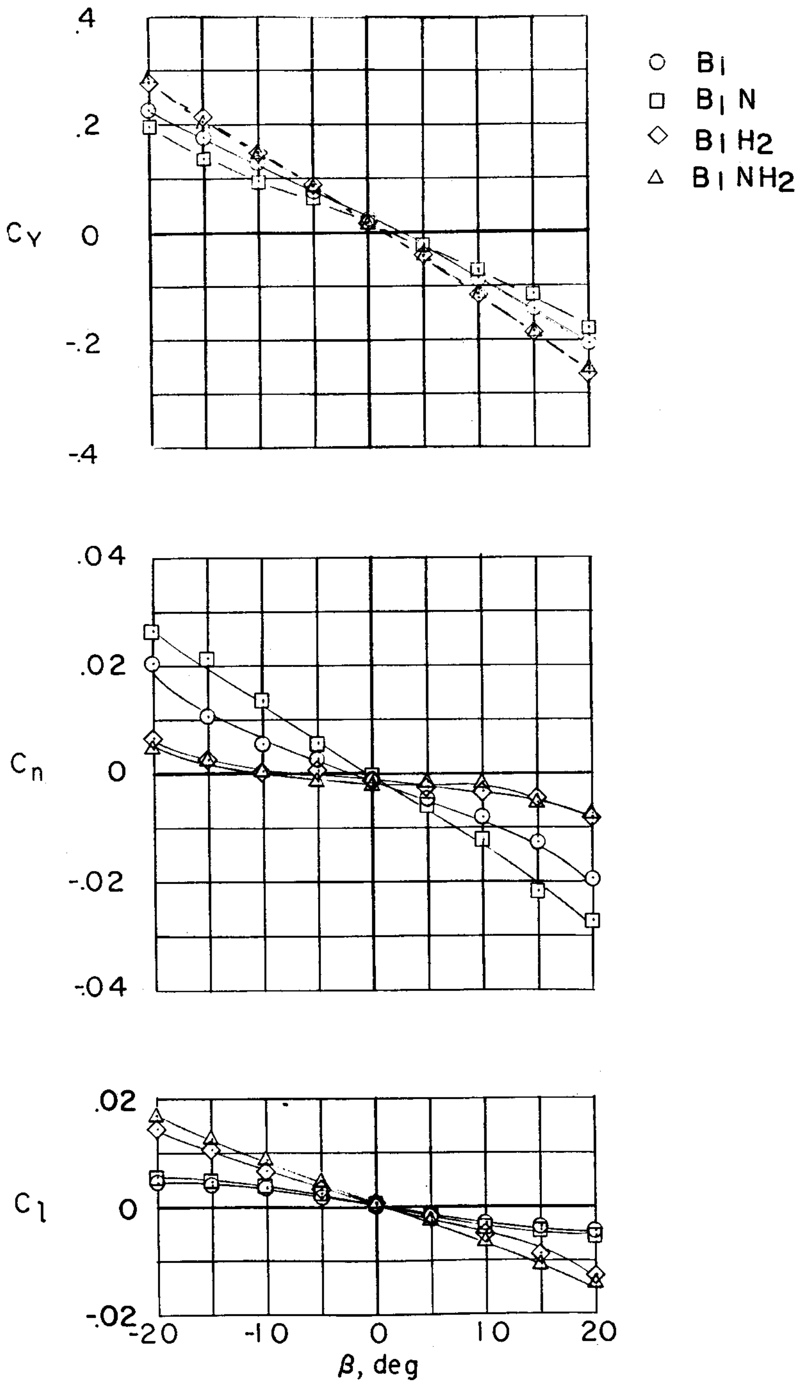

(c) $\alpha = 20^{\circ}$.

Figure 21.- Continued.

L-575

L-575

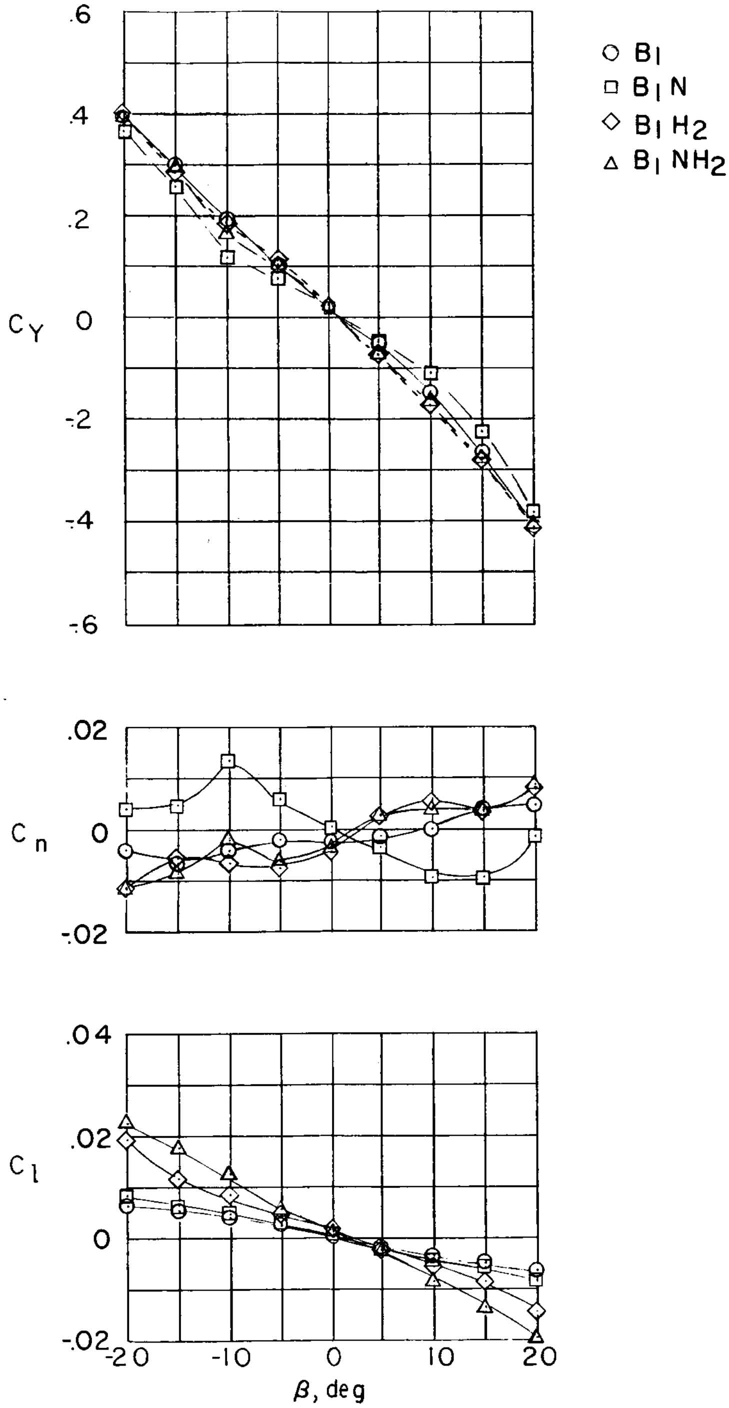

(d) $\alpha = 30^{\circ}$.

Figure 21.- Concluded.

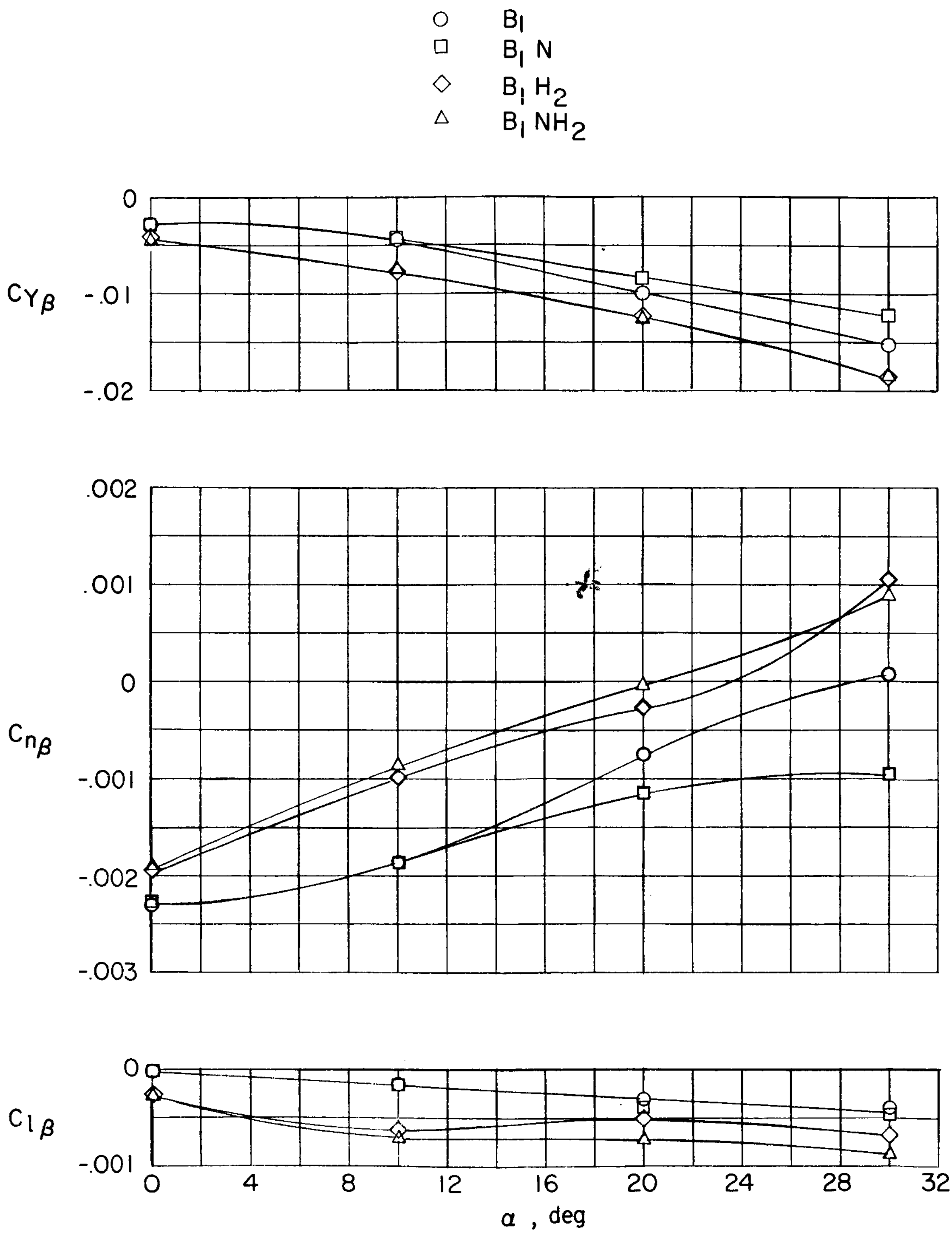

Figure 22.- Effect of components on static lateral stability derivatives of model with body B_1 and vertical tail off. Power off; $i_j = 0^o$.

L-575

L-575

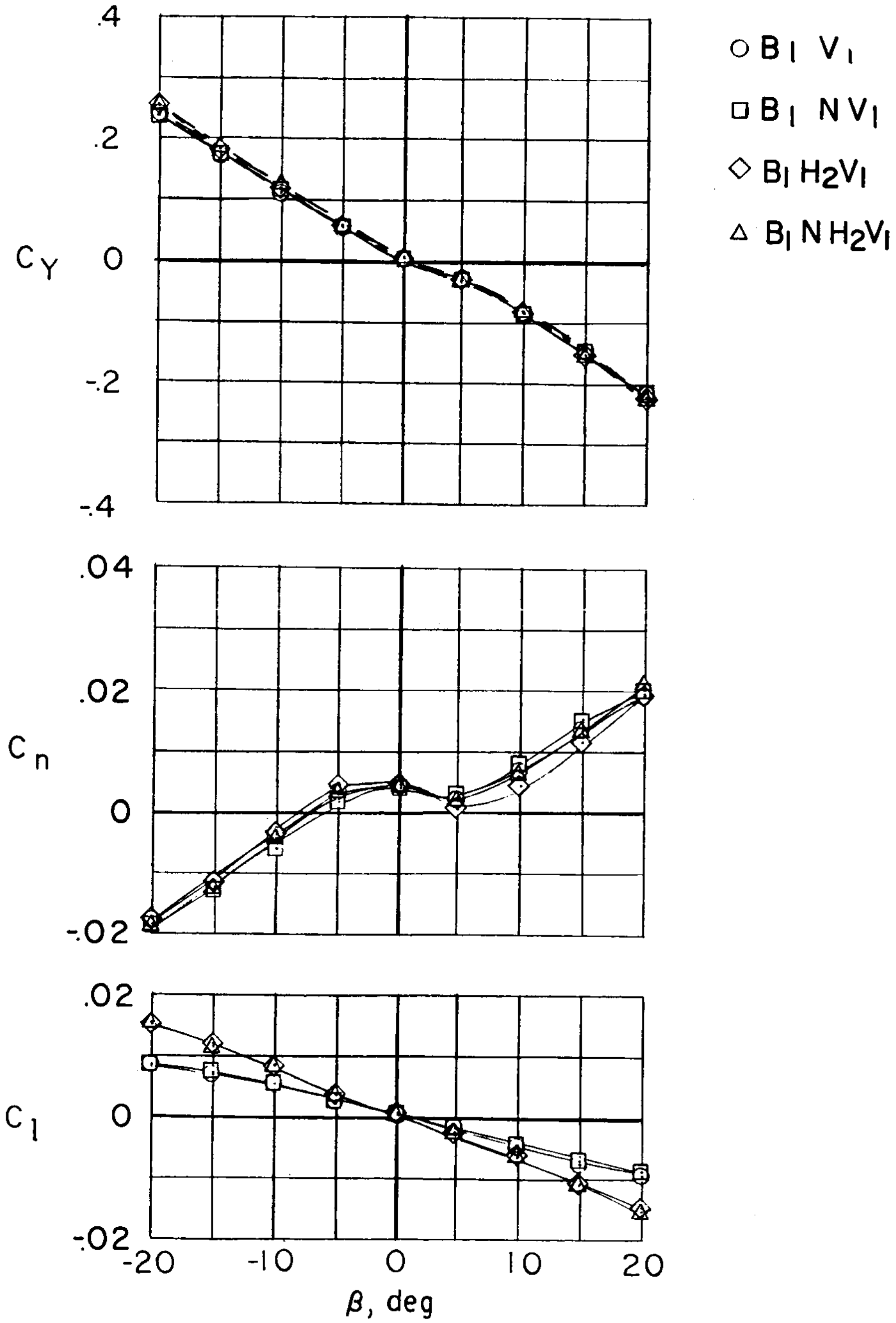

(a) $\alpha = 0^{\circ}$.

Figure 23.- Effect of components on lateral characteristics of model with body B_1 and vertical tail V_1. Power off; $i_j = 0^{\circ}$.

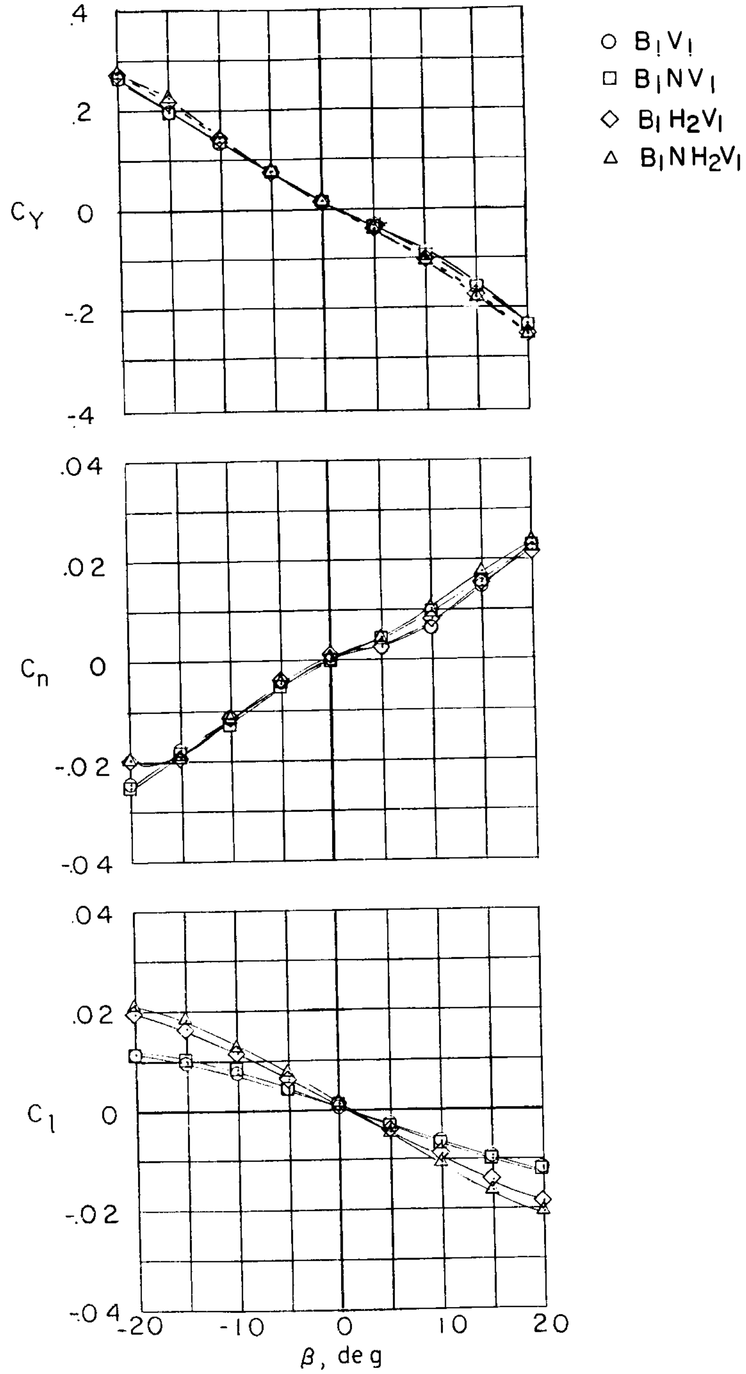

(b) $\alpha = 10^{\circ}$.

Figure 23.- Continued.

L-575

L-575

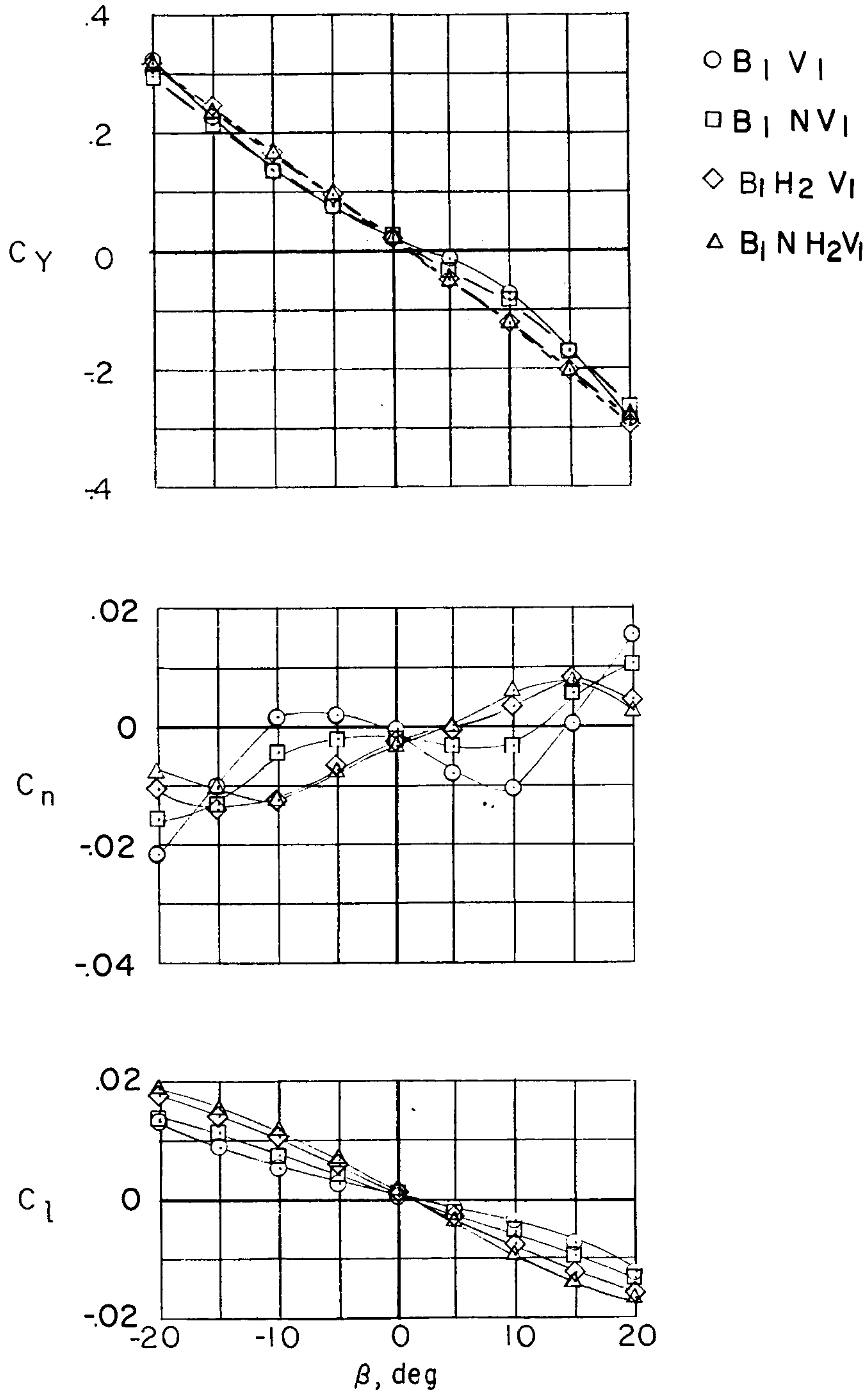

(c) $\alpha = 20^{\circ}$.

Figure 23.- Continued.

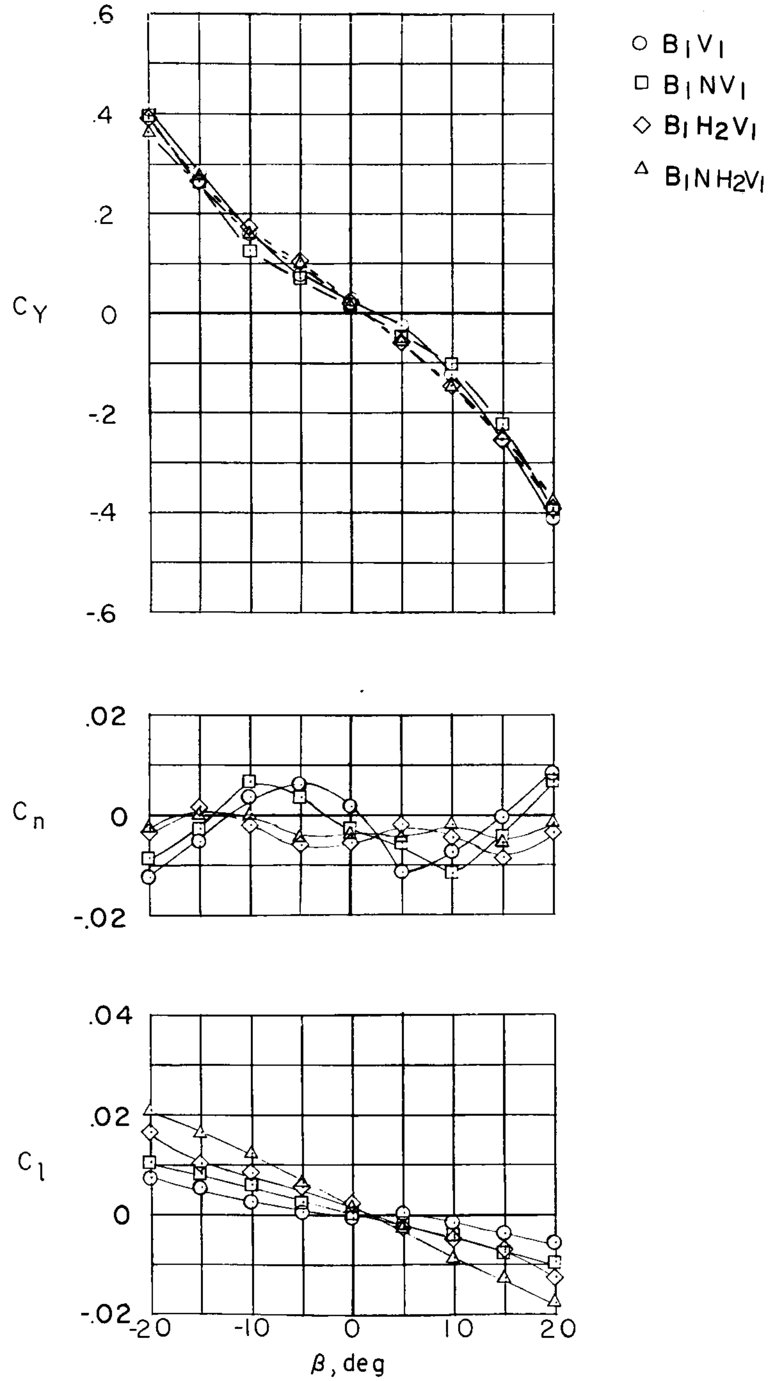

(d) $\alpha = 30^{\circ}$.

Figure 23.- Concluded.

L-575

L-575

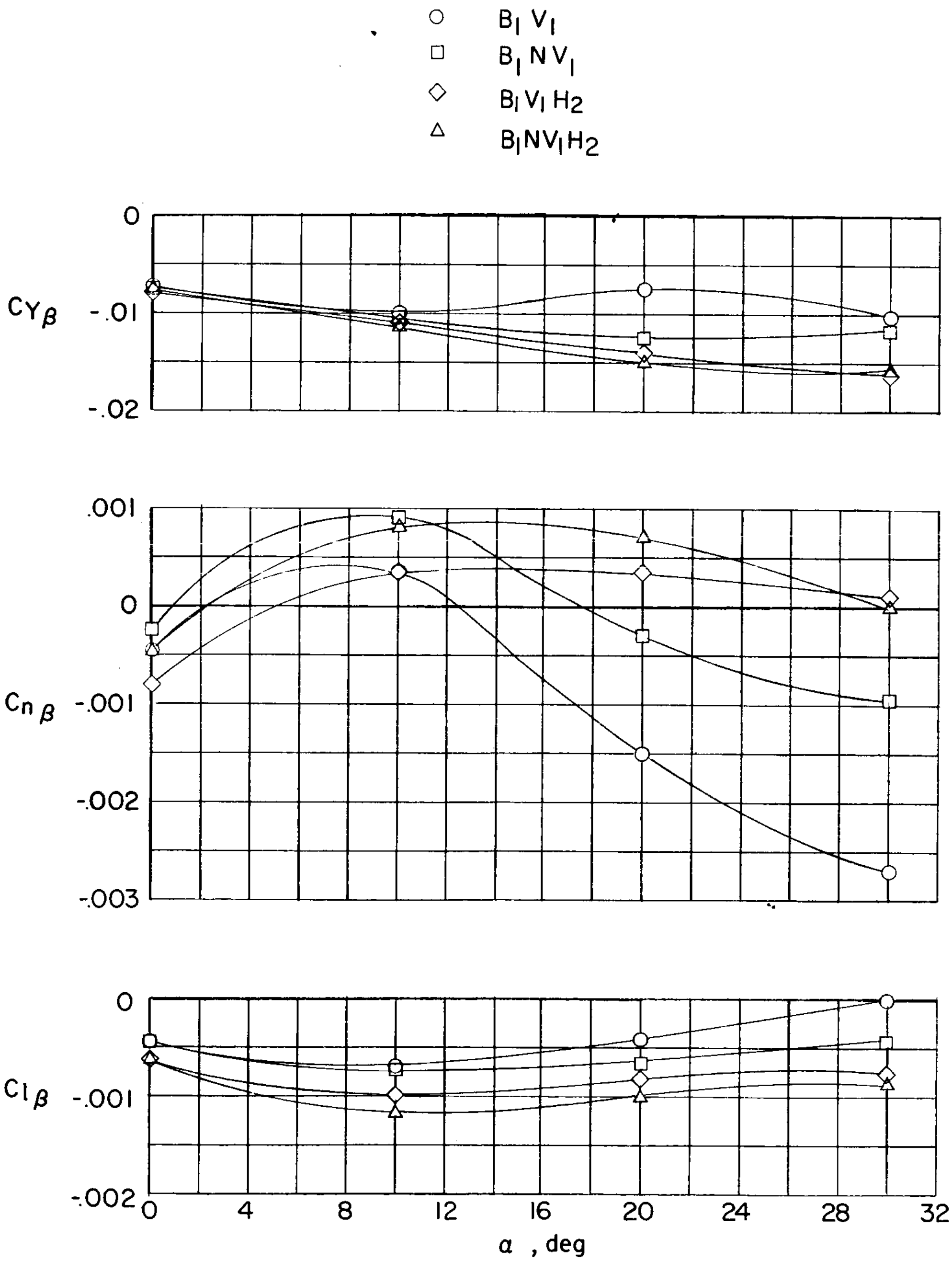

Figure 24.- Effect of components on static lateral stability derivatives of model with body B_1 and vertical tail V_1. Power off; $i_j = 0^o$.

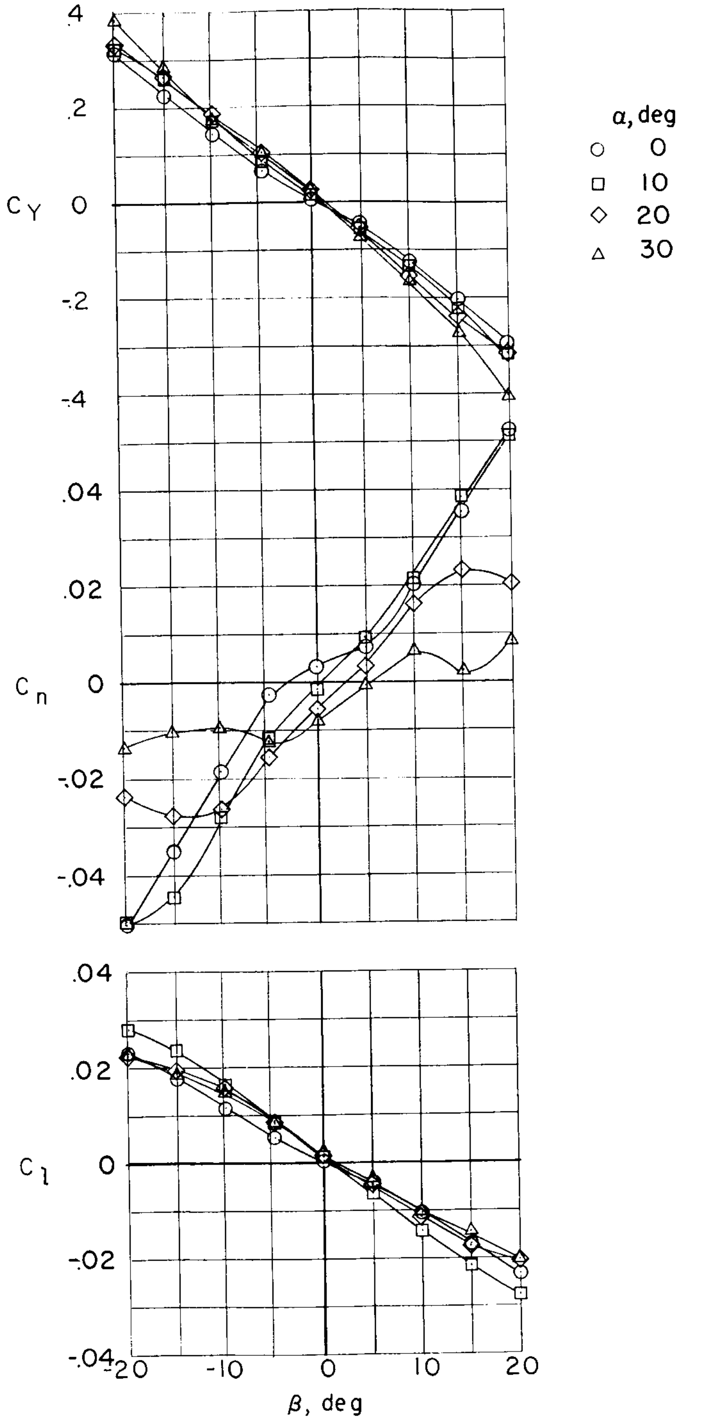

Figure 25.- Lateral characteristics of model in configuration $B_1NH_2V_2$. Power off; $i_j = 0^{\circ}$.

L-575

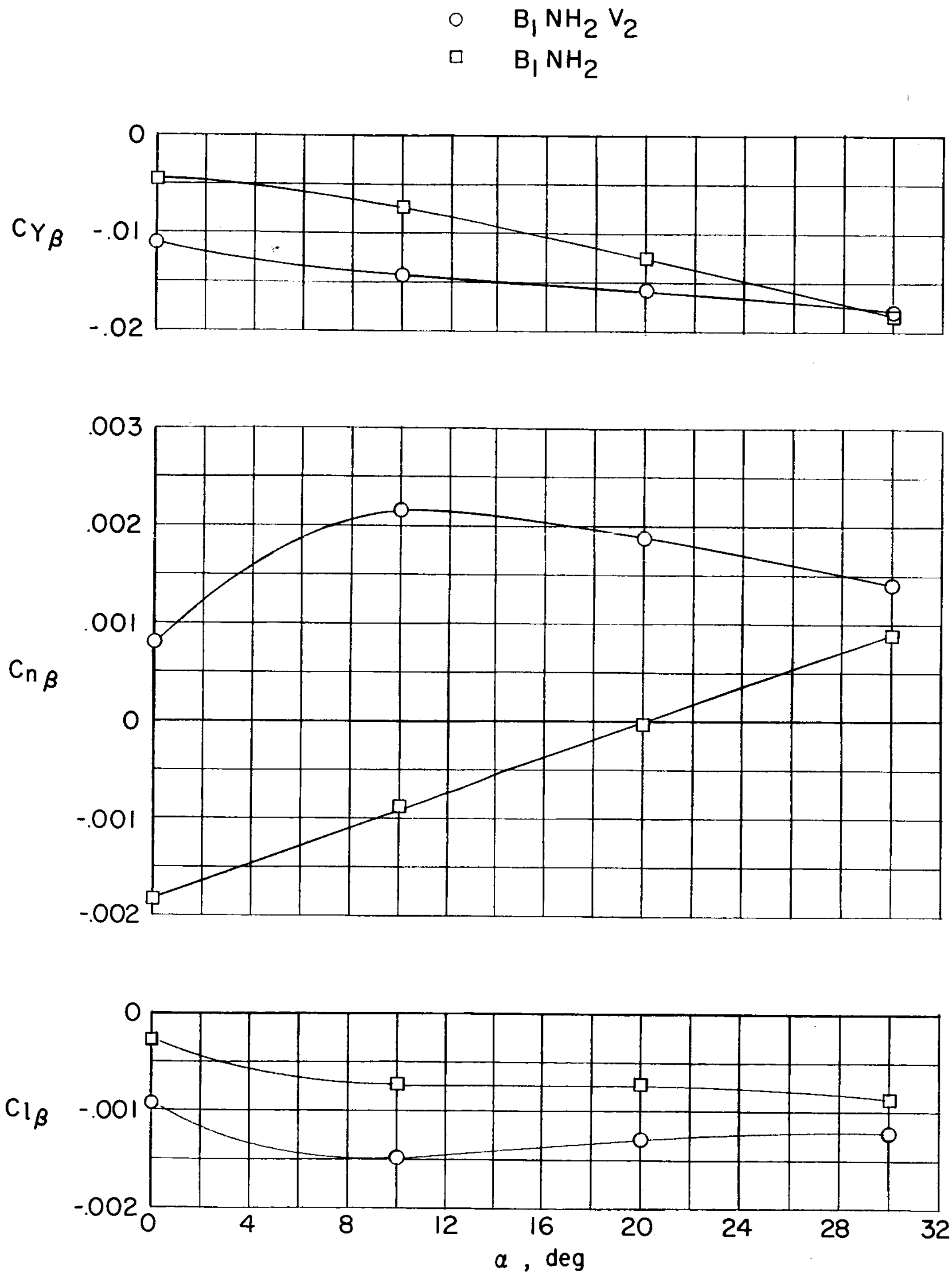

Figure 26.- Static lateral stability derivatives of model in configuration $B_1NH_2V_2$. Power off; $i_j = 0^o$.

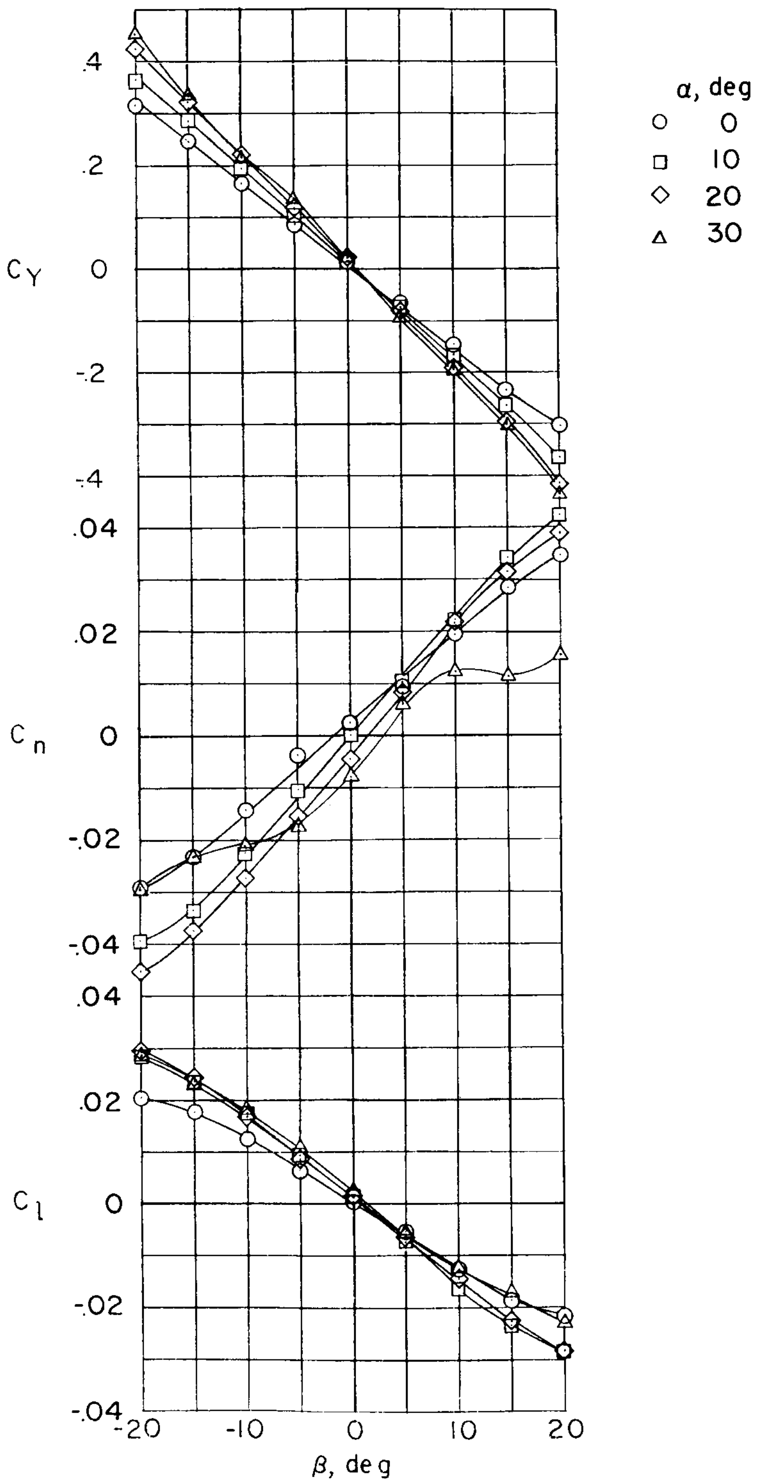

L-575

Figure 27.- Lateral characteristics of model in configuration $B_1NH_2V_3$. Power off; $i_j = 0^\circ$.

L-575

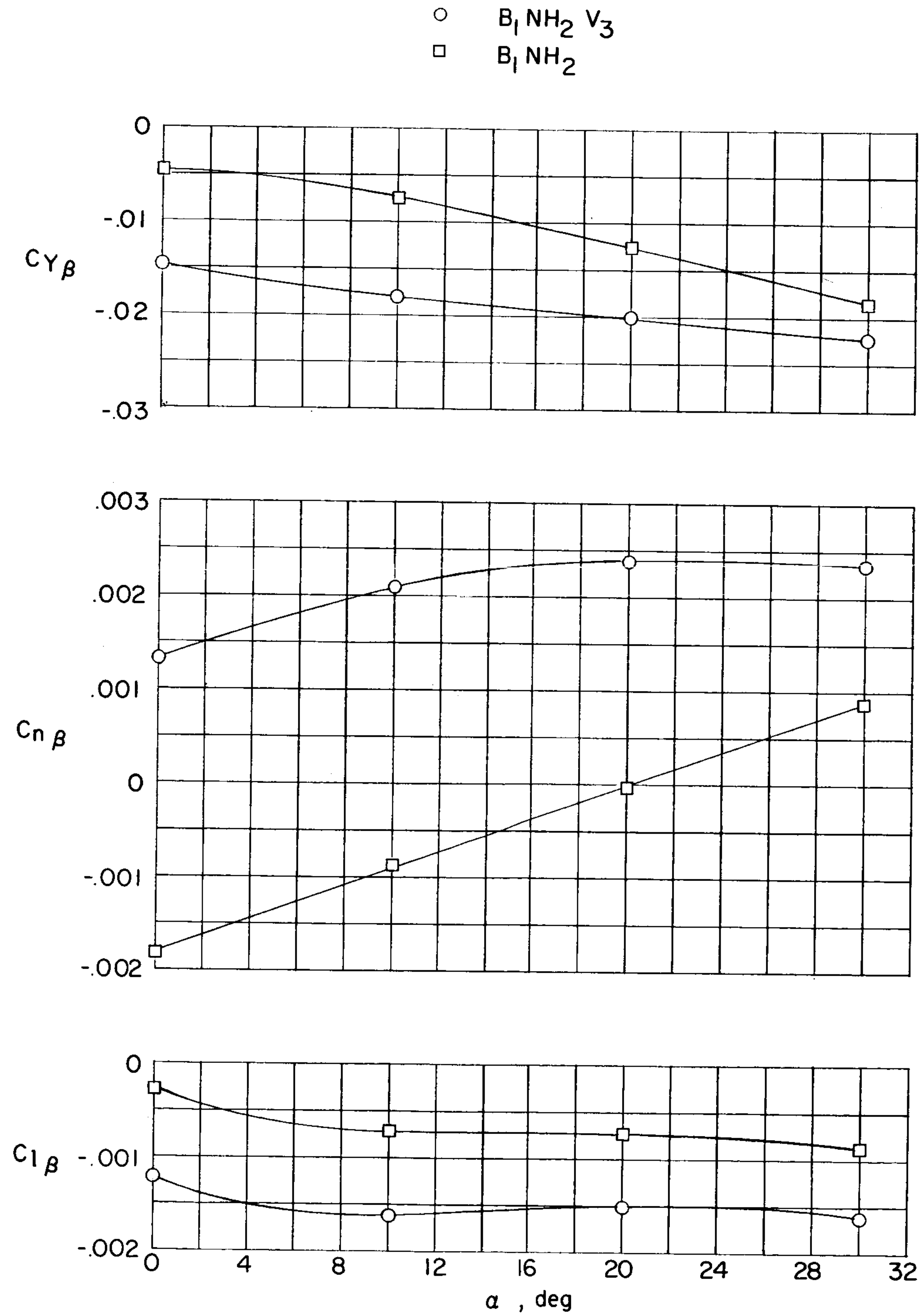

Figure 28.- Static lateral stability derivatives of model in configuration $B_1NH_2V_3$. Power off; $i_j = 0^\circ$.

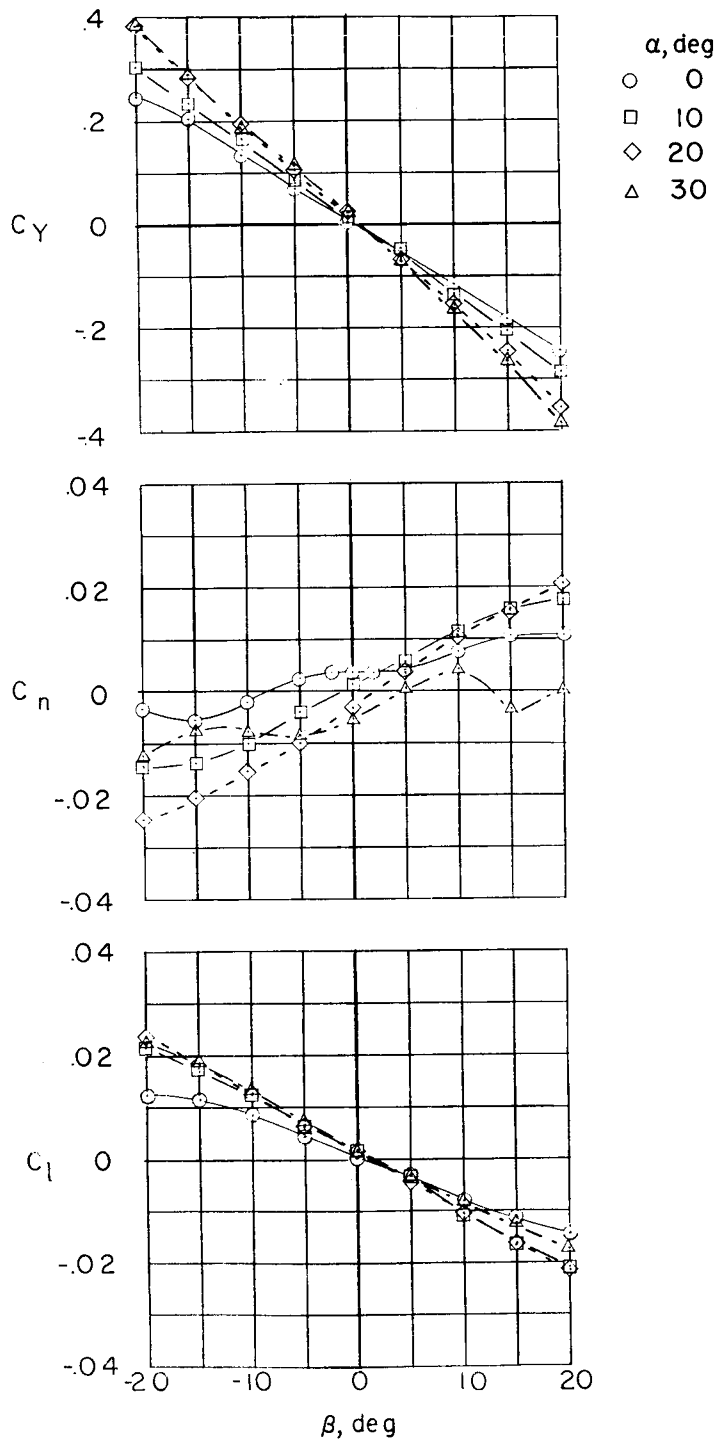

L-575

Figure 29.- Lateral characteristics of model in configuration $B_1NH_2V_4$. Power off; $i_j = 0^{\circ}$.

L-575

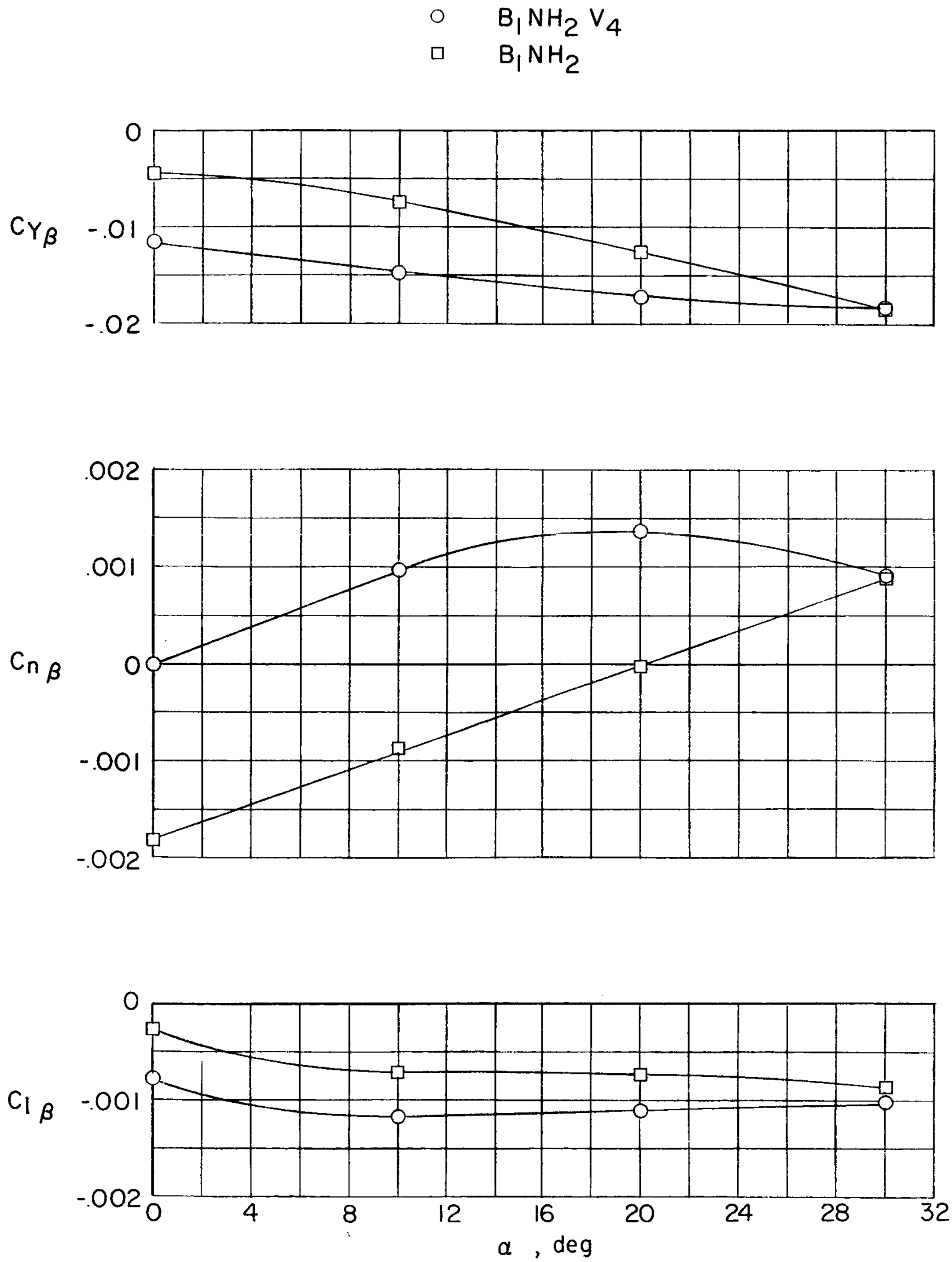

Figure 30.- Static lateral stability derivatives of model in configuration $B_1NH_2V_4$. Power off; $i_j = 0^\circ$.

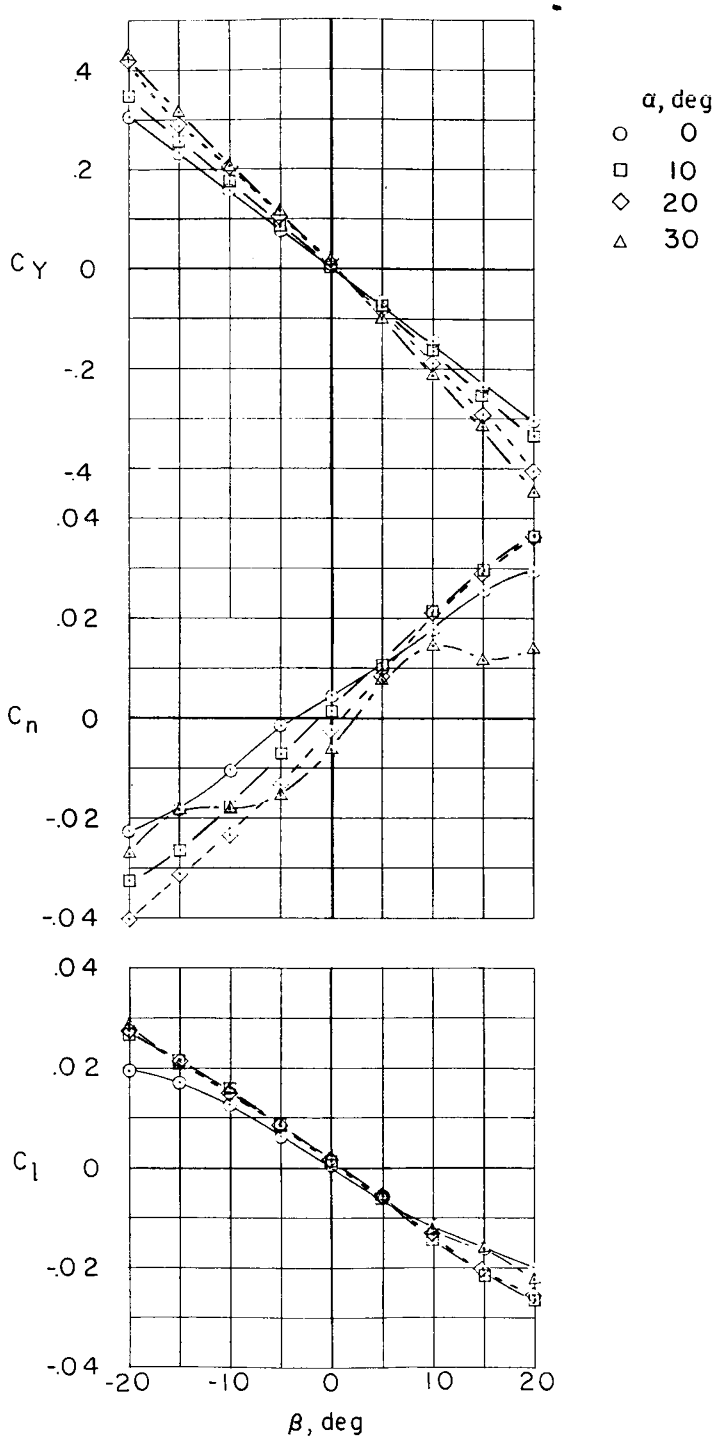

Figure 31.- Lateral characteristics of model in configuration $B_1NH_4V_5$. Power off; $i_j = 0^{\circ}$.

L-575

L-575

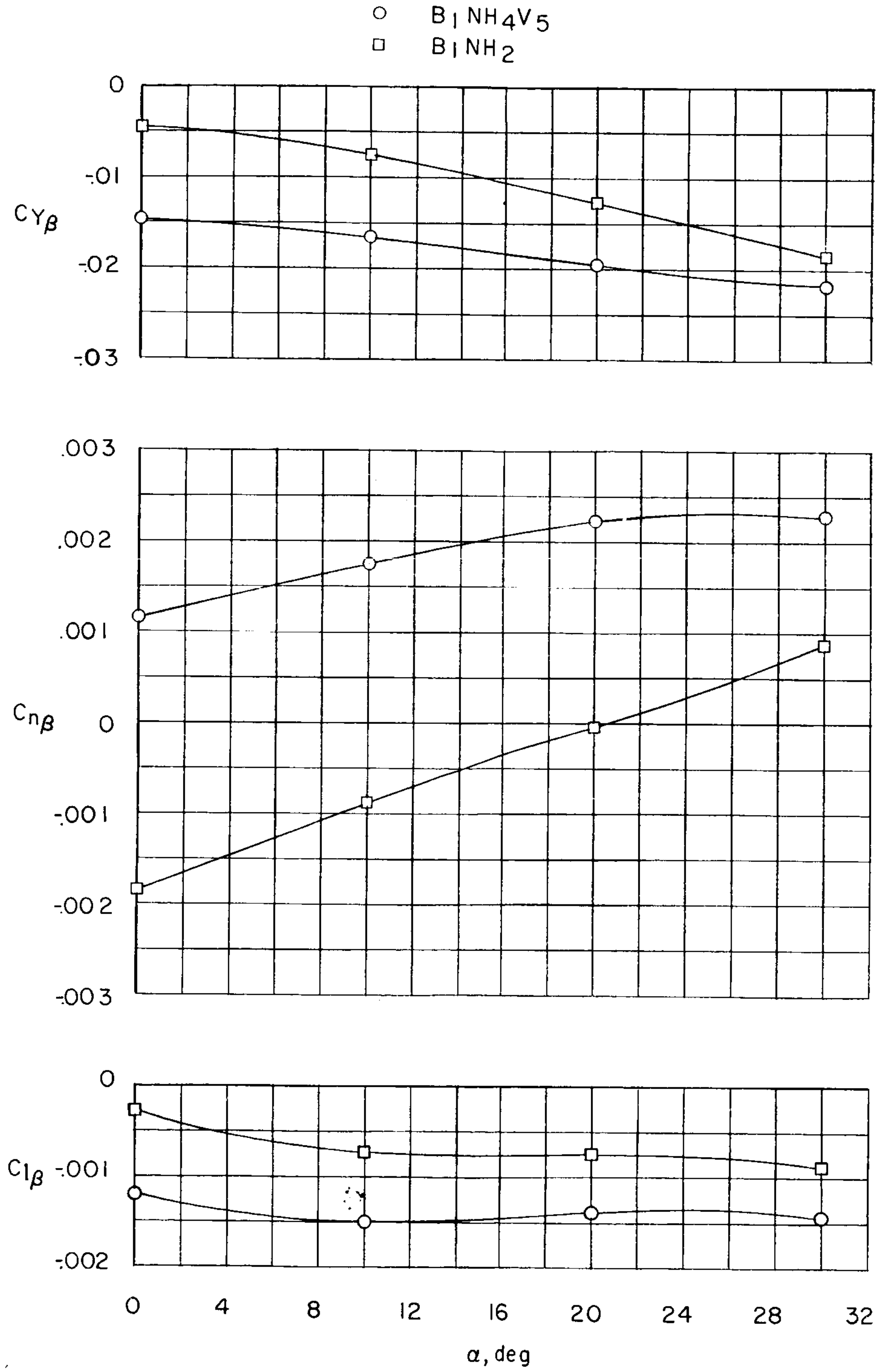

Figure 32.- Static lateral stability derivatives of model in configuration $B_1NH_4V_5$. Power off; $i_j = 0^\circ$.

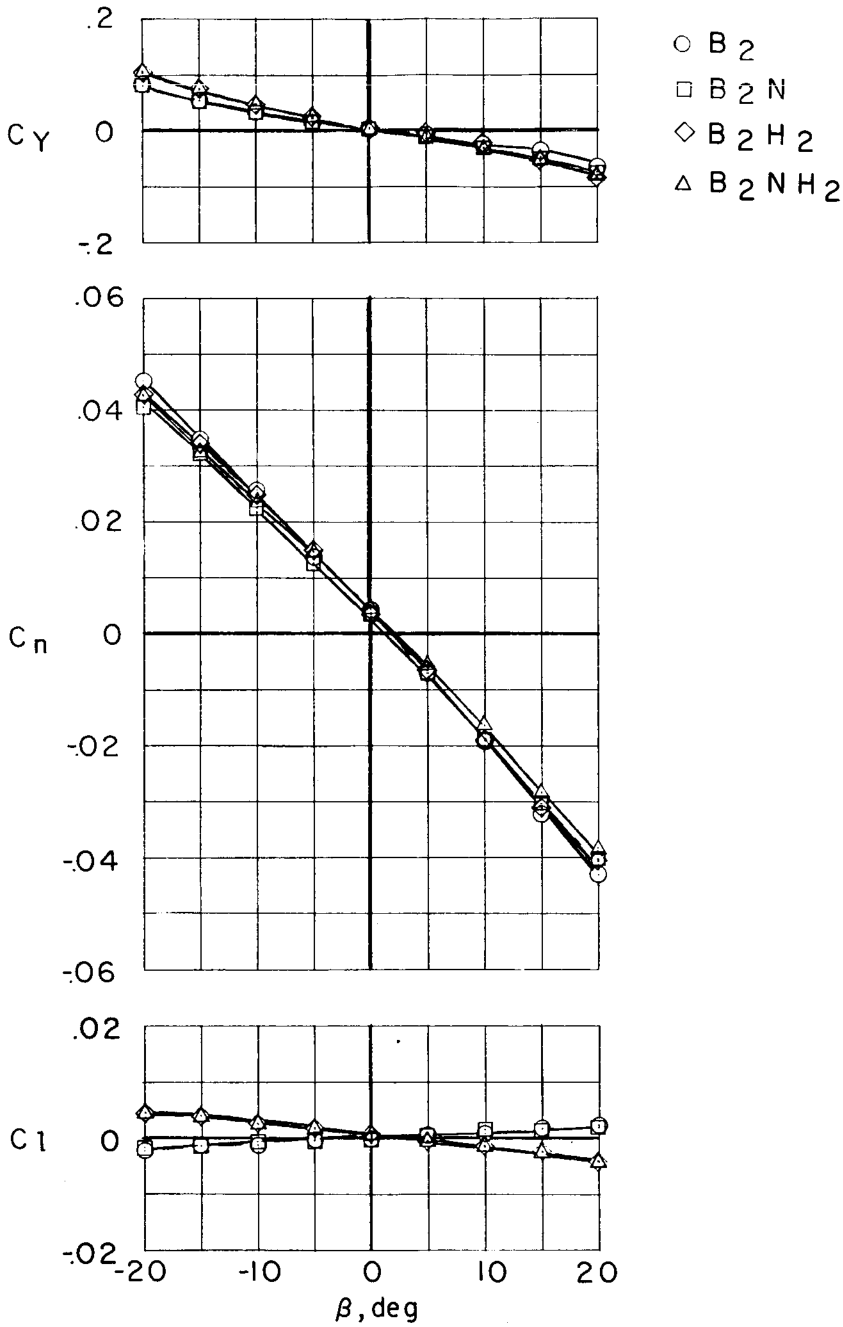

(a) $\alpha = 0^{\circ}$.

Figure 33.- Effect of components on lateral characteristics of model with body B_2 and vertical tail off. Power off; $i_j = 0^{\circ}$.

L-575

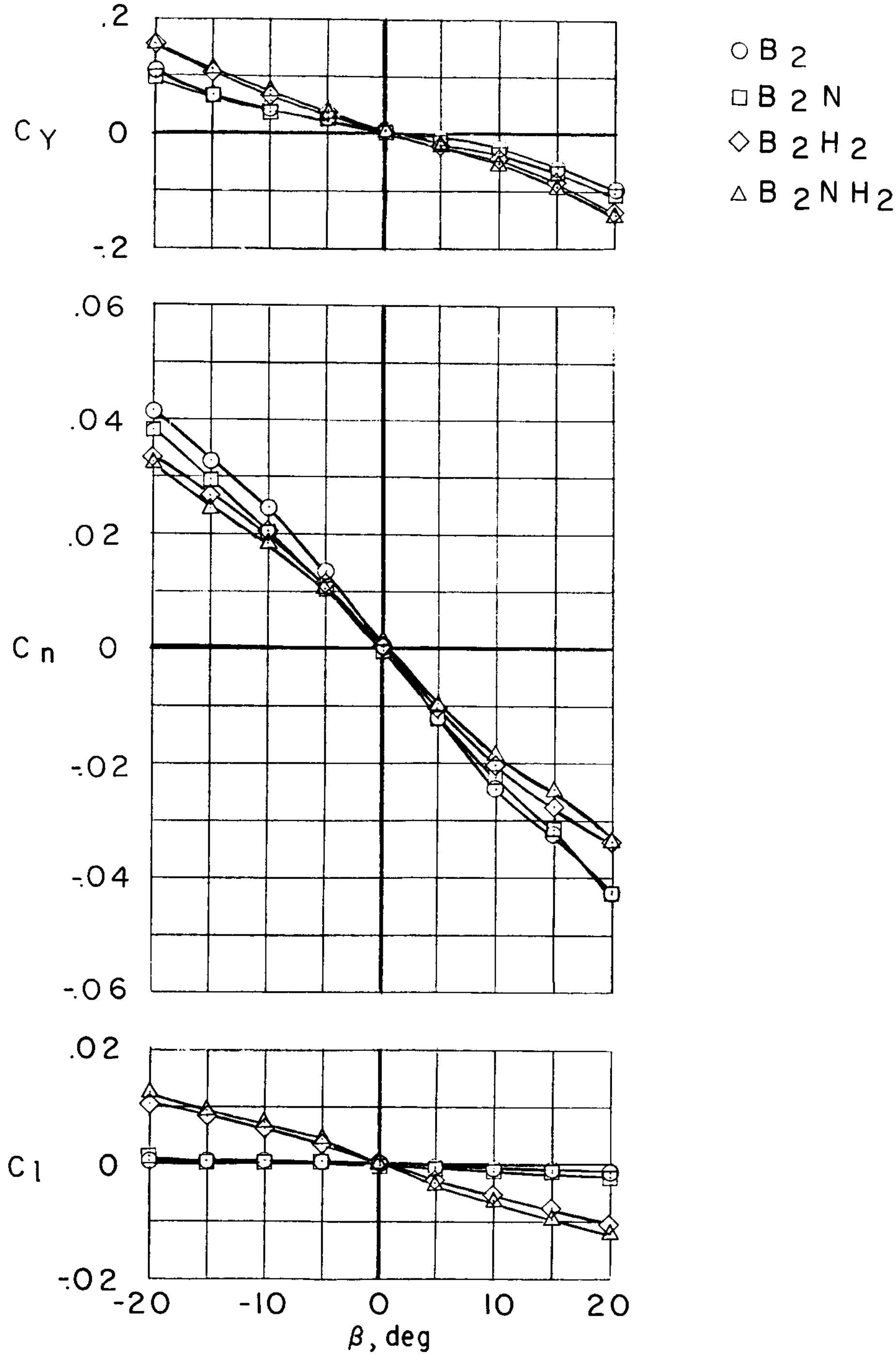

(b) $\alpha = 10^{\circ}$.

Figure 33.- Continued.

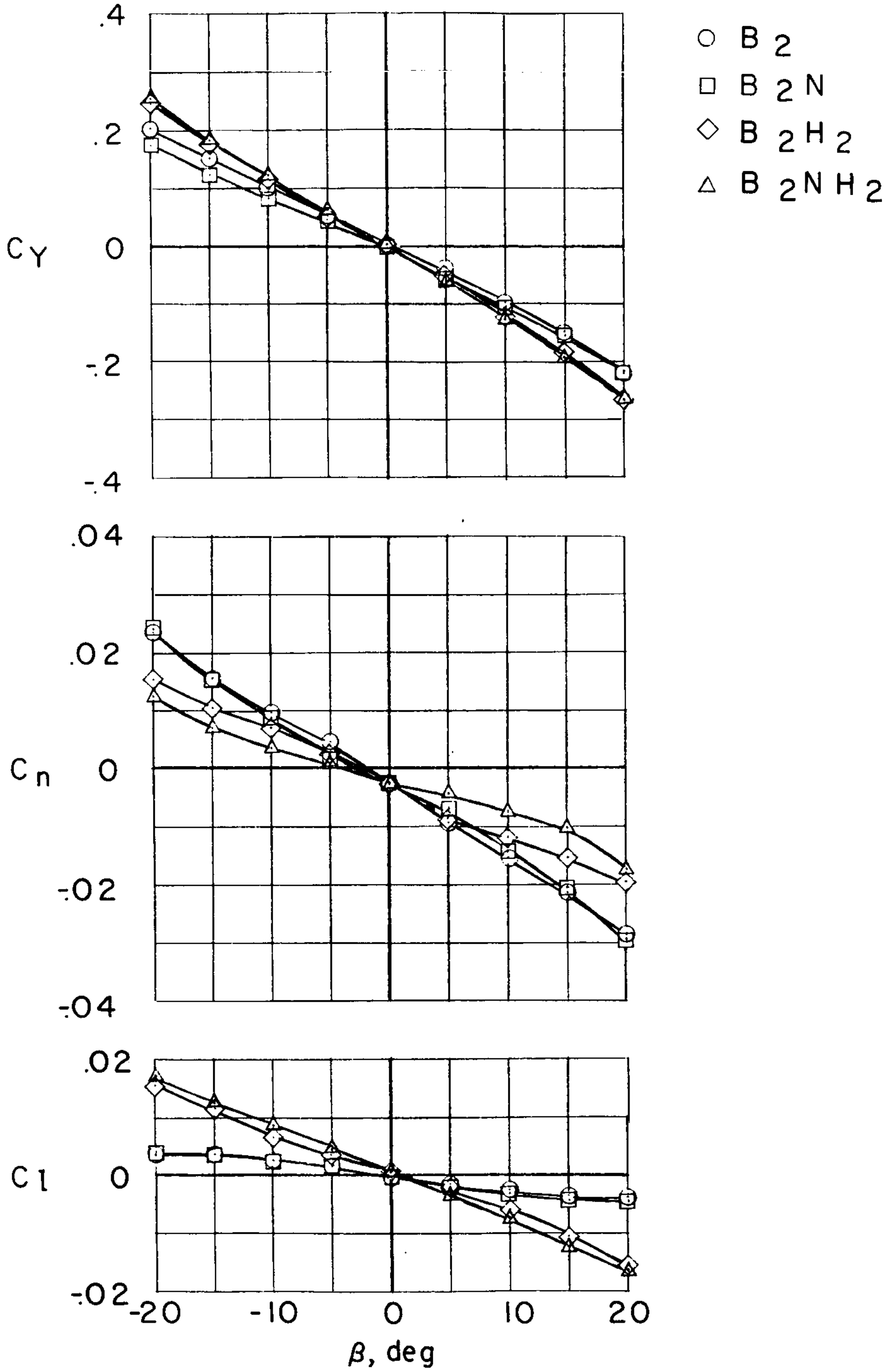

(c) $\alpha = 20^\circ$.

Figure 33.- Continued.

L-575

L-575

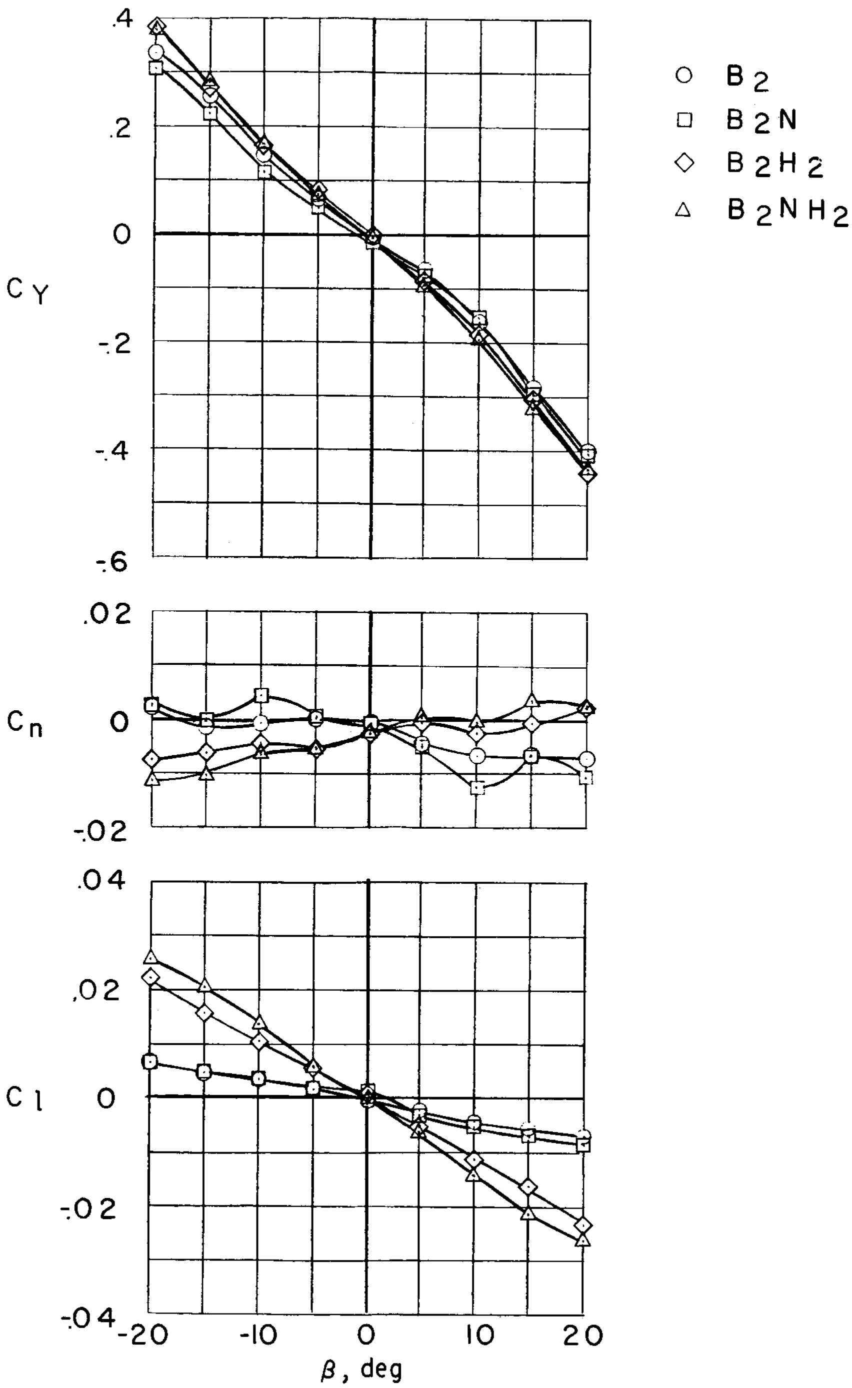

(d) $\alpha = 30^\circ$.

Figure 33.- Concluded.

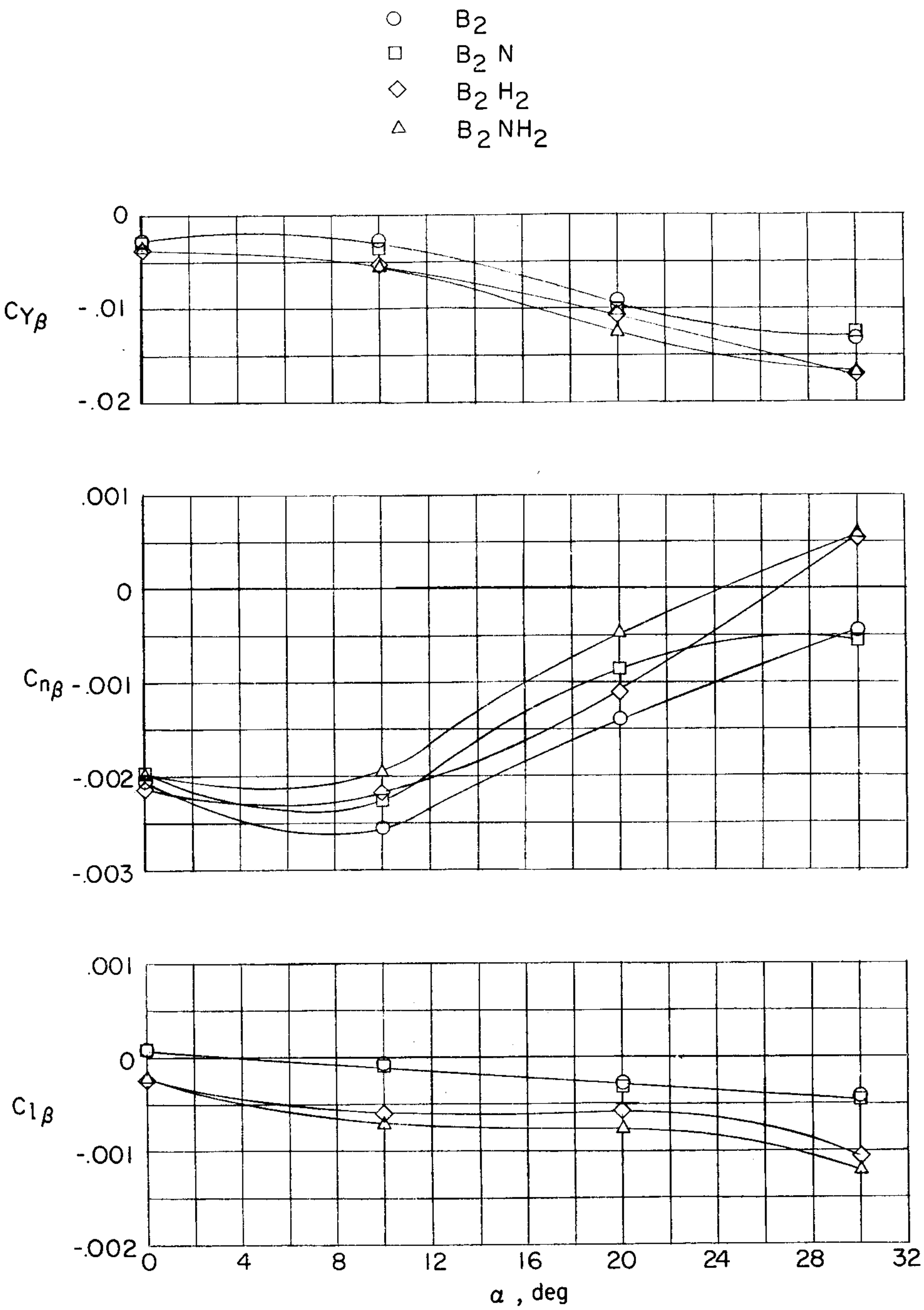

Figure 34.- Effect of components on static lateral stability derivatives of model with body B_2 and vertical tail off. Power off; $i_j = 0^{\circ}$.

L-575

L-575

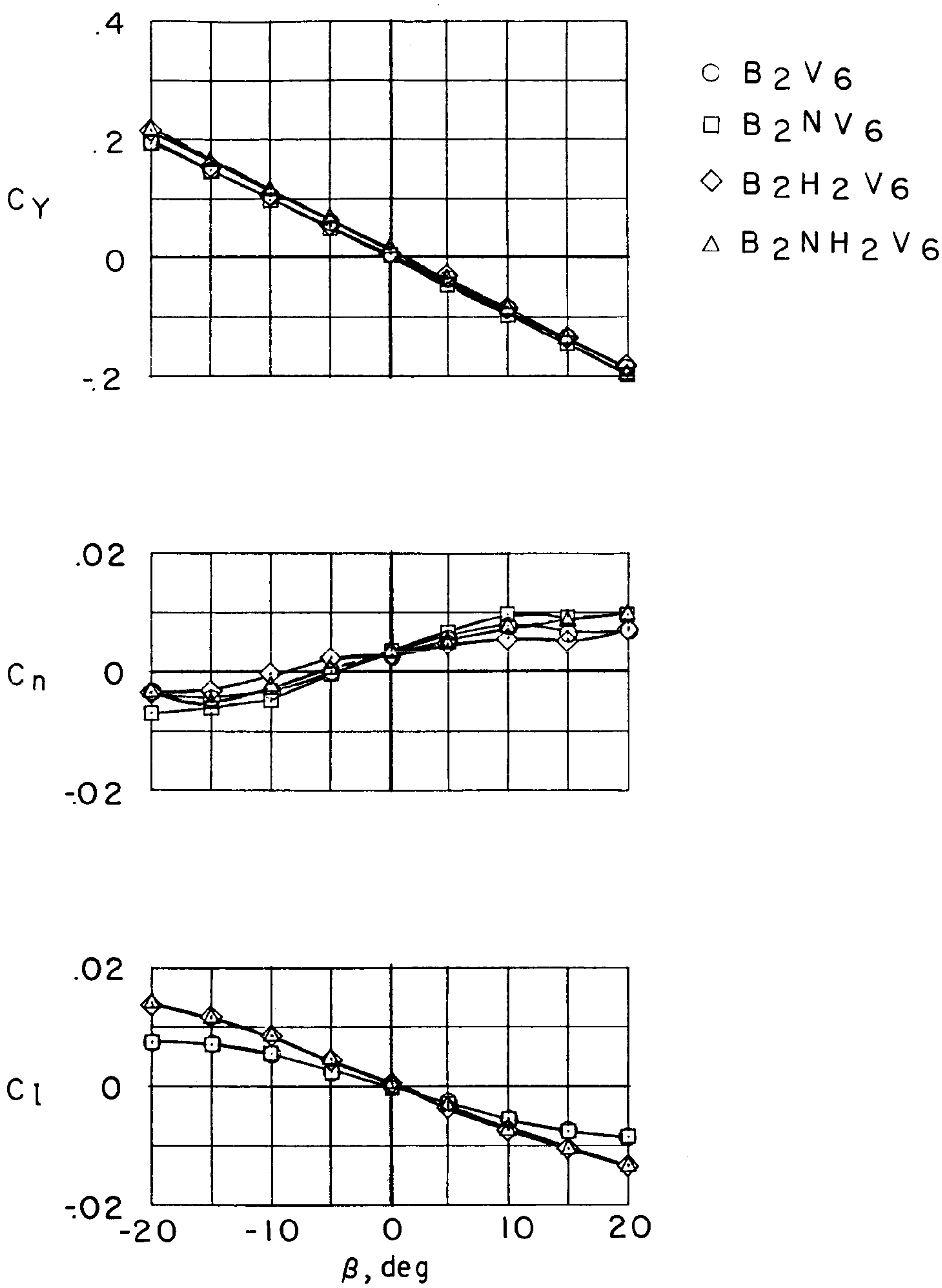

(a) $\alpha = 0^{\circ}$.

Figure 35.- Effect of components on lateral characteristics of model with body B_2 and vertical tail V_6. Power off; $i_j = 0^{\circ}$.

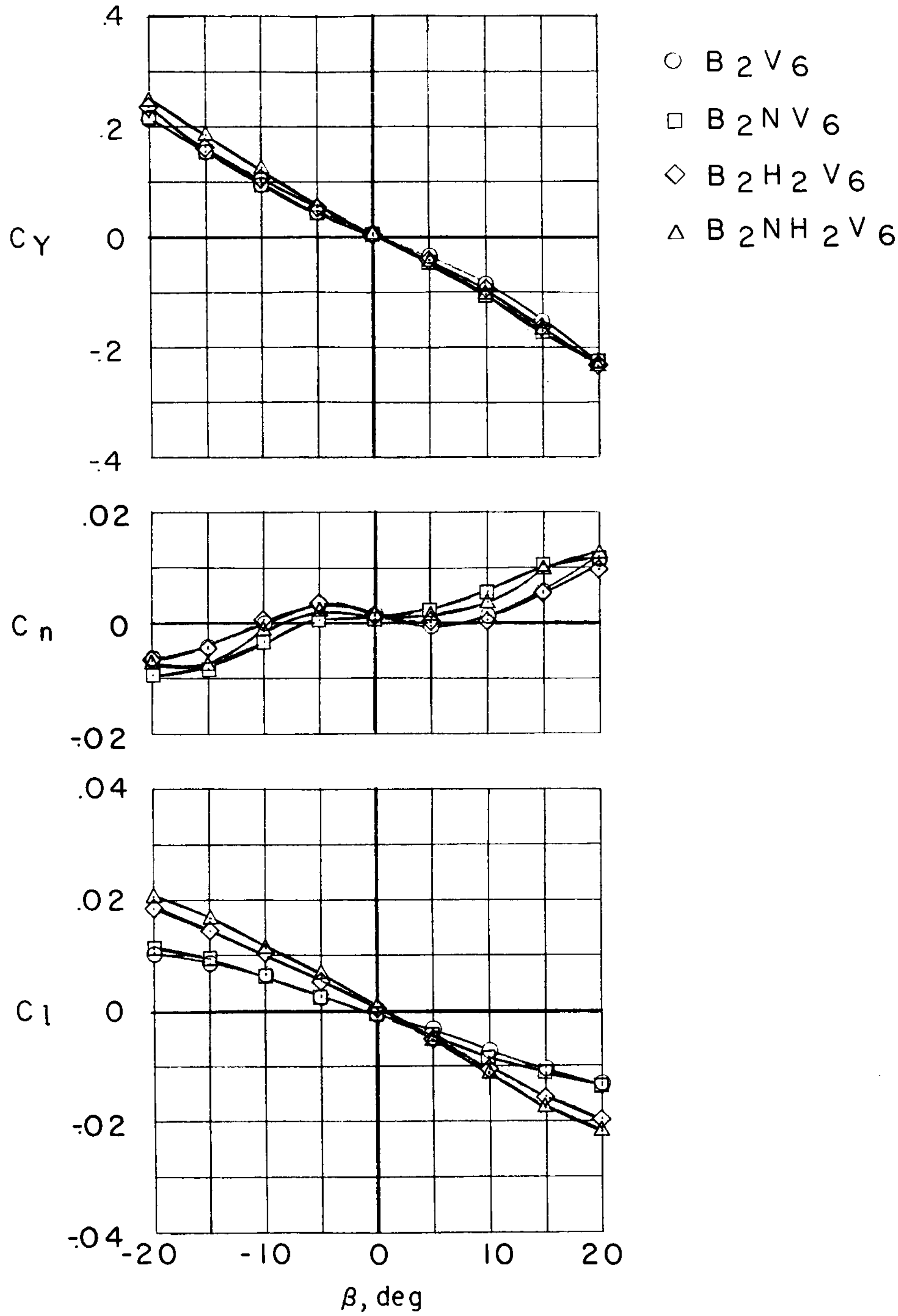

(b) $\alpha = 10^{\circ}$.

Figure 35.- Continued.

L-575

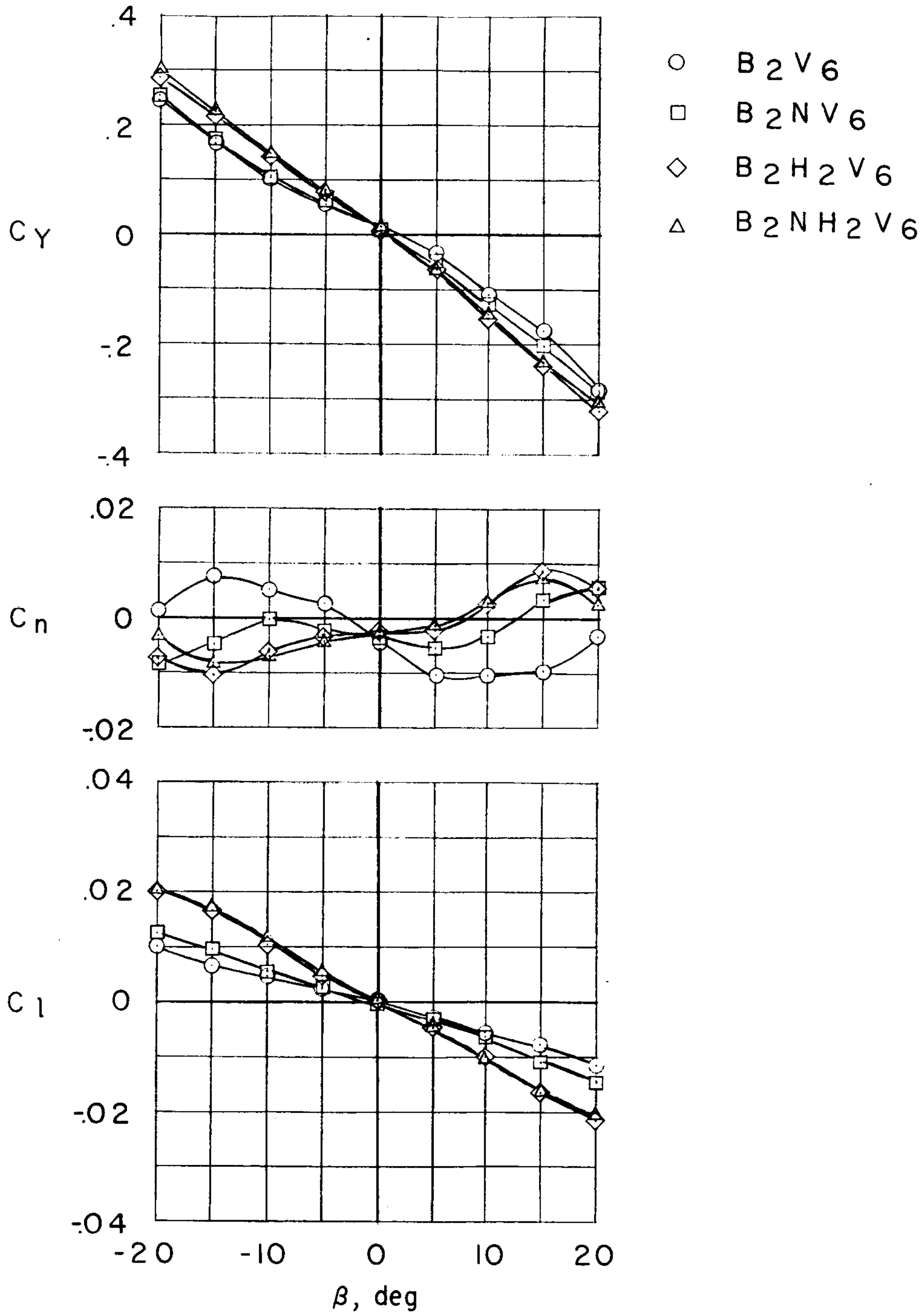

(c) $\alpha = 20^{\circ}$.

Figure 35.-- Continued.

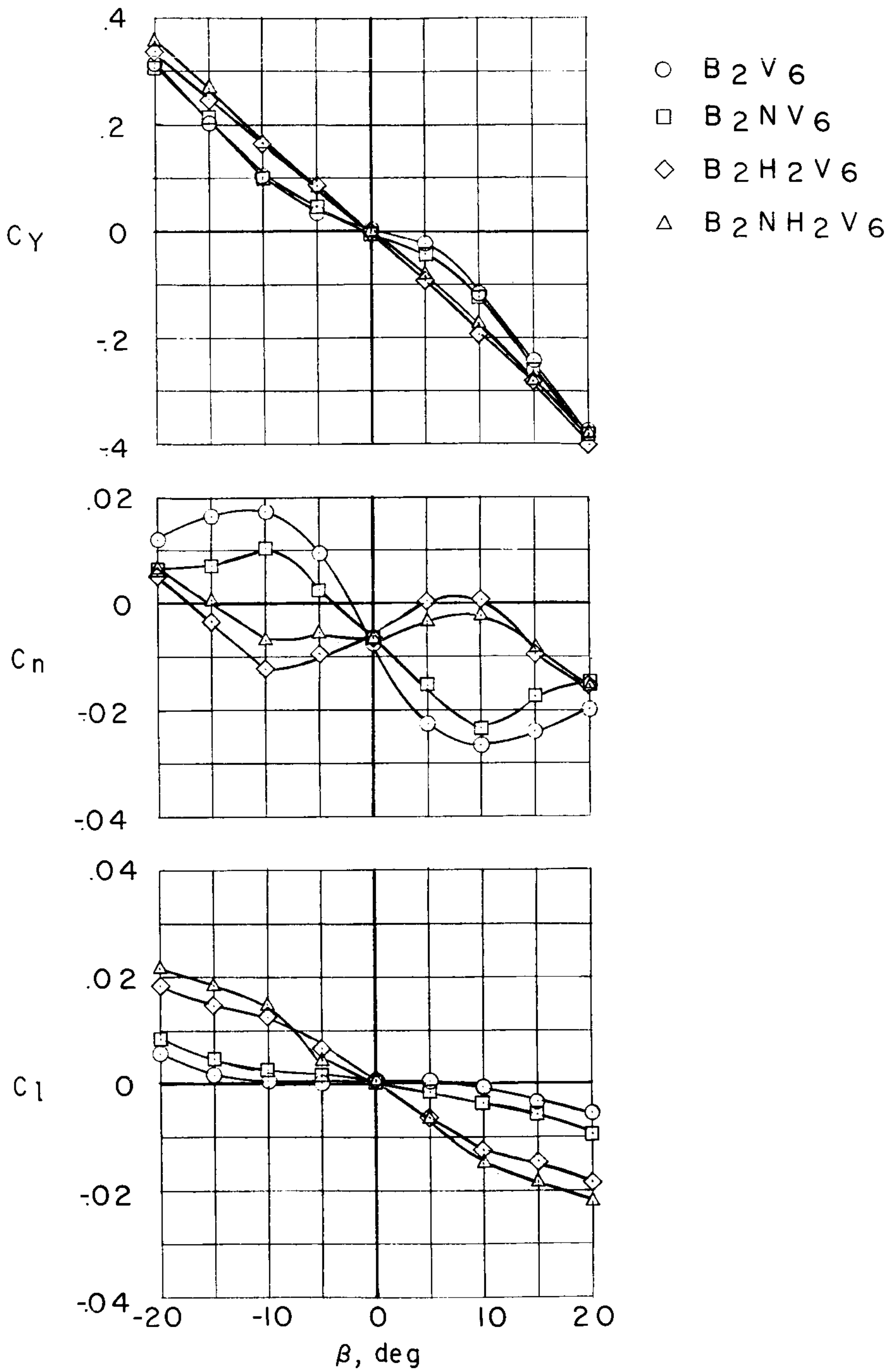

(d) $\alpha = 30^{\circ}$.

Figure 35.- Concluded.

L-575

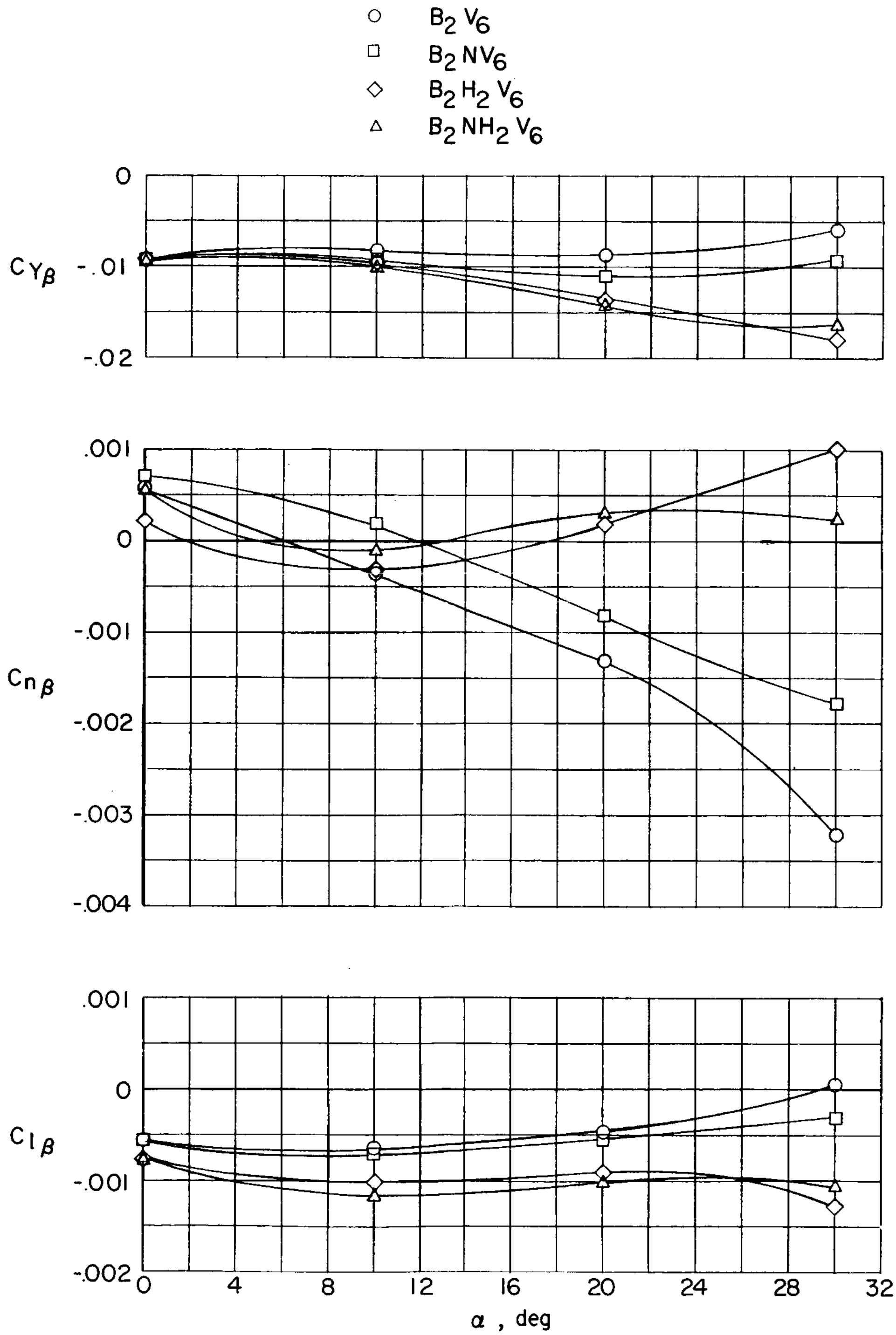

Figure 36.- Effect of components on static lateral stability derivatives of model with body B_2 and vertical tail V_6. Power off; $i_j = 0^o$.

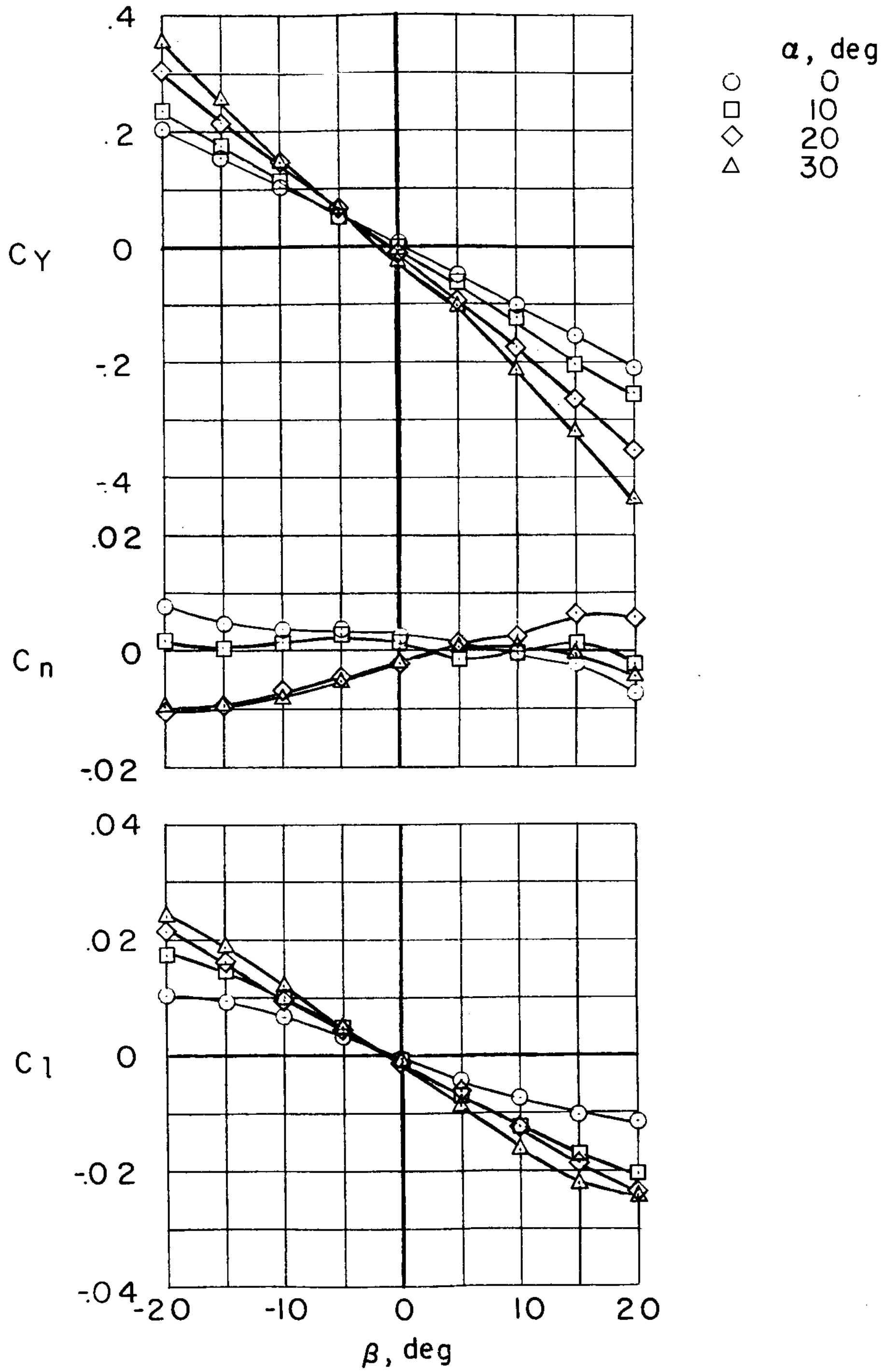

Figure 37.- Lateral characteristics of model in configuration $B_2NH_2V_7$. Power off; $i_j = 0^{\circ}$.

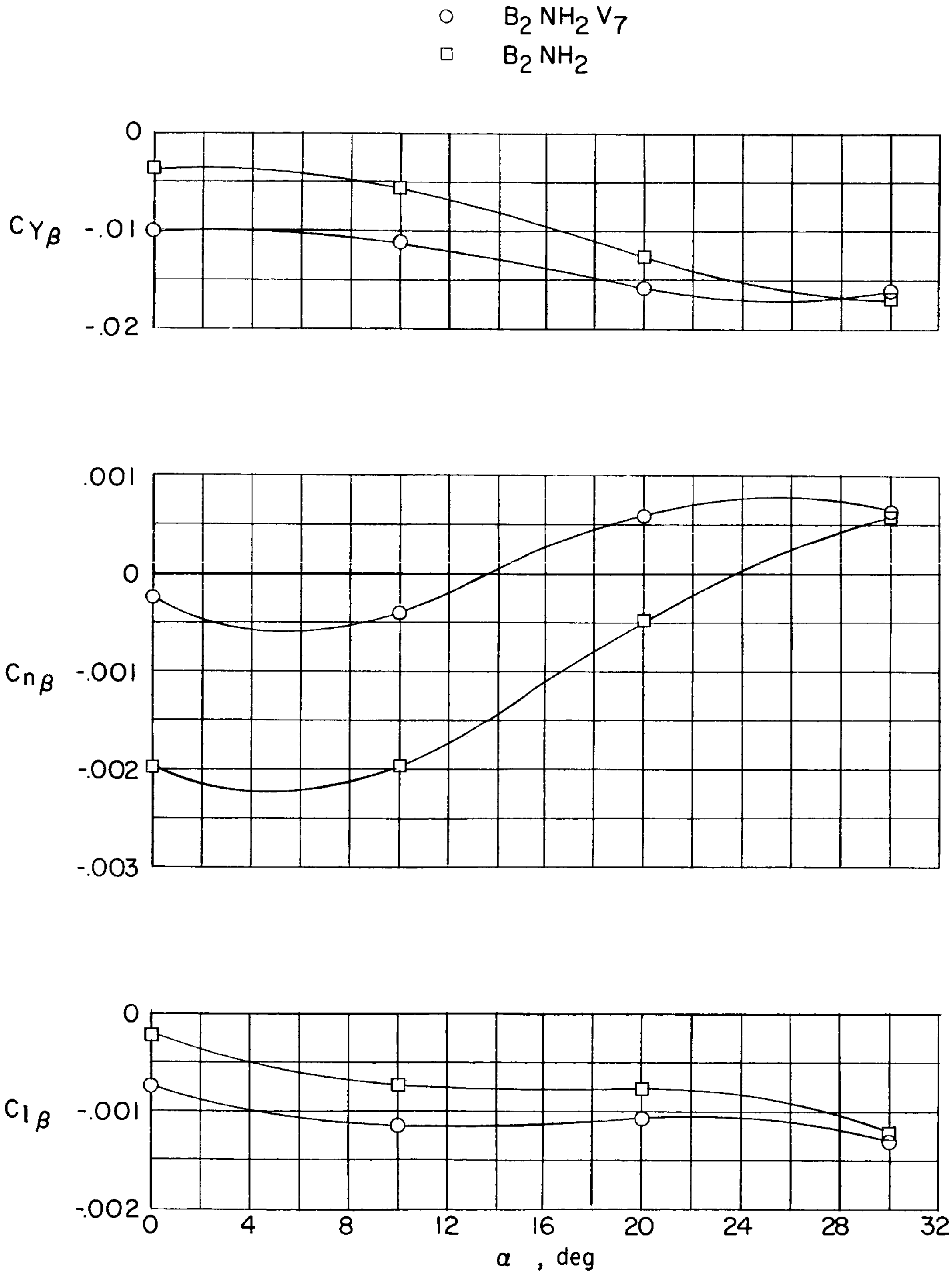

Figure 38.- Static lateral stability derivatives of model in configuration $B_2NH_2V_7$. Power off; $i_j = 0^{\circ}$.

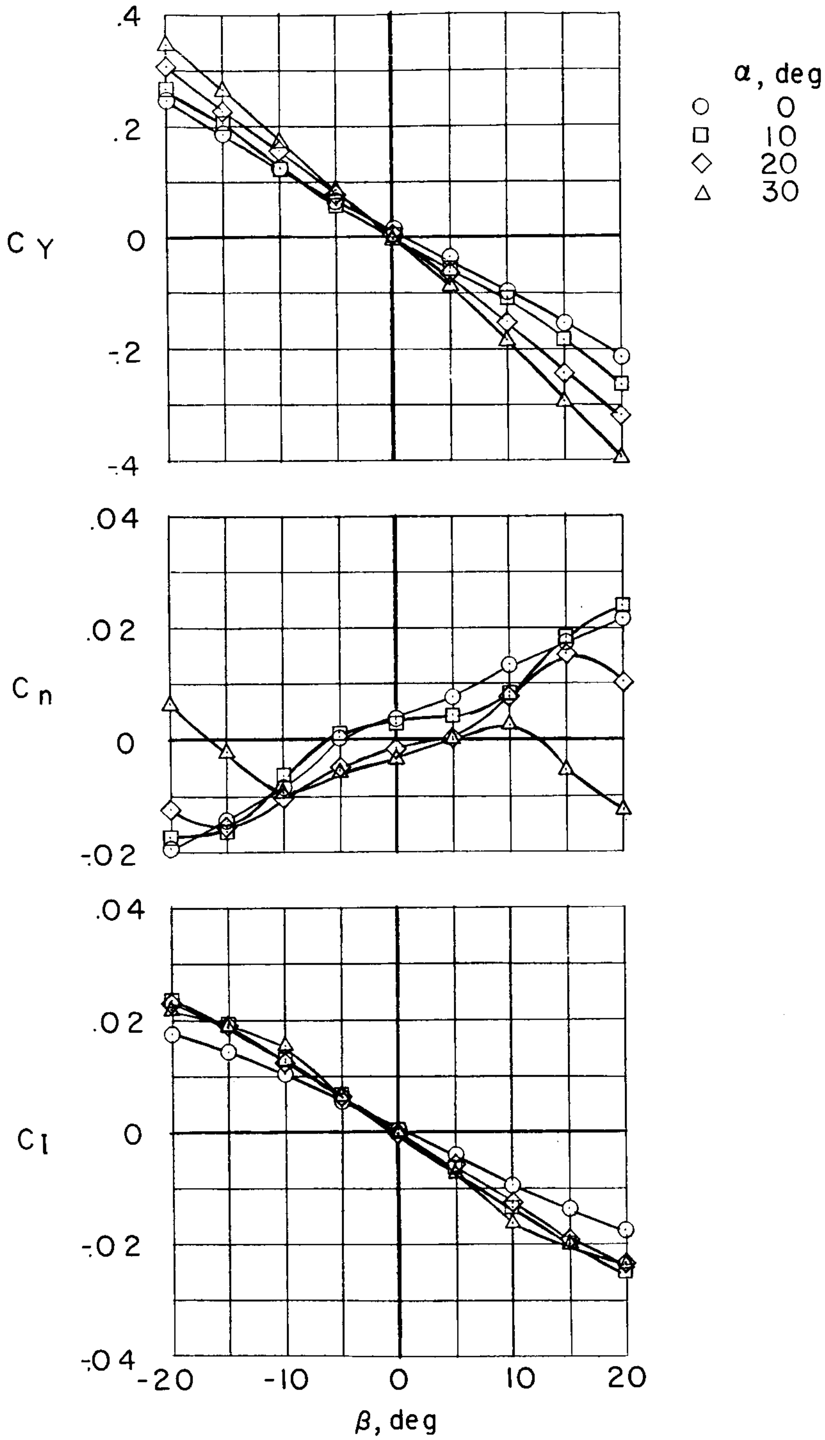

Figure 39.- Lateral characteristics of model in configuration $B_2NH_2V_8$. Power off; $i_j = 0^o$.

L-575

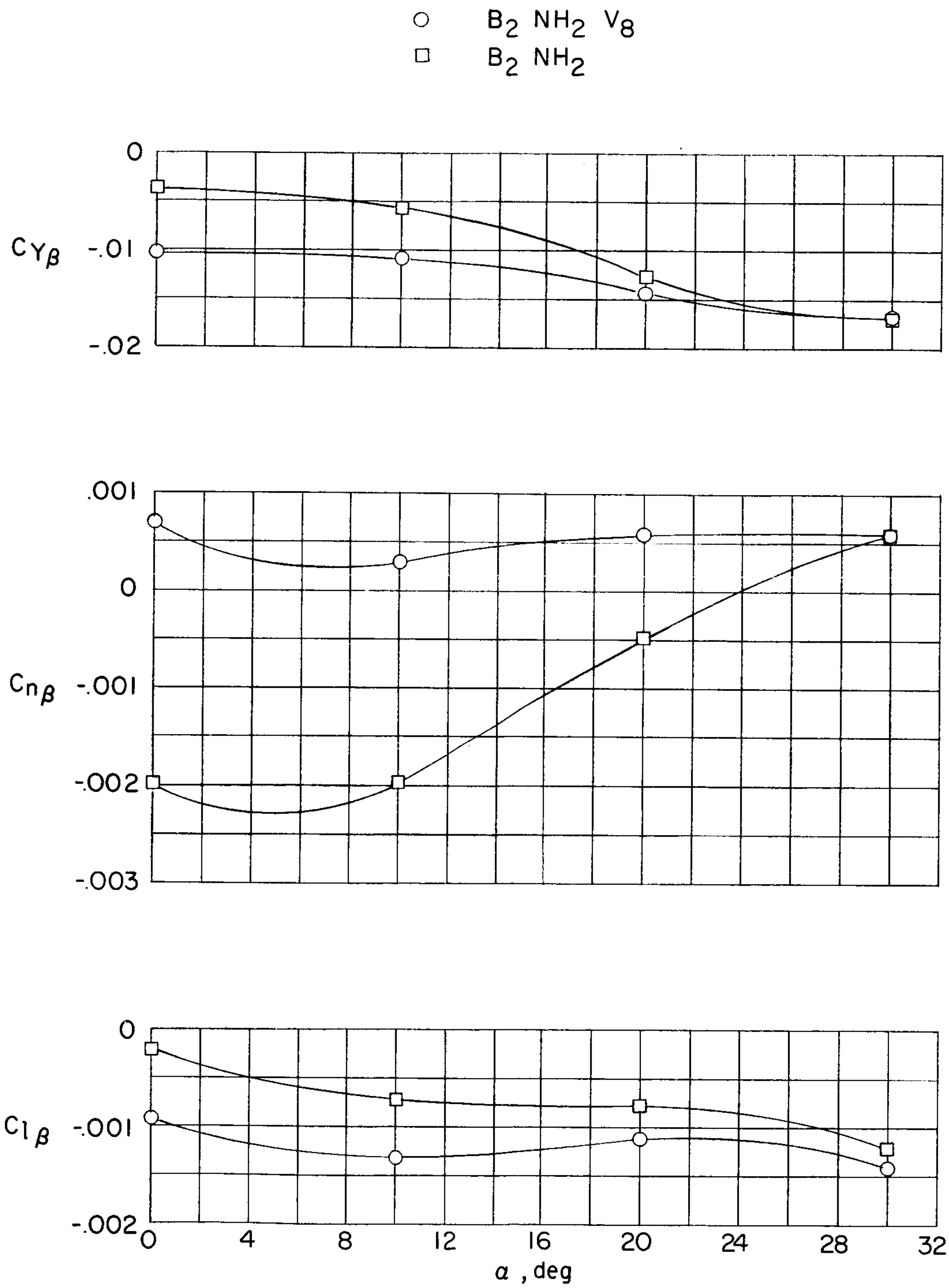

Figure 40.- Static lateral stability derivatives of model in configuration $B_2NH_2V_8$. Power off; $i_j = 0^o$.